Electronic components & applications

Vol. 3, No
May 198

ISSN 0141–6219

Electronic components & applications

Volume 3, No. 3 May 1981

Like an exclamation mark punctuating the skyline south of Utrecht, the main antenna tower of the Dutch Broadcasting Authority emphasises the dominant role of broadcast communication in today's society. Credit for that dominance goes not only to the producers and artists who capture the public's attention, but also to the technology that enables them to do so. Four articles in this issue focus on aspects of that technology: transmitting tubes; a miniature camera tube that opens new horizons to electronic news gathering; a significant improvement in camera tube signal-to-noise ratio; and a new television sound system for high-fidelity, stereo, and even bilingual programmes.

Contents

Portable TV cameras need to be small, light, easy to handle, and resistant to microphony. Thanks to the novel construction of a new Plumbicon tube with 8 mm scan diagonal, they can be. And the power they save is enough to make a welcome difference in the weight of the cameraman's battery pack.

Miniature Plumbicon® tube for portable TV cameras

A. A. J. FRANKEN

Portability is an essential attribute of cameras for electronic field production and electronic news gathering (EFP and ENG). To meet that need the 2/3-inch Plumbicon tube with 11 mm scan diagonal introduced in 1975 went a long way toward making cameras both smaller and lighter. Now a new Plumbicon tube with 8 mm scan diagonal, the 80XQ, makes it possible to cut the size and weight of the camera head by roughly another half, and the power consumption by almost three-quarters so that battery packs can be lighter too. In respect of performance, cameras using the new tube are in every way a match for their larger predecessors. As an added benefit, they are also much better suited to integration in a single unit with a recorder.

CONSTRUCTION OF THE TUBE AND DEFLECTION COIL

The construction of the 80XQ departs significantly from earlier practice (Ref.1). The glass envelope, no longer merely a housing and vacuum seal, is an essential structural element supporting and locating principal electrodes (Ref.2). Apart from the target (already glass-supported in previous tubes), these include an electrostatic focusing electrode, the collector, and the mesh. Special manufacturing techniques keep critical tolerances of the envelope and the electrodes to within a few micrometres, ensuring excellent registration. Other benefits of the new construction are that it gives more stable performance characteristics and virtually eliminates microphony.

To keep heater consumption low and at the same time allow for high cathode-current density, a special impregnated cathode has been developed. The heater operates at 9 V instead of the usual 6.3 V. This matches the supply voltage customarily used elsewhere in EFP and ENG cameras and eliminates losses due to stabilisation of an additional voltage.

The electron gun is an improved diode gun with grid 1 positive with respect to the cathode (Ref.3). Since there is no crossover in the electron paths and the potential in the region of greatest current density is only about 20 V (compared to about 320 V in the 2/3-inch diode-gun Plumbicon tubes XQ2427 and XQ3427), the beam temperature and beam resistance are low. This shortens decay lag and makes for fast response.

To minimise power consumption the beam is focused electrostatically rather than electromagnetically. The focusing electrode consists of a metal film electroless-deposited on the glass. This electrode, at about 30 V, and the collector, at 250 V, together form an accelerating

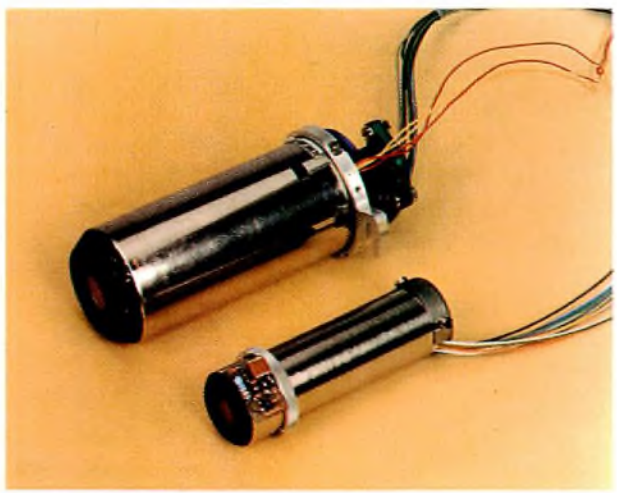

Fig.1 The 80XQ Plumbicon tube in its deflection coil housing, shown for comparison alongside a 2/3-inch Plumbicon tube and coil. The small circuit board near the faceplate end of the 80XQ carries the FET preamplifier and the mesh decoupling capacitor

lens by means of which it is possible to obtain a spot of a given diameter in less distance than with the customary unipotential lens. Such an accelerating lens not only shortens the tube but, in combination with the diode gun, also tends to prevent ions present from poisoning the cathode.

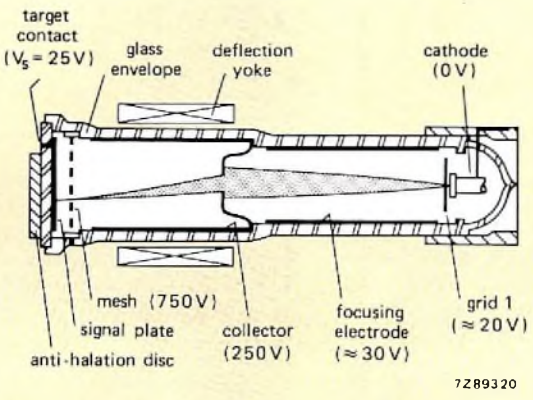

Fig.2 Arrangement of the electrodes, deflection coil, and base connector of the 80XQ

The collector is also an electroless-deposited metal film. Because of its thinness it absorbs little energy from the deflection field and is thus conducive to good linearity at the beginning of scan (Ref.4). Furthermore, because of the low voltage on it the electron velocity inside it is low, so little deflection power is required. A domed metal diaphragm, defining the entrance to the collector and forming part of the accelerating lens, restricts the electron beam and minimises spherical aberration so that sharpness in the corners of the target is very nearly equal to that in the centre.

To ensure the best possible registration the seating surfaces of the target and the mesh support ring are formed simultaneously by precision tooling so that the mesh is clamped exactly parallel to the target. Furthermore, because of the smallness of the mesh it is relatively stiff and therefore resistant to microphony. This is especially important in camera/recorder combinations in which even small-amplitude vibrations due to tape and head drives might otherwise affect image quality.

The connection to the mesh is on the adjoining outer surface of the glass, so there is no risk of long internal leads picking up interference from the deflection flyback pulses. Moreover, the mesh can be decoupled by a capacitor on the same printed wiring board as the signal FET, at the faceplate end of the deflection coil housing (see Fig.1). At the specified mesh voltage of 750 V, distortion is less than 0.5% and landing errors are smaller than 0.5 V (Ref.2).

The target is a low output-capacitance one (Ref.5) that does not cover the entire faceplate but is only slightly larger than the scanning area. It is at 25 V, instead of the usual 45 V, to minimise beam bending and distortions at the edge of the image. Connection to it is made via a metallised contact area adjoining a cut-away segment of the anti-halation disc.

There are no base pins. Connections to the collector, focusing electrode, grid 1, cathode, and heater are made via contact surfaces recessed in a sleeve enclosing the base of the tube. These engage contacts in the tube/deflection-coil housing from which a cable-form provides for connection to the associated circuitry. This construction not only makes the tube/deflection-coil assembly significantly shorter and lighter, it also allows the mu-metal shield to be extended far enough to the rear to ensure that external magnetic fields have no effect on the electron beam.

Because of the precision with which the glass envelope and deposited electrodes are formed there is no need for alignment coils or magnets; thus, the entire assembly is in fact as simple, compact, and uncluttered as appears in Fig.1.

PROPERTIES OF THE TUBE AND DEFLECTION COIL

Table 1 compares significant properties of the 80XQ and the 2/3-inch XQ2427. Both the diameter and length of the new tube in its deflection coil are significantly smaller, reducing the volume from about 130 cm^3 to about 30 cm^3; the weight reduction from 255 g to 65 g, due mainly to the lighter coil, is proportionate. The 66% saving in power consumption is due mainly to the use of electrostatic instead of electromagnetic focusing.

Because of the smaller scanned area there is some loss of sharpness. However, in a three-tube colour camera it is not nearly so serious as the difference between 65% and 45% modulation depth at 4 MHz, as reported in the table, would suggest. Due to the superior registration of the 80XQ the image on the monitor remains excellent and no loss of sharpness is discernible. (The 45% modulation depth reported in the table is, moreover, not a wholly accurate statement of the characteristic of the tube but, if anything, a somewhat pessimistic one. For so small an image the modulation transfer characteristic of the lens also begins to play an important part; the reported measurement was made using an f/4.0 Summicron lens for which the modulation transfer characteristic for an 8 mm scan diagonal in green light was 75% at 4 MHz).

Figure 4 is a plot of the sharpness in the centre and corners as functions of focus voltage variation. Without dynamic focusing the sharpness in the corners is about 80% of that in the centre; with dynamic focusing the difference can be reduced to only a few per cent. A focus voltage modulation of about 0.5 V is sufficient to give good sharpness uniformity over the entire image.

TABLE 1
Comparative data of 80XQ and XQ2427 Plumbicon tubes

tube	80XQ	XQ2427	
yoke	DT1120	AT1109	
focusing	electro-static	electro-magnetic	
scan diagonal	8	11	(mm)
length overall	78	115	(mm)
yoke diameter	22	38	(mm)
tube mass	15	25	(g)
yoke mass	50	230	(g)
total mass	65	255	(g)
filament power	0.5	0.6	(W)
focusing power		0.9	(W)
total power	0.5	1.5	(W)
modulation depth at 4 MHz*	45	65	(%)
sensitivity	280	320	(μA/lum)
output capacitance	3.5	6.5	(pF)
decay lag after 60 ms**	6.5	9	(%)

* Measured in green light with:
I_s/I_b = 100 nA/200 nA for 80XQ, 200 nA/400 nA for XQ2427.

** Measured in green light, without bias lighting, at:
I_s/I_b = 20 nA/200 nA for 80XQ, 20 nA/300 nA for XQ2427.

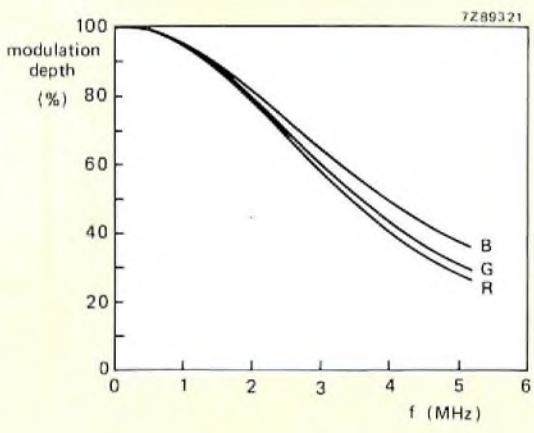

Fig.3 Square-wave modulation transfer function of the 80XQ in red (I_s/I_b = 50 nA/100 nA), green (I_s/I_b = 100 nA/200 nA), and blue (I_s/I_b = 50 nA/100 nA); the curves shown are not corrected for the transfer characteristic of the f/4.0 Summicron lens used in measurement

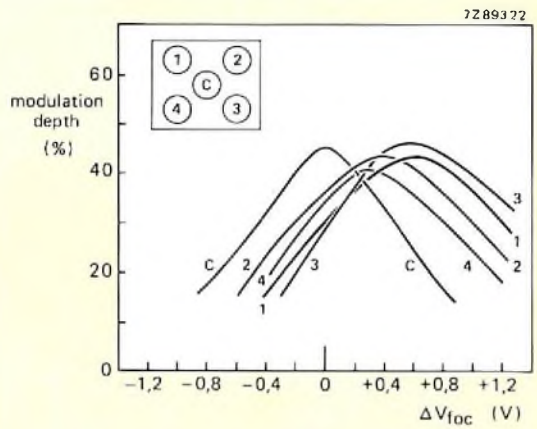

Fig.4 Modulation depth in the centre and corners of the 80XQ target, at 4 MHz, as a function of focus-voltage variation ΔV_{foc}; measured in green light with I_s/I_b = 100 nA/200 nA, corners optically focused

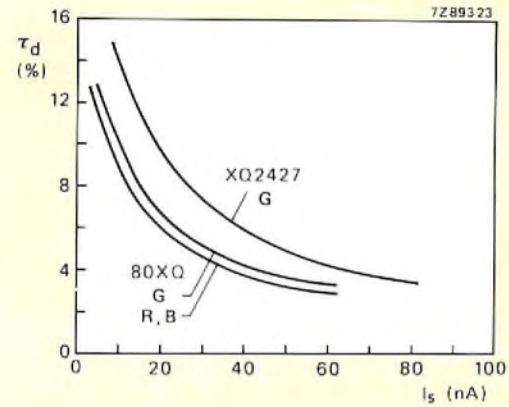

Fig.5 Decay lag of the 80XQ and XQ2427, after 60 ms, as functions of signal current I_s. For the 80XQ, measured with I_b = 200 nA (green), 100 nA (red and blue); for the XQ2427, with I_b = 300 nA (green)

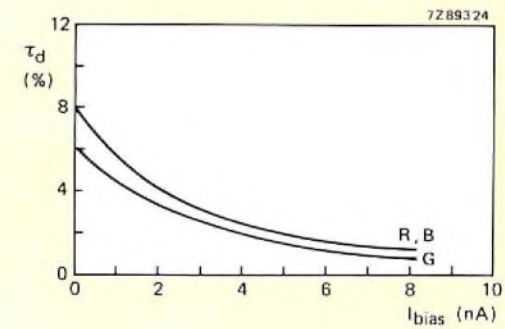

Fig.6 Showing the effect of front bias lighting on the decay lag of the 80XQ in red (I_s/I_b = 10 nA/100 nA), green (I_s/I_b = 20 nA/200 nA) and blue (I_s/I_b = 10 nA/100 nA); i_{bias} is the photocurrent due to the bias lighting

To conserve modulation depth the photoconductive layer of the 80XQ is made slightly thinner than in larger tubes. This reduces sensitivity somewhat, but on the other hand the smallness of the signal plate halves the output capacitance of the tube in its deflection coil and thereby increases the signal-to-noise ratio (Ref.5). The tube can therefore be operated at smaller signal currents, down to the level at which decay lag becomes a limiting factor. Thanks to the improved electron gun and the reduced capacitance of the smaller target, the decay-lag limited signal-current level of the 80XQ is about half that of the 2/3-inch XQ2427 (see Fig.5).

Decay lag can be further reduced by applying front bias light (Fig.6). As the lag does not differ appreciably from one colour channel to another, the light may be adjusted to give substantially the same bias current in all three channels, say 2 to 3 nA.

The 80XQ has sufficient beam reserve to allow the application of dynamic beam control (Ref.6) to deal with highlights up to 3 or 4 lens-stops overexposure. Because of the low target voltage and small layer capacitance, the resulting signal currents (500 to 700 nA) are not large enough to impose any severe demands on the dynamic characteristics of the preamplifier.

In respect of dark current, flare, burn-in, colour rendition, life expectancy and ability to withstand temperature variations, the 80XQ embodies the well-known qualities of all Plumbicon tubes. In respect of registration it is at least the equal of the XQ2427 but also has an important advantage over that tube: because of its very low dissipation it is now possible to construct three-tube colour cameras in which the temperature difference between the camera head and the environment is so small that there is no longer any threat to the stability of the registration.

CAMERA COMPARISONS

Three-tube cameras using 80XQ and XQ2427

Cameras with different image sizes cannot be accurately compared in all respects: so many parameters can be varied, particularly in the optics, and so many different compromises can be adopted. The comparison summarised in Table 2 is therefore based on a more or less typical specification for a camera with a zoom range of 12:1 and a maximum lens aperture of f/1.7.

Let the focal length range of the camera with XQ2427 tube be 9 mm to 108 mm; for the same zoom range and angle of view, that of the 80XQ camera will then be 6.5 mm to 78 mm. If both cameras were to have lenses of the same diameter, that of the 80XQ camera could then have an aperture of f/1.2 because of the shorter focal length; however, the usual three-piece colour-splitting prism limits the usable aperture to f/1.4, so there is no point in choosing a larger one. The f/1.4 lens of the 80XQ camera will have a smaller diameter than the f/1.7 lens of the XQ2427 camera and will weigh less. Together, the optics, camera tubes, and deflection coils of the 80XQ camera will weigh about half as much as those of the XQ2427 camera (Table 2). The volume reduction is sufficient to allow the 80XQ camera to be designed so that the cameraman can see over it while it is resting on his shoulder: a particularly valuable asset in ENG, where the cameraman often has to react quickly to the unexpected.

The reduced power consumption shown in Table 2 reflects not only the saving due to the tubes and deflection coils themselves but also that due to the circuitry. The calculations were based on the use of a nominal 12 V battery pack.

To compare the sensitivities of the two cameras, the one with XQ2427 tubes can be taken to have a signal-to-noise ratio of 50 dB at a scene illumination of 600 lux, a reflectivity (ρ) of 60%, and a lens aperture of f/2. Under the same conditions the S/N ratio of the one with 80XQ is down 5.5 dB because the scanned area is smaller and 1.2 dB because the sensitivity of the photoconductive layer is less; however, the lower output capacitance restores 2.8 dB of that loss, so the net is S/N = 46.1 dB.

More to the point, however, is a comparison under conditions when noise is most likely to cause trouble;

TABLE 2
Comparative data of three-tube colour cameras using 80XQ and XQ2427

tube	80XQ	XQ2427	
lens focal length (zoom) range	6.5 - 78	9 - 108	(mm)
lens aperture	f/1.4	f/1.7	
lens mass	1.1	1.6	(kg)
prism mass	0.2	0.4	(kg)
tube and yoke mass (× 3)	0.2	0.8	(kg)
total	1.5	2.8	(kg)
filament power	1.5	1.8	(W)
filament circuitry power*	0.4	1.5	(W)
focusing power		2.7	(W)
focusing circuitry power		1.5	(W)
total	1.9	7.5	(W)
S/N ratio			
at 600 lux, ρ = 60%, f/2	46.1	50	(dB)
at maximum aperture	52.3	52.7	(dB)

* Based on nominal 12 V battery pack, stabilisation of 9 V filament supply for 80XQ, 6.3 V filament supply for XQ2427.

namely, at low light level and maximum lens aperture. Then, the signal-to-noise ratio of the XQ2427 camera at f/1.7 is 52.7 dB; and of the 80XQ camera at f/1.4, 52.3 dB.

Comparison with a camera with a single stripe-filter tube

Several methods of colour separation using single camera tubes with stripe filters are in use; for example,

- cross-filter systems in which colour signals are obtained via high-pass filters and phase-amplitude detection
- two-carrier frequency separation using bandpass filters
- step energy systems
- three-electrode systems
- two-electrode systems with high-pass filters and phase amplitude detection.

Detailed comparison with all these is not practical. Nevertheless, a three-tube camera can be shown to be preferable to all of them in nearly all respects, for the following reasons.

- Its signal-to-noise ratio is better because in a stripe-filter tube a smaller fraction of the light reaches the photoconductive layer. In stripe-filter tubes with multiple signal electrodes there is also capacitive cross-talk between signals. Moreover, the colour information of a stripe-filter tube is often modulated on a comparatively high-frequency carrier, and where the modulation depth is small the noise contribution of the preamplifier is comparatively large. To avoid moiré effects it is necessary to use optical low-pass filters which usually cause serious attentuation of high signal frequencies. If a low carrier frequency is used resolution is lost.
- The sampling principle of stripe-filter tubes limits resolution, sacrificing sharpness particularly in the red and blue.
- In a camera with a stripe-filter tube high-frequency colour signals interfere with high-frequency luminance signals, causing beat patterns that do not occur in three-tube cameras.
- Residual chromatic aberration of present-day zoom lenses may cause size differences amounting to as much as 100 ns of scan in the three colour images on the target. In a three-tube camera these can be compensated by small adjustments to the scan of each tube. In a stripe-filter tube no correction is possible.

Moreover, compared with a three-tube camera using the 80XQ, any saving of weight or power consumption that one with a single stripe-filter tube might appear to offer is likely to prove illusory. It will be more than made up by the additional circuitry required for colour separation and signal processing.

Conclusion

The 80XQ Plumbicon tube opens new opportunities to reduce size, weight, and power consumption, particularly of cameras combined with recorders. The sensitivity of such a camera would be roughly equal to that of one equipped with 2/3-inch tubes and would be susceptible of further improvement as lower-noise FETs become available. What little the tube sacrifices in static resolution is more than compensated by its excellent registration and shorter decay lag, so that in respect of dynamic resolution it is at least on a par with its larger predecessors. Compared with present cameras using 2/3-inch tubes or a single stripe-filter tube, a three-tube camera using the 80XQ promises to be superior in nearly all respects.

REFERENCES

1. ROOSMALEN, J. H. T. van. 1971. IEEE Trans. El. Dev. 18 no. 11, 1087–1093. See also U.S.A. patent no. 3,831,058.
2. ROOSMALEN, J. H. T. van. 1981. Philips Technical Revue 39, no. 8, 201–210.
3. FRANKEN, A. A. J. 1979. Electronic Components and Applications 1 no. 2, 71–77.
4. FRANKEN, A. A. J. 1981. 'A new high resolution Plumbicon tube' 15th annual SMPTE Television Conference, San Francisco, February 6-7.
5. FRANKEN, A. A. J. 1981. Electronic Components and Applications 3 no. 3, 156–158.
6. FRANKEN, A. A. J. and LOHUIS, W. 1980. Electronic Components and Applications 3 no. 1, 17–20.

The tuner in a TV receiver converts the incoming v.h.f. or u.h.f. signals into an i.f. signal at about 37 MHz, but as the tuner is not very selective unwanted signals must be suppressed by a bandpass filter. Nowadays, surface-acoustic-wave filters are often used for this, mainly because they are smaller than LC filters and need no trimming; however, they do introduce losses. This article describes a single-transistor preamplifier to compensate those losses. The linear input characteristic of the BF370 transistor, combined with its high transition frequency and low feedback capacitance, ideally suits it to this application.

Single-transistor preamplifier for surface-acoustic-wave i.f. filters

Surface-acoustic-wave (SAW) filters are rapidly replacing conventional LC filters in tv receiver i.f. stages, principally because they are smaller and require no trimming. They do, however, have higher insertion losses (in the region of 20 dB), so the use of a preamplifier is essential for keeping the sensitivity and signal-to-noise ratio at acceptable levels. On the basis of cost, a single transistor preamplifier is preferred for domestic receivers. This article describes such a preamplifier using a new npn bipolar transistor, the BF370. This transistor has been designed to meet the rather special requirements of the SAW preamplifier, notably:

- voltage gain of about 24 dB to compensate the insertion losses of the SAW filter
- ability to handle the wide range of signal voltages, from say 200 μV to about 100 mV, generated at the tuner output
- output impedance sufficiently low to minimise reflections in the SAW filter, this being best achieved by means of a shunt feedback network.

Since these are to some extent conflicting requirements, the preamplifier design must embody a high degree of compromise. The BF370 allows this compromise to be more easily achieved.

The BF370 is supplied in TO-92 encapsulation. Table 1 gives its main characteristics. They include many features that suit it particularly well to the present application, the most important being:

- a linear input characteristic, minimising distortion in the emitter circuit
- a high transition frequency f_T (about 490 MHz) and a substantially linear f_T/I_C characteristic with a maximum relatively independent of I_C (Fig.1)
- low feedback capacitance (<2.2 pF), this results in a small capacitive component to the input impedance, easing trimming of the preselection circuit and allowing maximum advantage to be taken of the shunt feedback network.

TABLE 1
BF370 transistor characteristics

collector-base voltage (open emitter)	V_{CBO}	≤40 V
collector-emitter voltage (open base)	V_{CEO}	≤15 V
d.c. collector current	I_C	≤100 mA
total power dissipation up to T_{amb} = 25 °C	P_{tot}	≤500 mW
junction temperature	T_j	≤150 °C
d.c. current gain at V_{CE} = 1 V; I_C = 10 mA	h_{FE}	≥40
transition frequency at V_{CE} = 10 V; I_C = 40 mA	f_T	≥490 MHz
feedback capacitance at V_{CE} = 10 V; I_C = 0, f = 1 MHz	C_F	1.6(≤2.2) pF

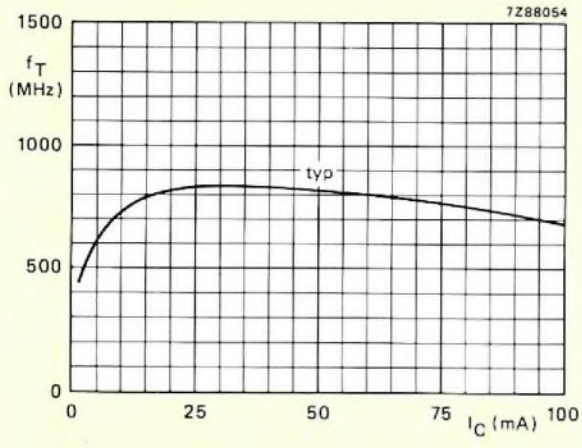

Fig.1 f_T/I_C characteristic of the BF370 transistor. The relationship is substantially linear up to its maximum, and is thereafter relatively independent of I_C

PREAMPLIFIER CIRCUIT

Figure 2 shows the BF370 in a single stage common-emitter preamplifier circuit using a shunt feedback network. The conflicting requirements of high gain and low cross-modulation are not easily met in a single stage preamplifier; but a double-tuned bandpass filter eases the problem considerably by providing i.f. preselection at the tuner output. The bandpass filter shown in Fig.2 attenuates the interfering signals by about 17 dB at a distance of at least two channels, and eases matching between the preamplifier and tuner. Note: if the tuner design permits, a less expensive single tuned bandpass filter can be used instead.

PREAMPLIFIER PERFORMANCE

Figure 3 gives the response of the double-tuned bandpass filter. The filter passes signals between 33 and 40 MHz, the normal passband for tv i.f. amplifiers.

The performance of the preamplifier can be assessed from the data given in Table 2 (obtained with the SAW filter simulated by a 1 kΩ resistor shunted by a 15 pF capacitor). The amplifier can provide a voltage gain of about 24 dB at acceptable levels of cross-modulation (1% at an input of 120 mV).

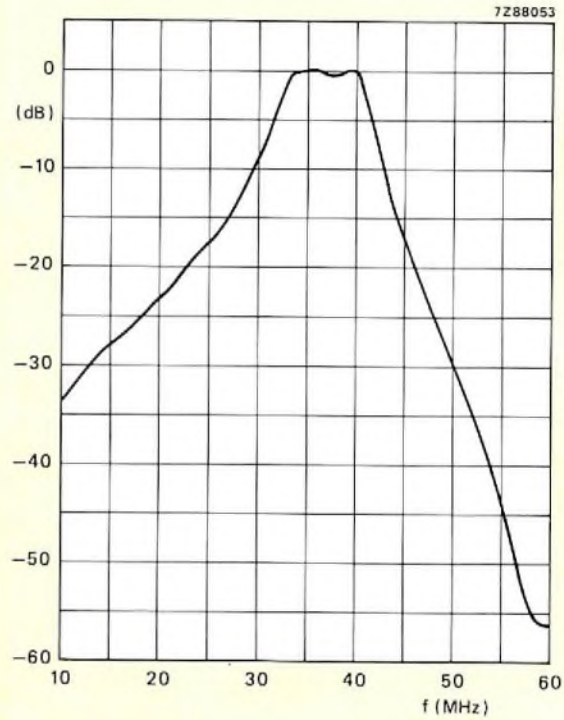

Fig.3 Response of the double-tuned bandpass filter coupling tuner and preamplifier

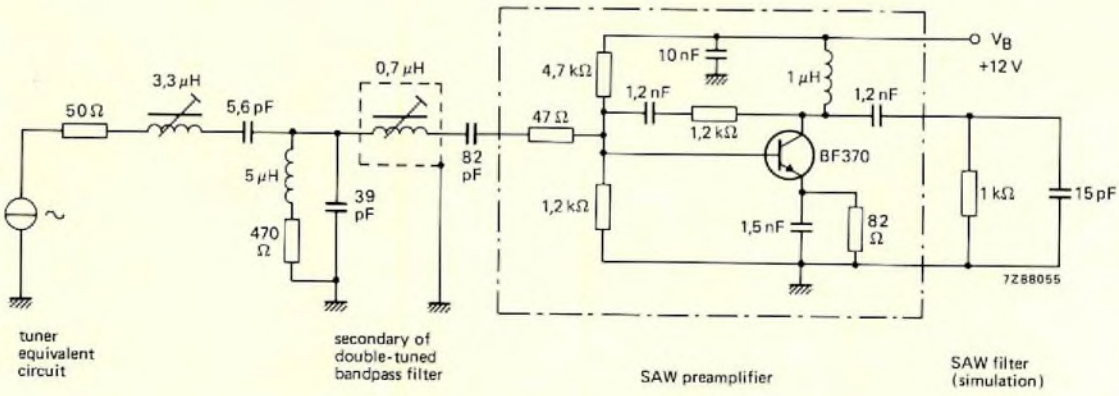

Fig.2 I.F. preamplifier circuit equipped with transistor BF370. The figure also shows details of the coupling between tuner and preamplifier, i.e. the double-tuned bandpass filter

System performance

Figure 4 shows a basic tv receiver front end incorporating the preamplifier and SAW filter, and the voltage levels for the front end operating at a vision carrier frequency of 38.9 MHz. The gain of the preamplifier, tuner and i.f. amplifier (TDA2541), and the attenuation of the SAW filter, are all contributing factors determining receiver sensitivity. In Fig.4, the sensitivity is about 12.5 μV.

Noise

The preamplifier contributes little to the total noise of the i.f. stage. With an available tuner gain of say 20 dB and a noise of 7 dB, a noise of 9 dB in the preamplifier contributes no more than 0.1 dB overall.

TABLE 2
Preamplifier performance

power consumption	240 mW
voltage gain	24 dB (16×)
input impedance	approx. 50Ω//1 pF
output impedance	100Ω
noise	8.5 dB at 50Ω source
input voltage for 1% cross-modulation	120 mV
3rd order intermodulation distortion	52 dB below input voltage (120 mV)*
input voltage for 1 dB gain compression	430 mV

* Measured according to the 'two signal' method.

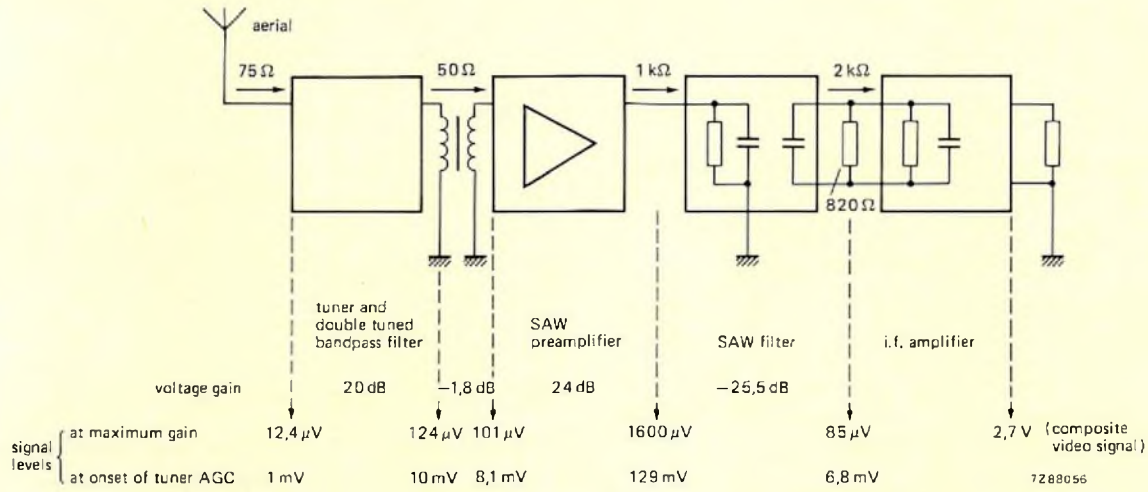

Fig.4 Block diagram of a tv receiver front end incorporating a SAW filter and preamplifier

Storage oscilloscope tubes that keep isolated waveforms on display are useful for studying fast one-shot events. However, ions generated in the operation of the tube are attracted to the dielectric mesh on which the trace is stored and limit the display time by gradually lightening the background. The transfer-storage tube described here extends the display time by using two meshes in cascade: a small-capacitance one for 100 MHz bandwidth, and a large-capacitance one for long storage.

Wideband, variable persistence oscilloscope tube

K. ZEPPENFELD

The L14-140GH/95 is a 100 MHz oscilloscope tube with 5.3 V/cm vertical deflection sensitivity and 9 mm/ns storable writing speed for one-shot events. Advanced features of its design and construction include:

- 3 kV writing-gun with electrostatic quadrupole lenses for vertical scan magnification and separate horizontal and vertical focusing
- 7 kV post-acceleration with proximity focusing between storage mesh and screen
- very-low-voltage 'laminar flow' flood-guns
- quick-heating cathodes in writing and flood-guns for five-second start-up
- burn-resistant secondary emitters in the storage system
- short vertical deflection plates with side contacts for low capacitance and negligible time-of-flight distortion.

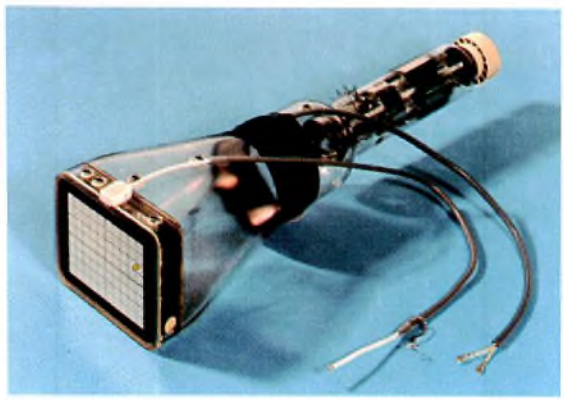

The L14-140GH/95 transfer-storage oscilloscope tube. A visually striking feature is that the collimator bands on the inside of the cone are transparent; unlike the customary graphite, the material used is not hygroscopic

The flat faceplate has a 14 cm diagonal and an internal 8 x 10 graticule with 9 mm divisions.

The L14-140GH/95 can be used as an ordinary wideband oscilloscope tube, as a wideband tube with conventional storage facility and variable persistence (Fig.1), or as a transfer-storage tube with very high writing speed.

WRITING SPEED AND STORAGE TIME

The maximum writing speed of a conventional storage oscilloscope, under specified background conditions, is the speed at which the beam is just able to write a discernible trace; for a gaussian spot profile,

$$S_w \sim \frac{I_b}{W_t} \cdot \frac{\delta - 1}{Q}$$

where

- S_w is maximum writing speed
- I_b is the beam current
- W_t is the trace width
- δ is the secondary emission ratio
- Q is the charge required to drive an element of the storage mesh from the specified background condition to just discernible transmission.

The first factor, I_b/W_t, called line current density, is a function of writing-gun design. It is the same as for high writing speed in a normal cathode-ray tube but is subject to another limitation: in a normal c.r.t. line brightness continues to increase as the acceleration voltage increases; in a storage tube it increases with the secondary emission, which reaches a maximum at moderate beam velocities corresponding to an acceleration voltage between 1 kV and 3 kV. (For that reason post-acceleration can be applied only behind the storage mesh, and

post-deflection acceleration by means of a domed mesh is not practical.)

The second factor, $(\delta - 1)/Q$, is called storage sensitivity. For high writing speed Q must be small. $Q = \Delta V \cdot C$, where ΔV is the voltage change required to drive an element of the mesh into discernible transmission, and C is the capacitance of the mesh per unit area. Low drive voltage ΔV can be achieved with a fine mesh and very narrow flood-electron energy and angular distributions obtained by careful flood-gun and collimator design. Low capacitance can be obtained by using a secondary emitter of low dielectric constant applied as a porous layer; the thicker the layer, the lower the capacitance.

Because the vacuum in the tube is never perfect, long viewing time is incompatible with high writing speed. Positive ions generated by flood electrons gradually neutralise the negative bias of unwritten parts of the mesh so that the background lightens and contrast fades. Fading can be delayed by pulsing the flood-gun current, but for a given tube design and hardness of vacuum the viewing time ultimately depends on the amount of charge needed to distinguish a written from an unwritten part of the mesh. The greater the charge the longer the time; but also, the slower the writing speed. One can be traded off for the other in the design of the mesh, but their product remains constant. For a tube of the type shown in Fig.1 this appears to represent the state of the art.

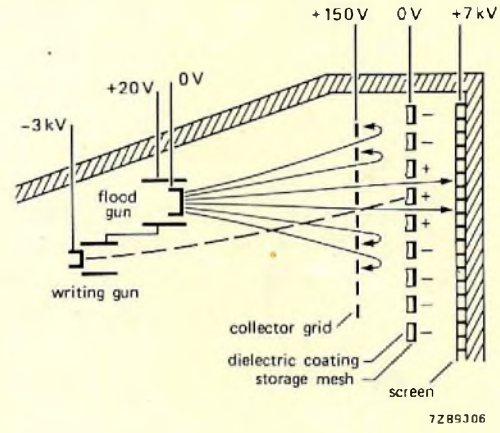

Fig.1 Storage tube principle. Where fast electrons from the writing gun strike the dielectric-coated storage mesh the mesh becomes positively charged by secondary emission. To display the stored charge pattern the flood gun emits a flood of slow electrons which are transmitted by the positively charged parts of the mesh and accelerated toward the screen; other flood electrons, repelled by the negative bias on uncharged parts of the mesh, are absorbed by the collector grid. As the electron transmittance of the storage mesh is a continuous function of positive charge, good halftone rendering is possible

TRANSFER-STORAGE PRINCIPLE

In the L14-140GH/95 the conflict between high writing speed and long viewing time is resolved by embodying the two functions in separate meshes: a small-capacitance mesh for fast writing and a large-capacitance one for long storage. Flood electrons transfer the image from the fast-writing mesh to the storage mesh and, as in a conventional storage tube, from the storage mesh to the screen.

Figure 2 illustrates the principle. Voltages given in the figure and the following description are for explanatory purposes only and are not exact. Exact values, together with practical timing schemes and adjustment procedures, are given in the tube data sheets.

The operating cycle starts with an erase sequence in which the storage mesh is first equalised at a high potential and then stabilised at flood-gun cathode potential. A 500 V pulse on the storage mesh triggers an intense flux of flood electrons which charges the whole mesh positive. At the end of the pulse the mesh is returned briefly to 0 V before the 10 V erase pulse is applied; at this voltage the secondary emission ratio is less than unity, so the storage surface of the mesh discharges to flood-gun cathode potential. At the end of the erase

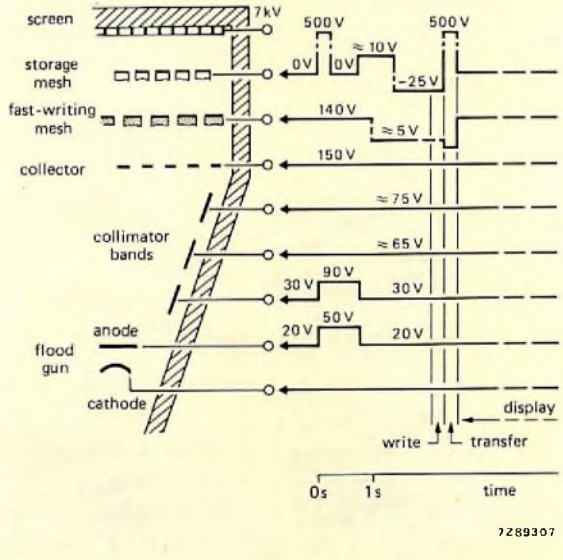

Fig.2 Transfer-storage principle: electrode voltages and timing for the erase-write-transfer-store sequence

pulse, when the storage mesh is returned to 0 V, capacitive coupling drives the surface of the mesh below flood-gun cathode potential and flood electrons are cut off.

During the erase sequence the fast-writing mesh, biased at 140 V, acts as collector for secondary electrons emitted from the storage mesh, and its own surface becomes positively charged by secondary emission. To remove this charge the bias is dropped from 140 V to 0 V. The surface then stabilises at a small negative potential due to the velocity distribution of the flood electrons, some of which continue to land until their energy is insufficient to overcome the gradually increasing potential barrier.

After the erase sequence the writing gun is unblanked and writes the signal to be displayed on the fast-writing mesh, where it is temporarily stored as a positive charge pattern. At the end of the unblanking pulse a 500 V pulse on the storage mesh transfers the pattern from the fast-writing to the storage mesh. During this pulse, flood electrons are accelerated through the positively charged parts of the fast-writing mesh and strike the storage mesh, duplicating the pattern there by exciting secondary emission.

For one-shot events, the cycle is stopped at this point and the image is kept on display. For periodic events, the transfer pulse is also the equalising pulse for the next erase sequence and the cycle starts anew.

During the erasing sequence the flood-gun anode voltage can be increased to increase the flood current density and improve flood homogeneity; collimator potentials can also be adapted. Depending on the erasing pulse amplitude, the storage mesh potential can be set for erasure to any required level of background illumination; for instance, to 'just black', or to 'blacker than black' for longer storage time.

ELECTRON-OPTICAL SYSTEM

Writing gun and scan magnifier

The writing gun of the L14-140GH/95 works with a single-stage acceleration voltage of 3 kV, which is sufficient to produce high secondary emission from the fast-writing mesh and to give high current density in the spot.

The vertical deflection plates are short, so their capacitance is low and time-of-flight effects are negligible A quadrupole scan magnifier situated between the vertical and the horizontal deflection plates expands the vertical scan by a factor of 1.8 but does not affect the horizontal scan. Maximum vertical deflection sensitivity is 4.8 V/div (5.3 V/cm).

Because of the scan magnification the beam has to be highly astigmatic to produce a round spot. Two additional quadrupole lenses that take the place of the normal focusing lens provide the required astigmatism (Fig.3). A quadrupole lens has two perpendicular planes of symmetry, one of which is convergent and the other divergent. In the vertical plane, the order of the scan magnification and the two additional quadrupole lenses is: divergent, convergent, divergent. The second lens is therefore responsible for focusing in the vertical direction. It brings the beam to a first focus between the gun and the writing mesh; the scan magnification lens shifts the focus onto the mesh.

In the horizontal plane the lenses are convergent, divergent, convergent, giving a beam crossover between the second lens and the scan magnifier. The vertical line to which this crossover corresponds is focused by the scan magnifier to a spot on the mesh.

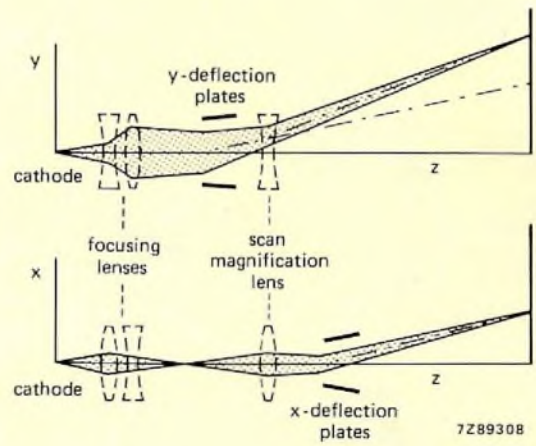

Fig.3 Action of the focusing and scan-magnification quadrupole lenses: top, vertical deflection; bottom, horizontal deflection

The quadrupole lenses are built up from identical flat plates with non-circular apertures rotated 90° with respect to each other. Lens aberrations of the quadrupoles are corrected by the spacing and biasing of the plates. For a fixed scan magnification factor of 1.8, only the x and y focus voltages, and not the quadrupole bias voltages, need be adjusted. A small horizontal correction is also required.

Flood guns and collimator

To ensure the narrow energy spread required for obtaining a steep storage-mesh drive characteristic, the two flood guns are designed to operate as diodes (grid 1 connected to cathode), giving 'laminar flow' with no crossover. The only adjustment required is balancing the cathode potentials to equalise the background illumination.

The flood-gun and writing-gun cathodes are of the quick-heating type (10% emission in 5 seconds, 90% in 10 seconds) proved in many millions of television picture tubes. The flood-gun filaments are connected in series and fed via the base to obviate contact difficulties.

The collimation system consists of the flood-gun anodes at 20 V, three collimator bands on the inside of the cone at 30 V, 65 V and 75 V, and the collector mesh with integral field-shaping electrode at 150 V. Computer-aided design optimised the geometry for near-normal landing and constant current density over the whole storage mesh.

CHARGE-TRANSFER STORAGE SYSTEM

Storable writing speed over the central 80% of the screen is 1 div/ns. The key to this performance is the three-mesh array consisting of collector, fast-writing mesh, and storage mesh.

The collector is of wire mesh with more than 80% transmission to minimise absorption of flood-gun and writing-beam current.

The fast-writing mesh is electroplated nickel with a thick, porous coating (about 30% bulk density) giving a dielectric constant close to unity.

The storage mesh, also of electroplated nickel, has a thin, dense, high-capacitance coating which gives a storage time of at least a minute when the screen has been erased to 'just black' and full flood-gun current is applied. Persistence can be varied by varying the duty factor of short erasing pulses. This mesh can also be written on directly, with a storable writing speed from 0.25 div/μs against 'just black' to 5 div/μs against a light background.

Stereo/dual sound TV transmission soon to be introduced necessitates reorganising receiver sound channels. This article describes new integrated circuits for high-fidelity TV sound systems and gives details of a soon to be available IC for decoding the stereo/dual sound transmissions.

High-fidelity stereo/dual sound for TV

U. BUHSE and H. SCHWARZ

Modern television receivers are a far cry from the cumbersome, power-consuming sets of a few years ago. Almost complete integration of the circuits, the use of switched-mode power supplies and the development of self-aligning picture tubes with short necks and simplified deflection circuitry have reduced manufacturing costs, improved reliability and lowered power consumption. The development of LSI circuits has allowed innovations such as remote control, microcomputer-controlled tuning, on-screen tuning information and data display systems such as teletext and viewdata. The next step is improvement of the sound circuits to allow hi-fi reproduction together with facilities for receiving stereo and dual channel (e.g. bilingual) sound.

In West Germany, the inauguration of stereo/dual-channel sound transmissions is planned for this year, and other countries will undoubtedly follow suit within a very short time. It is envisaged that many of the colour sets manufactured in West Germany this year will be equipped to receive the new transmissions. Within a few years, dual channel/stereo sound facilities will be commonplace in full-performance colour sets made in Europe and will also be available in some black and white sets.

PHILOSOPHY FOR HIGH-FIDELITY TELEVISION SOUND

The conventional intercarrier sound system shown in Fig.1 provides a compromise between cost and performance and is used in nearly all existing television sets. In this system, the vision and sound i.f. signals are amplified together and both passed through the same quasi-synchronous demodulator to obtain a video signal, and a frequency-modulated sound signal with an intercarrier frequency equal to the difference between the frequencies of the sound and vision i.f. carriers (5.5 MHz in most of Continental Europe). The frequency-modulated sound signal is then separated from the video information and is amplified and amplitude-limited before being passed through an f.m. demodulator. In this system, the shape of the transfer characteristic of the bandpass filter following the tuner must be a compromise between the requirements of the sound and vision channels. Furthermore, non-linearities in the common amplification path lead to spurious amplitude modulation of the sound signal which causes the well-known intercarrier buzz in the sound channel.

At first glance, an obvious solution appears to be to split the vision and sound channels immediately after the tuner as shown in Fig.2. The vision and sound channels are then entirely separated and each can be optimised for performing its own function. Theoretically, this system would be ideal for hi-fi sound reproduction but, in practice, there are several drawbacks. For example, the system is prone to local-oscillator instability.

A practical solution lies in the quasi-split sound system shown in Fig.3. Here, the vision and sound signals are again split immediately after the tuner so that the filter characteristics can be optimised for each channel. Furthermore, the reference frequency for both the sound and vision demodulators is 38.9 MHz (the vision i.f.). As shown in Fig.3, a deep sound trap in the vision channel minimises sound interference in the picture and allows the bandwidth of the vision channel to be extended. The filter at the beginning of the sound channel has a response with two peaks and a trough between them. One peak is centred on the vision carrier frequency, and the other

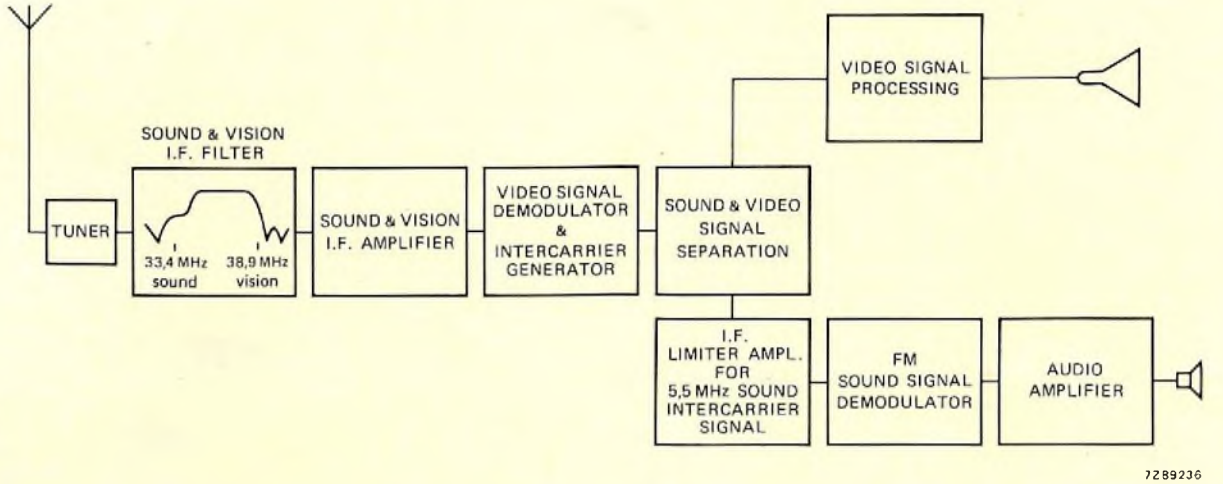

Fig.1 Conventional intercarrier sound system

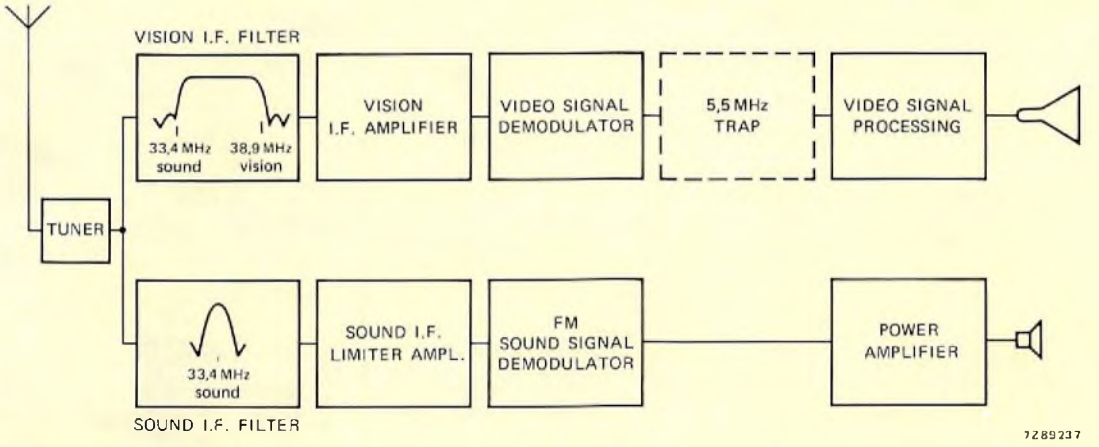

Fig.2 Split sound system

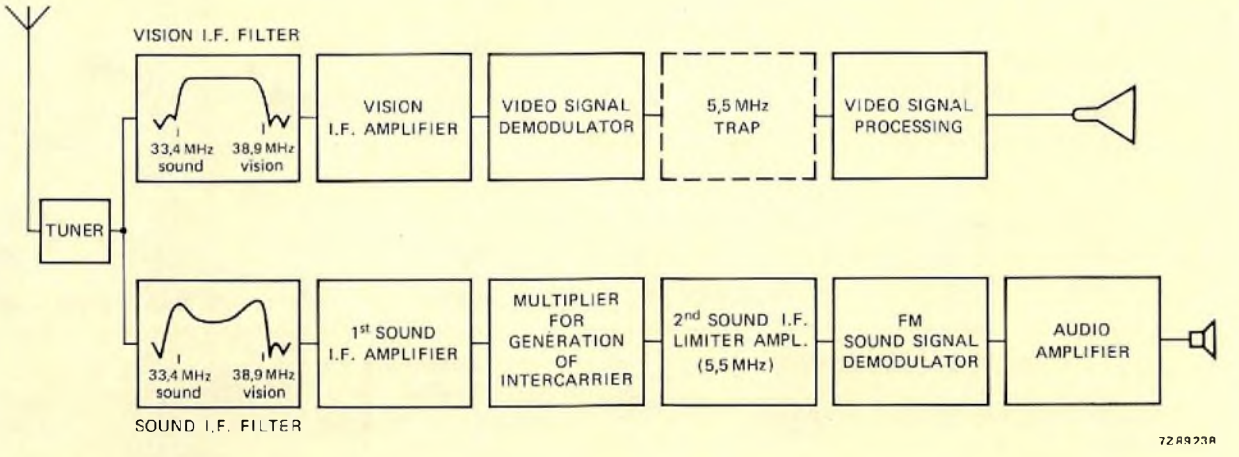

Fig.3 Quasi-split sound system

is centred on the sound carrier frequency. The filter therefore attenuates i.f. frequencies which might cause second harmonics yielding 5.5 MHz during demodulation. Since there is no attenuation of the sound i.f. carrier, the signal-to-noise ratio of the quasi-split sound system is better than that of a conventional system. The group delay characteristic of the i.f. filter should be identical for the sound and vision passband. Since no Nyquist slope is necessary, the amplitude and phase characteristics of the filter can be symmetrical around the vision carrier frequency. This is essential for phase-linear regeneration of the reference carrier for the sound demodulator because it allows the reference circuit to be symmetrically aligned (no compensation). A linear quadrature demodulator should be used to demodulate the f.m. sound, because this type of circuit generates low harmonic distortion and few intermodulation products (residual sidebands caused by the video modulation).

The quasi-split sound system with quadrature f.m. demodulation is also insensitive to the varying ratio of vision to sound signal amplitude which causes sound-chroma beats and poor quality sound in some other systems. We have therefore selected the quasi-split system for our hi-fi television sound channel and have developed a number of new integrated circuits for mono and dual-channel/stereo sound channels using the system.

MONO HI-FI SOUND

A mono quasi-split hi-fi sound channel

Figure 4 shows the arrangement of our integrated circuits for a mono hi-fi quasi-split sound channel. It uses the new 1st i.f. amplifier and intercarrier demodulator circuit TDA2545 which is shown in block form in Fig.5 and is further described in Ref.1. The TDA2791 shown in Fig.6 provides d.c. control of volume with physiological correction, and d.c. control of treble and bass. The TDA1512 audio power amplifier shown in Fig.7 provides a power output of 13 W to high-fidelity standard.

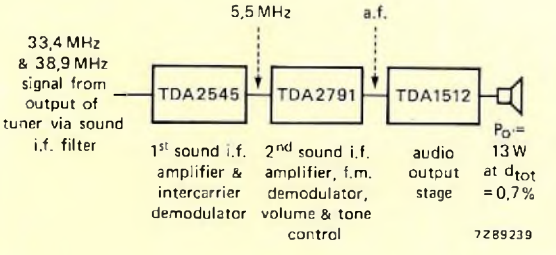

Fig.4 Mono hi-fi sound system

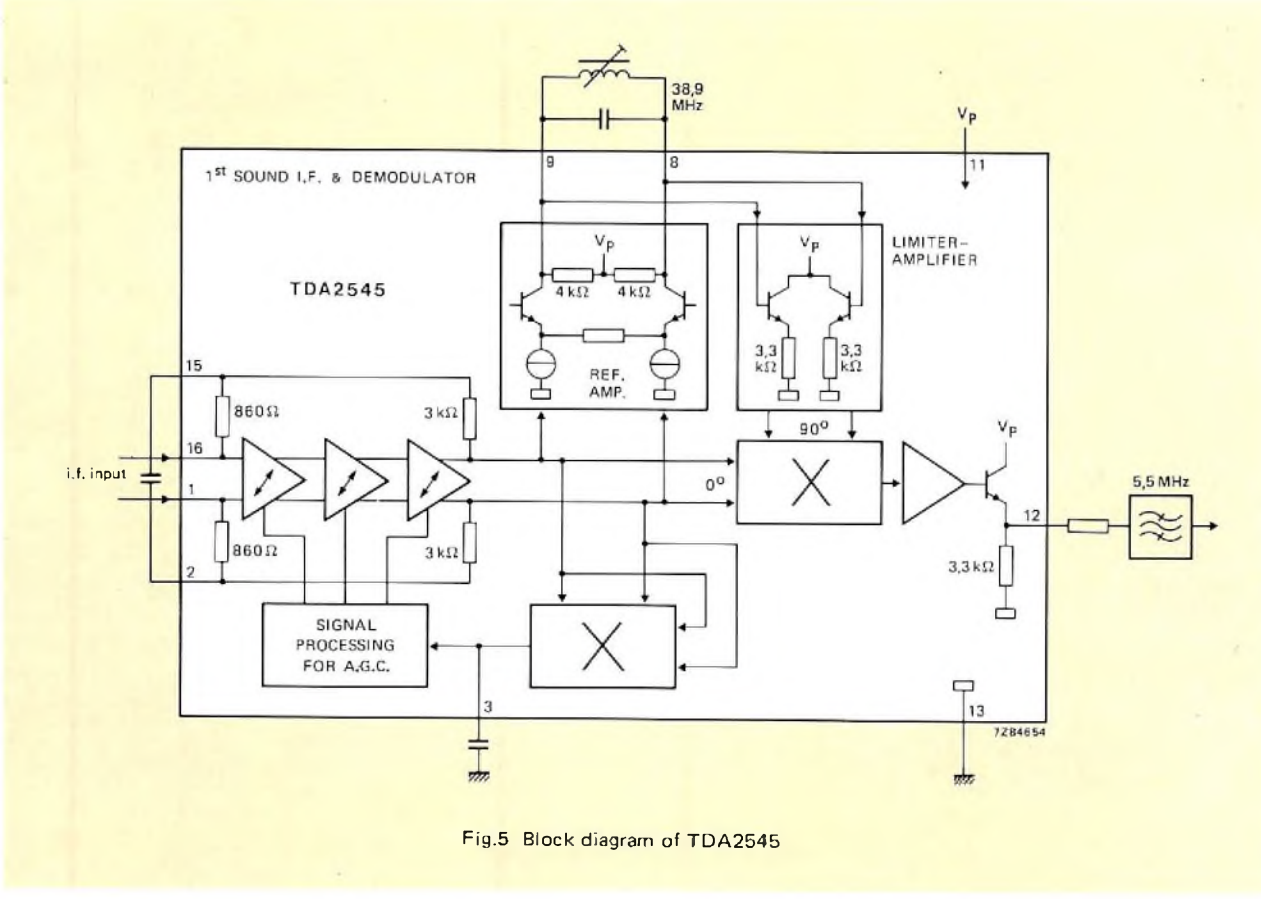

Fig.5 Block diagram of TDA2545

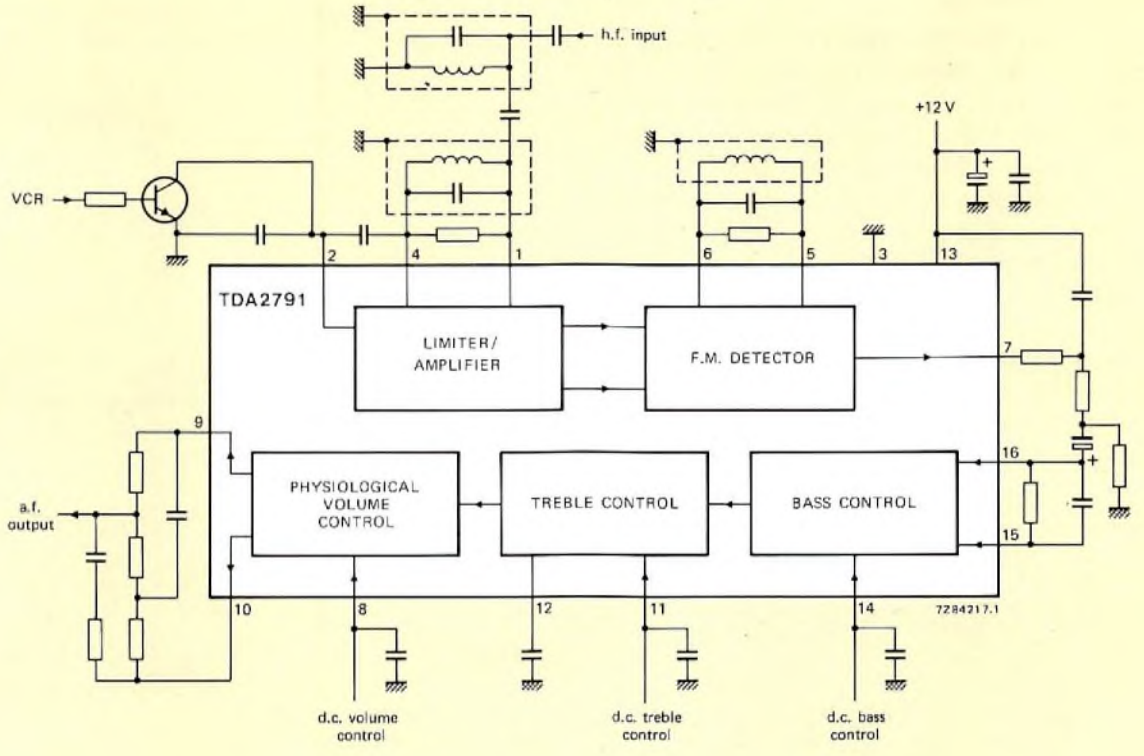

Fig.6 Block diagram of TDA2791

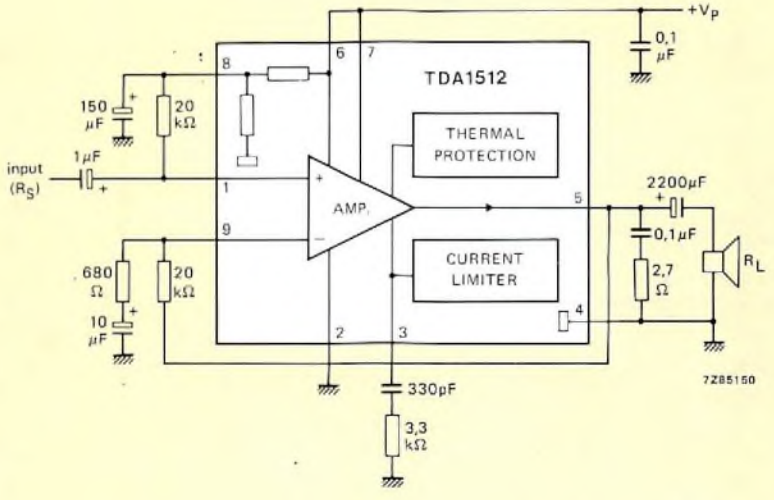

Fig.7 Block diagram of TDA1512

STEREO/DUAL CHANNEL SOUND

Transmission standards

The West German stereo/dual sound television standards are given in Table 1. Transmissions will consist of the normal vision carrier, a first sound carrier (frequency difference 5.5 MHz) and a second sound carrier (frequency difference 5.5 MHz + 242.1875 kHz). The i.f. spectrum of the three carriers is shown in Fig.8. To ensure that standard sets can still receive mono sound from the new stereo transmissions, the normal sound carrier (SC1) is frequency modulated with L + R information. The additional sound carrier (SC2) is frequency modulated with 2R information. The maximum frequency deviation of the modulation is ±50 kHz (CCIR). The maximum frequency deviation transmitted by the West German broadcasts will however be limited to ±30 kHz. To identify the type of signal being transmitted (stereo, dual sound or mono), SC2 is also frequency modulated (±2.5 kHz deviation) with an identification signal. This identification signal consists of a

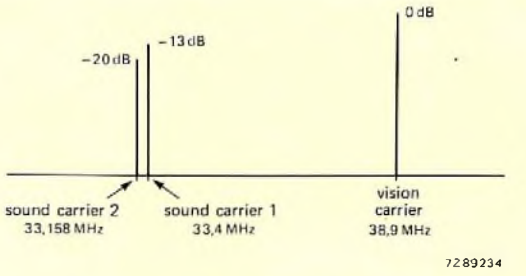

Fig.8 Spectrum of the i.f. carriers of the West German stereo/dual sound transmission

TABLE 1
Transmission standard for stereo/dual sound system

Sound carriers (note 1)		
	channel 1	*channel 2*
Sound carrier frequencies	f_V + 5.5 MHz	f_V + 5.7421875 MHz
Sound carrier stability	±500 Hz	±500 Hz
Vision/sound power difference	13 dB	20 dB
Sound bandwidth	40 Hz to 15 kHz	40 Hz to 15 kHz
Required frequency deviation due to 500 Hz modulation for maximum volume	±30 kHz	±30 kHz
Pre-emphasis	50 μs	50 μs
Frequency deviation due to modulation with ident. signal (pilot carrier + modulation)	–	±2.5 kHz (±500 Hz)
Identification of transmission mode (note 2)		
		channel 2
Pilot carrier frequency		54.6875 kHz (±5 Hz)
Type of modulation		a.m.
Modulation depth		50%
Modulation frequency		
mono		unmodulated
stereo		$f_{line}/133 \approx 117.5$ Hz
dual sound		$f_{line}/57 \approx 274.1$ Hz
Sound signal components (note 3)		
	channel 1	*channel 2*
Mono transmission	mono	mono
Stereo transmission	L + R	2R
Dual sound transmission	channel A (mono)	channel B (mono)

Notes:
1. To minimise interference, the two sound carriers are separated by 242.1875 kHz which is an uneven multiple of half the horizontal scan frequency.
2. The pilot carrier frequency is within 5 Hz of 3.5 times the horizontal scan frequency with which it is normally synchronised. If, for any reason, the line sync. pulses cease (interruption of vision signal transmission), the accuracy of the pilot carrier frequency is ±50 Hz.
3. The main channel (channel 1) always contains mono sound information compatible with a standard tv sound transmission.

54.6875 kHz pilot carrier which is unmodulated for mono transmissions or 50% amplitude modulated with 117.5 Hz (horizontal scan frequency/133) for stereo or 274.1 Hz (horizontal scan frequency/57) for dual sound transmissions. After intercarrier mixing, the frequency spectrum of the two intercarriers is as shown in Fig.9.

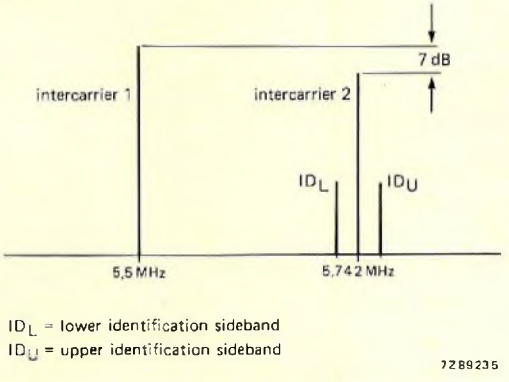

Fig.9 Intercarrier frequency spectrum of the West German stereo/dual sound transmission

After bandpass filtering and f.m. demodulation, the audio signals extracted from IC1 (5.5 MHz) and from IC2 (5.742 MHz) are as given in Table 1. The stereo information can therefore be simply dematrixed by amplifying the demodulated IC1 signal (L + R) by a factor of 2 and subtracting the demodulated IC2 signal (2R) from it, i.e. 2(L + R) − 2R = 2L. After the identification signal has been demodulated, it is converted into a 2-bit binary code which is used to activate logic circuitry that drives status indicators and switches which route the required dematrixed audio information to the sound output circuits. Another input to the logic circuitry is a mode selection signal derived from a switch operated by the viewer. This allows the viewer to select stereo or mono during stereo transmissions and the required sound channel during dual sound transmissions.

Integrated circuit combinations

Our range of integrated circuits for standard and hi-fi stereo/dual channel quasi-split tv sound systems, together with the circuit functions and preferred combinations of integrated circuits for various applications, are presented in Table 2.

TABLE 2
Integrated circuits for quasi-split tv sound systems

function	integrated circuit type number									
	TDA 2545	TDA 2546	TBA 120S	TDA 2791	TDA 3800	V5630B	TDA 1029*	TCA 730A/740A or V5780**	TDA 1013	TDA 1512
1st sound i.f. intercarrier demod.										
2nd sound i.f./f.m. demod.										
ident. decoder/de-matrixing										
source selector										
volume control								2X		
tone control								2X		
audio output										
type of sound circuit	required integrated circuits									
mono hi-fi	X			X						X
economy dual-channel system with standard quality reproduction			2X			X			X	
dual-channel/stereo system with hi-fi reproduction and the minimum no. of ICs		X			X		X	X		2X
flexible dual-channel/stereo system with hi-fi reproduction. Very suitable for modular construction	X		2X			X	X	X		2X

* optional; ** contains ganged circuits for stereo operation.

The most economic dual sound system permits reception of mono sound or one viewer-selected channel of a dual sound transmission. This is a standard intercarrier system in which the second i.f. amplification and intercarrier demodulation are performed by a TBA120S in each channel.

For dematrixing, stereo/dual sound decoding, identification decoding and switching of the audio signals, we are developing the V5630B integrated circuit shown in Fig.10. A 2.5 W (d_{tot} = 0.5%) audio output and d.c. controlled volume are provided by the TDA1013 (Fig.11).

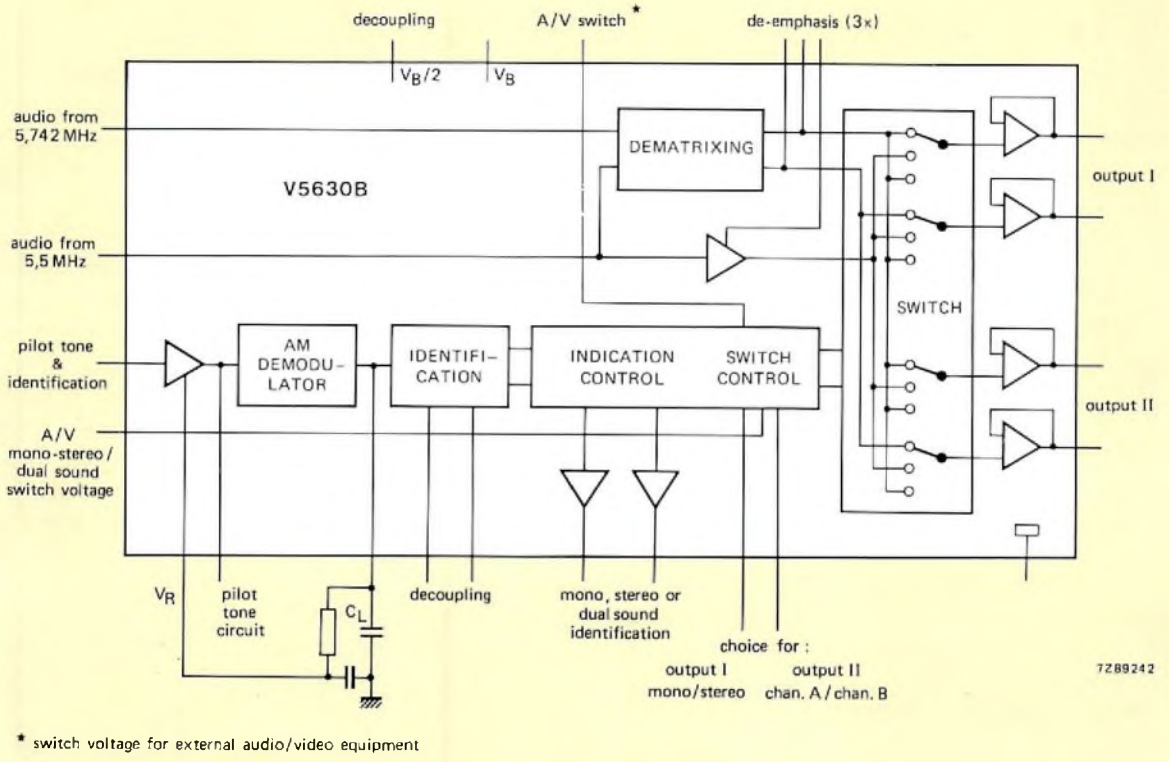

Fig.10 Block diagram of the V5630B

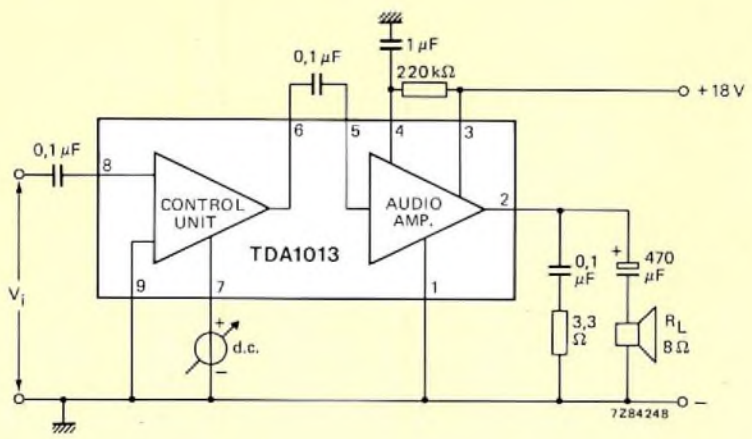

Fig.11 Block diagram of the TDA1013

For a full-performance hi-fi quasi-split stereo/dual sound system with the minimum number of integrated circuits as shown in Fig.12, we have developed the TDA2546 shown in block form in Fig.13. In this circuit, the first i.f. amplifier and intercarrier demodulator functions are combined with the second i.f. amplifier and f.m. demodulator for one of the stereo/dual sound channels. For this system we are also developing a stereo/dual sound decoder circuit similar to the V5630B but also including the second i.f. amplifier and f.m. demodulator for the other sound channel. This circuit, the TDA3800, is shown in Fig.14 and is optimally matched with the TDA2546. In this system, d.c. control of volume, treble and bass for both channels is performed by our well-known integrated circuits TCA730A and TCA740A (Ref.2). We are also developing a single integrated circuit, the V5780, to perform these functions. Audio switching for external equipment (e.g. tape recorder) can be provided by a stereo signal-sources switch TDA1029 (Ref.2). Two TDA1512 circuits (Fig.7) provide audio power outputs of 13 W per channel ($d_{tot} = 0.7\%$).

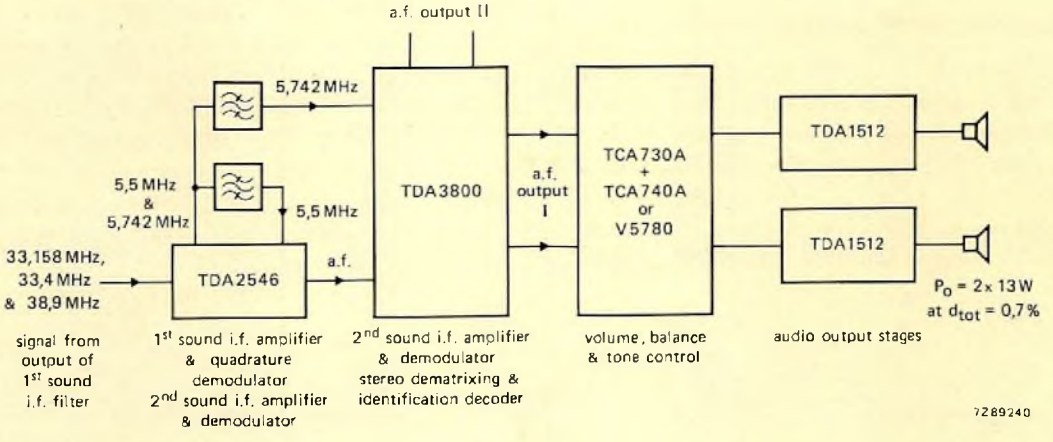

Fig.12 A stereo/dual sound system with hi-fi reproduction and the minimum number of integrated circuits

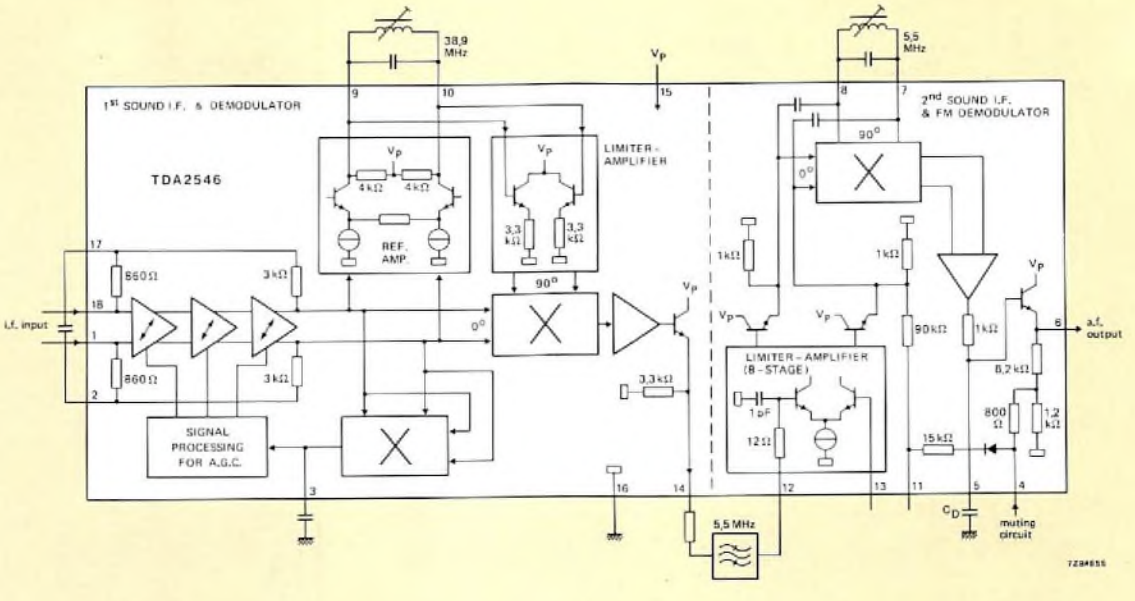

Fig.13 Block diagram of the TDA2546

The final combination of circuits shown in Fig.15 forms a full-performance hi-fi quasi-split stereo/dual sound system which is extremely flexible and lends itself to modular construction because the audio section can be completely separated from the i.f. section. In this system, the first i.f. amplification and intercarrier demodulation is performed by a TDA2545 (Fig.5) and the second i.f. amplification and f.m. demodulation for the two channels is performed by two TBA120S circuits (Ref.2). The dematrixing, stereo/dual sound decoding, identification decoding and switching of the audio signals is performed by the V5630B (Fig.11).

Decoder using currently available components

To enable manufacturers to construct hi-fi stereo/dual sound systems before the new integrated circuits TDA3800, V5630B and V5780 are available, we have designed a circuit which performs the same functions as the V5630B but uses integrated circuits TDA2795 and TDA1029 together with logic circuits from our current range. The audio control functions that will be available in the V5780 (volume, treble and bass) can be performed by our d.c.-controlled audio circuits TCA730A and TCA740A which are described, together with digitally-controlled audio source selector TDA1029 and audio output circuit TDA1512, in Ref.2. A block diagram of the system is given in Fig.16 and a complete circuit diagram is shown in Fig.17. Dematrixing of the left channel signal from the L + R and 2R signals of a stereo transmission is performed by operational amplifier NE5534 connected as a difference amplifier (Ref.3). After 50 μs de-emphasis, the L + R, 2R and 2L stereo signals are connected to the digitally-controlled audio source selectors TDA1029. The identification decoder integrated circuit TDA2795 is used in conjunction with standard logic elements for decoding the identification signals and providing binary signals for driving reception mode indicators and operating the switches in the TDA1029 circuits. These switches route the audio signals to one pair of outputs for connection to the stereo output stages, and to a second pair of outputs for connection to headphones or external equipment (e.g. hi-fi amplifier or tape recorder).

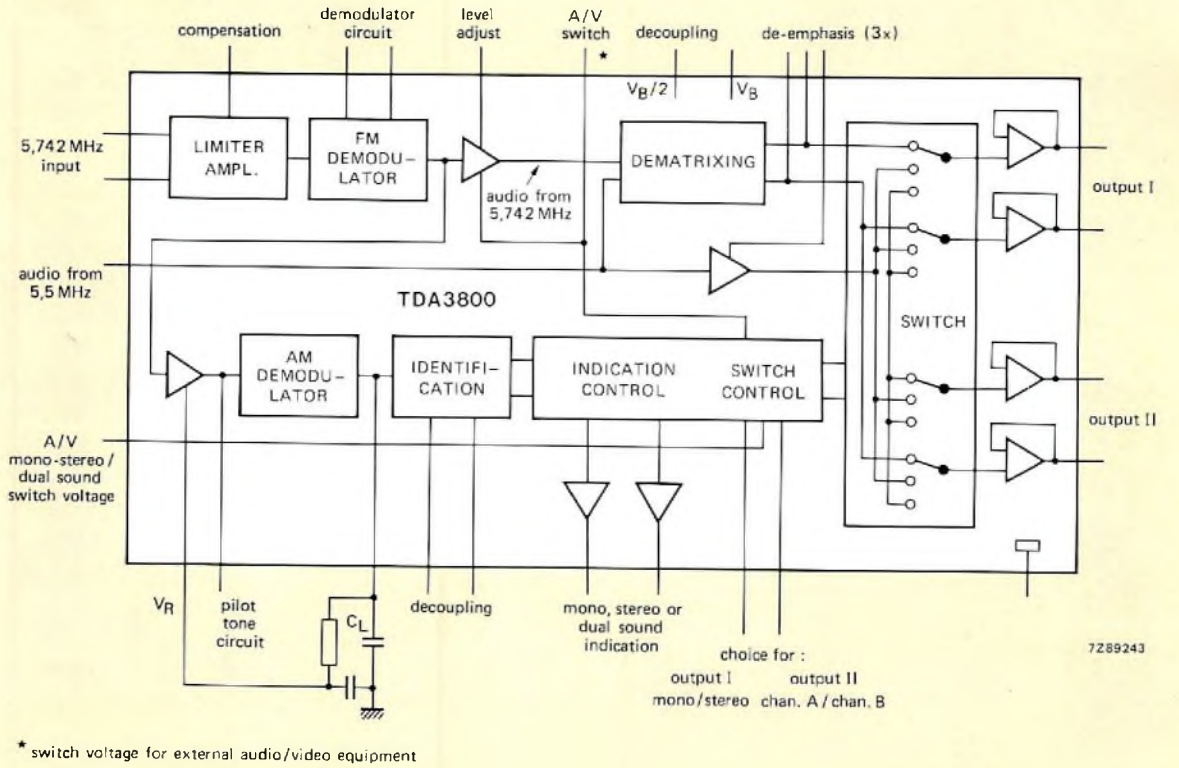

Fig.14 Block diagram of the TDA3800

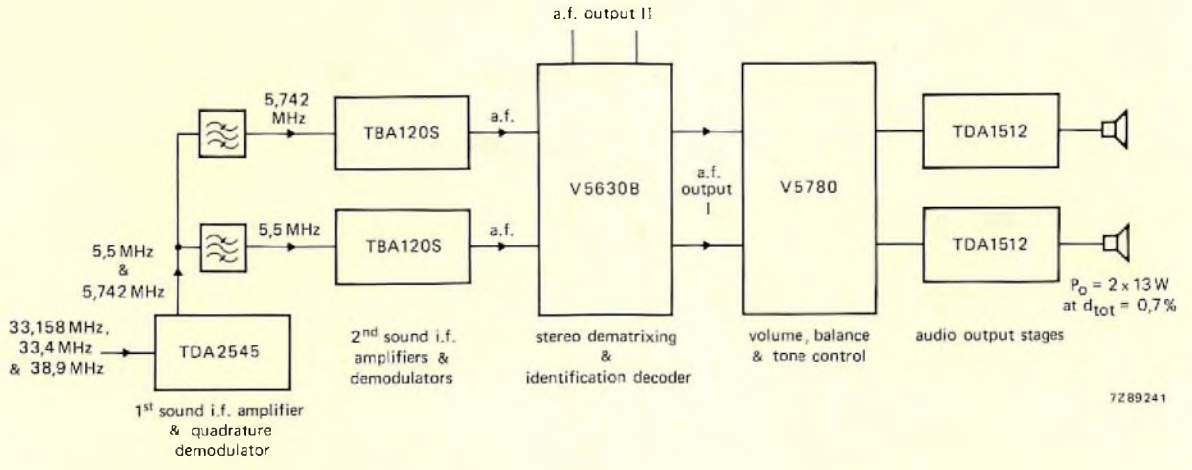

Fig.15 A stereo/dual sound system with hi-fi reproduction. This is a very flexible system in which the audio-frequency section can be completely separated from the high-frequency section

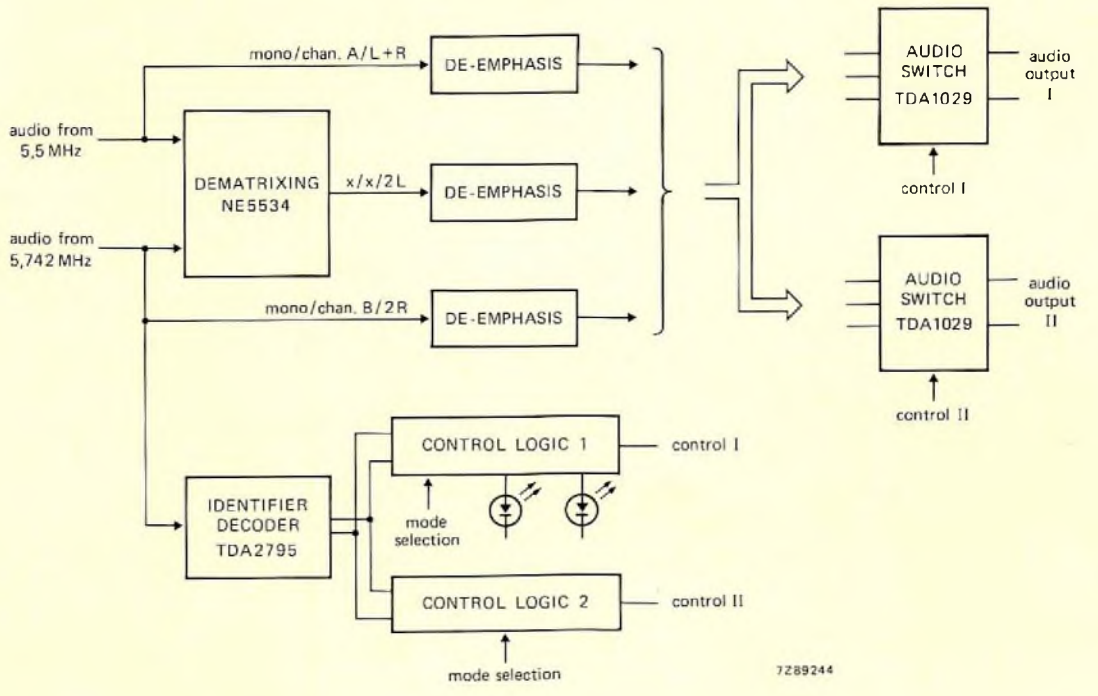

Fig.16 Block diagram of the simulated V5630B circuit

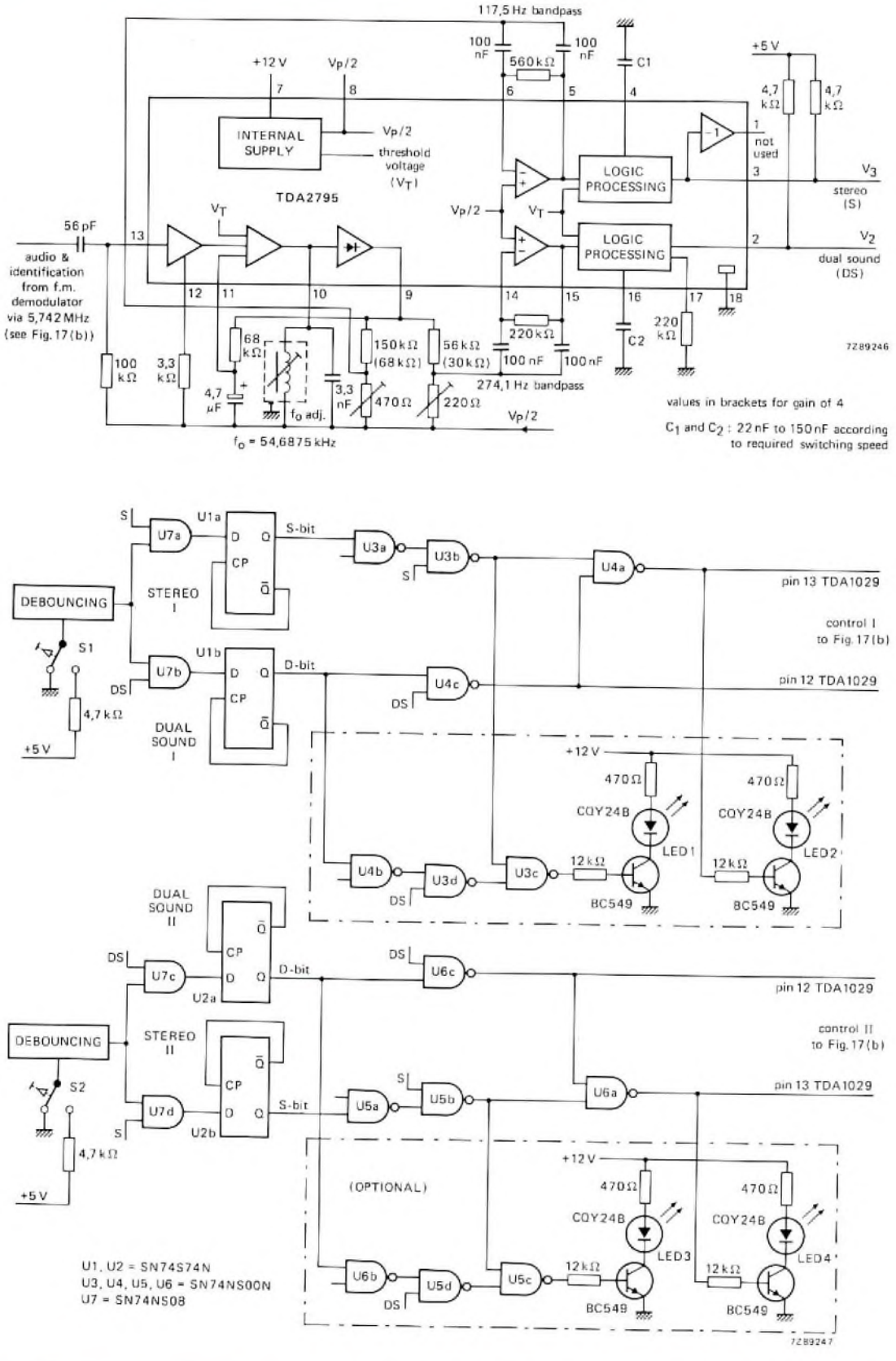

Fig.17(a) Identification signal decoding and control logic section of the circuit using currently available components

Dematrixing and de-emphasis. The L + R and 2R + identification information is derived from the outputs of two second i.f. amplifier/f.m. demodulator circuits (e.g. 2 × TBA120S) and applied to the input of the circuit in Fig.17(b). After 50 μs de-emphasis and buffering, these signals are applied to inputs of the two digitally-controlled audio switch pairs in the TDA1029 integrated circuits. They are also applied to the inputs of operational amplifier NE5534 connected as a difference amplifier with a gain of 2 at the non-inverting input, and unity gain at the inverting input. The dematrixed output from the NE5534 is therefore $2(L+R)-2R=2L$. This left-channel signal, after 50 μs de-emphasis and buffering, is applied to the remaining inputs of the digitally-controlled audio source selectors TDA1029. The de-emphasis is applied *after* dematrixing to avoid crosstalk due to amplitude and phase errors which would occur if it were applied at the inputs to the difference amplifier.

Identification decoder TDA2795. The identification signal decoder TDA2795 shown in Fig.17(a) performs the following functions:

- Gain-controlled amplification of the 54.6875 kHz identification carrier which is amplitude modulated with 117.5 Hz for stereo or 274.1 Hz for dual sound.
- Envelope detection of the 117.5 Hz and 274.1 Hz identification signals.
- Active bandpass filtration of the two identification signals.
- Integral evaluation and logic processing of the outputs from the bandpass filters.
- LED stereo lamp drive (not used in this application).

The amplitude-modulated 54.6875 kHz identification carrier is separated from the 2R audio information by a 28 kHz high-pass RC filter, comprising a 56 pF capacitor

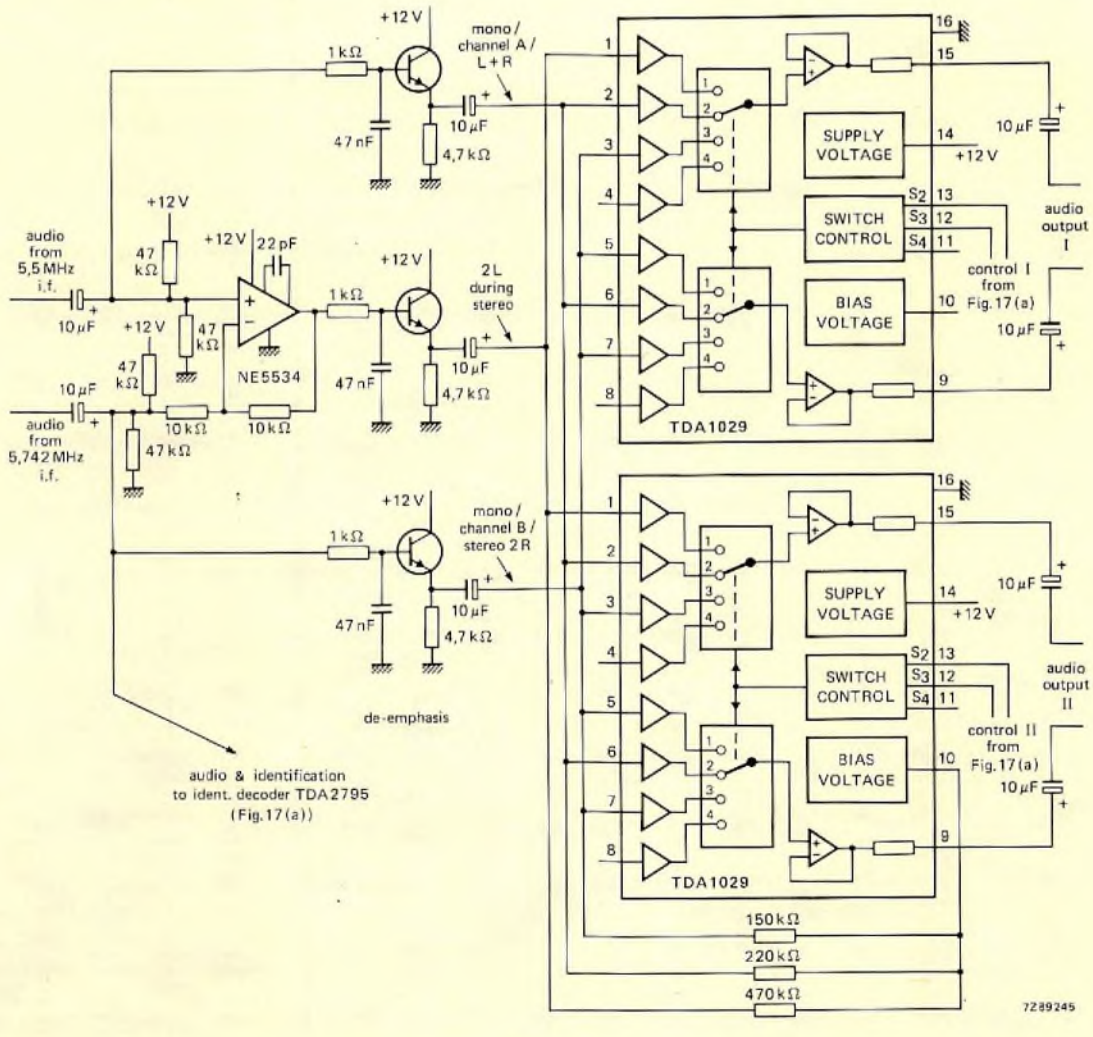

Fig.17(b) Dematrixing and audio signal switching section of the circuit using currently available components

and a 100 kΩ resistor, and applied to pin 13. After amplification, the identification signal modulation (if any) is extracted from the carrier by an envelope detector, the output from which is connected to pin 9. The identification signal is then applied to the inputs of two active bandpass filters at pins 6 and 14. The filter at pin 6 has a centre frequency of 117.5 Hz and the filter at pin 14 has a centre frequency of 274.1 Hz. The transfer characteristics of the filters are shown in Fig.18. After integral evaluation and logic processing, the logic states at the TTL-compatible open-collector outputs at pins 2 and 3 are as follows:

type of transmission	*pin 2*	*pin 3*
Mono (no identification signal, no second sound carrier or a weak signal):	0	0
Dual-channel (274.1 Hz identification):	1	0
Stereo (117.5 Hz identification):	0	1

Control logic for audio switches and status indicators. The stereo/dual channel sound system must allow the viewer to select mono or stereo reception during a stereo transmission, amd to select channel A or channel B during a dual-channel transmission. Furthermore, if there is too much noise on the received signal, the logic circuits should override the viewers choice of listening mode and automatically select mono during a stereo transmission, or channel A during a dual-sound transmission. Once the viewer has selected the required listening mode, the logic circuits must store the choice in case the transmitted identification signal is changed or interrupted during a programme or the viewer briefly tunes to another station. In a system incorporating a

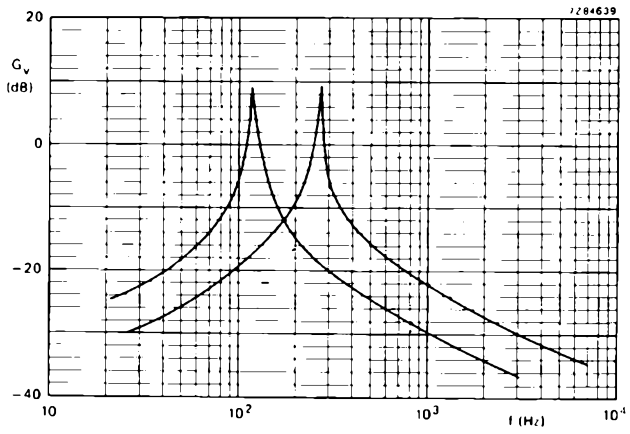

Fig.18 Transfer characteristics for the active bandpass filters in the TDA2795 shown in Fig.17(a)

second pair of outputs for headphone listening (simultaneous reception of both languages of a bilingual dual-channel transmission) or tape recording, the logic circuit must allow the listening mode for the second pair of outputs to be selected independently of that for the main outputs. The logic circuit must therefore consist of two functionally identical parts which allow independent operation and which have latched inputs. Such a circuit is incorporated in the TDA3800 and the V5630B which are both under development. The circuit which simulates the V5630B is given in Fig.17. The following description applies equally to the two identical parts of the logic circuit one of which is shown opposite.

The viewer's choice of listening mode is made with a toggle switch or pushbutton switch spring-biased to the grounded position. The choice is then stored in two D-type edge-triggered flip-flops. A debouncing circuit is in-

TABLE 3
Operating states for the circuits in Fig.14

trans-mission mode	TDA2795 output V_2	TDA2795 output V_3	selected reception mode	S-bit	D-bit	indication LED 1/3	indication LED 2/4	TDA1029 control* V_{12}	TDA1029 control* V_{13}	TDA1029 switch position	TDA1029 output pin 15	TDA1029 output pin 9	reproduced sound
mono	0	0	x	x	x	off	off	1	0	2	mono	mono	mono
stereo	0	1	stereo	0	x	on	on	1	1	1	2L	2R	stereo
stereo	0	1	mono	1	x	off	off	1	0	2	L + R	L + R	mono from stereo
weak stereo	0	0	x	x	x	off	off	1	0	2	L + R	L + R	mono from stereo
dual channel	1	0	channel A	x	0	on	off	1	0	2	channel A	channel A	dual sound channel A
dual channel	1	0	channel B	x	1	off	on	0	x	3	channel B	channel B	dual sound
weak dual channel	0	0	x	x	x	off	off	1	0	2	channel A	channel A	dual sound channel A

x = immaterial or indeterminate.

* V_{11} = 1 or disconnected.

corporated to eliminate the effects of switch contact bounce. The logic circuit also receives two inputs from the TDA2795 (S and DS) to indicate the type of transmission being received. The stereo bit (S-bit) at the output of the stereo flip-flop can only be altered during reception of a stereo programme (S = 1). The dual-channel sound bit (D-bit) at the output of the dual-channel sound flip-flop can only be altered during the reception of a programme with dual-channel sound (DS = 1). The use of a very simple logic array in the simulated circuit results in the states of the S-bit and the D-bit being indeterminate when the set is first switched on. If this is considered to be undesirable, more logic gates must be used to ensure that, at switch on, the circuit automatically selects stereo during a stereo transmission or channel A during a dual-channel transmission.

The logic section of the circuit controls the two switches in the audio source selector TDA1029 (Fig.17(b)) and also drives two LED status indicators. The operating states of the circuit for the various modes of operation are given in Table 3. Although two LED drives are provided by each of the two sections of the circuit, the V5630B which is under development only has sufficient pins to provide drives for two LED indicators for section I.

Performance. The circuit contributes negligible distortion and has hardly any influence on the signal-to-noise ratio of the hi-fi quasi-split sound system. The channel separation during stereo or dual-channel reception is greater than 60 dB over the audio frequency range 50 Hz to 12 kHz.

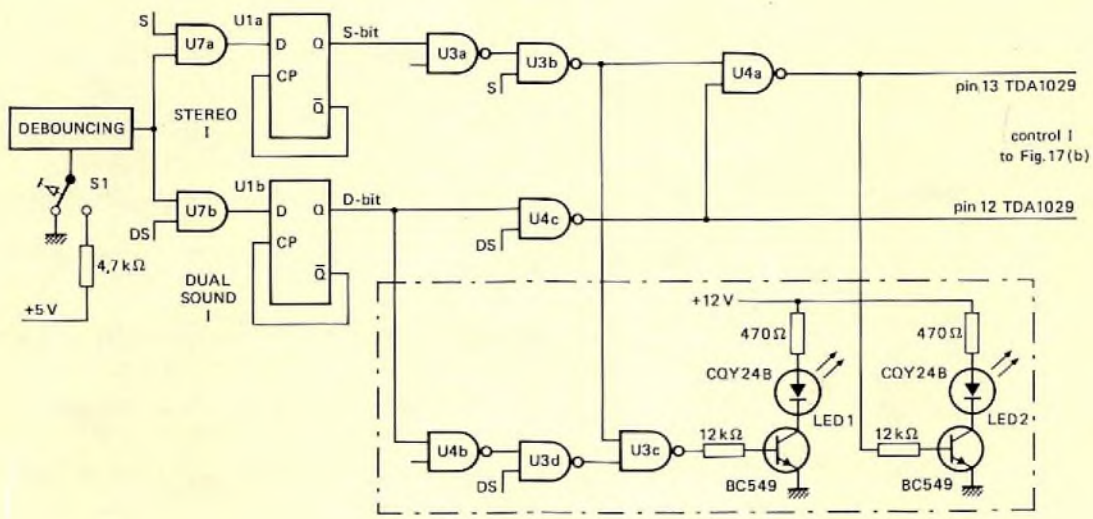

One half of the logic circuit from Fig.17(a) is repeated here to allow easy reference to the associated text

REFERENCES

1. H. ACHTERBERG, U. BUHSE und H. SCHWARZ; (Aufbereitung des Fernsehtonsignals mit den Integrierten Schaltungen TDA2545 und TDA2546 nach dem Quasi-Paralleltonverfahren'. Valvo Entwicklungsmitteilungen 79, Nov. 1980.
2. H. ACHTERBERG, W. G. GRAFFENBERGER und E. A. KILIAN; 'Stereo/Zweiton-NF-Verstarkerschaltung fur Fernsehgerate'. Valvo Technische Informationen fur die Industrie 800610, June 1980.
3. M. AIGNER und R. GOROL; 'Eine neue Stereomatrizierung fur den Fernsehton'. Rundfunktechnische Mitteilungen, Jahrg. 23, 1979, Heft 1.

ACKNOWLEDGEMENT

The authors wish to acknowledge the contribution made by W. Weltersbach during the early stages of the project. He was also responsible for the development of the quasi-split sound integrated circuits TDA2545 and TDA2546.

The sensitivity of a television camera increases with its signal-to-noise ratio; one way to increase that ratio is to reduce the output capacitance of the camera tubes. In the new range of low output-capacitance Plumbicon tubes this is done by reducing the size of the transparent conductive film in the target. The new tubes give about 3 dB improvement in signal-to-noise ratio.

Low output-capacitance Plumbicon® tubes

A. A. J. FRANKEN

The ever increasing demands of the TV industry have led in recent years to further development of the Plumbicon tube. This resulted in the introduction of the diode gun which enhanced resolution and, moreover, improved highlight handling by allowing the use of dynamic beam control (Ref. 1, 2 and 3). The new Plumbicon tubes found favour particularly in the fields of ENG and EFP, in which operating conditions are often less than ideal.

An important aspect of tv camera performance is signal-to-noise (S/N) ratio; the higher the S/N ratio the better the operational sensitivity of the camera. So increase of this ratio is obviously the next stage in upgrading camera performance.

$$S/N \approx 10 \log \frac{I_S^2}{4kTB\left(\frac{1}{R_t} + \frac{4\pi^2 B^2}{3}\left(\frac{C_O^2}{g_m}\right)\right)} \quad (dB)$$

In this expression, which relates to an uncoded video signal, the signal current I_S and bandwidth B, as well as the absolute temperature T, feedback resistance R_t and transconductance g_m of the preamplifier input FET are all subject to constraints that limit freedom to design for maximum S/N ratio.

With the output capacitance C_O, however, we are in a more fortunate position; by reducing it we can obtain an increase in S/N ratio. Since C_O includes contributions from the FET input capacitance C_f and the capacitance C_y of the tube in the yoke, it can be reduced either by choosing a lower capacitance FET, or by reducing C_y. A lower capacitance FET, however, will also have a lower transconductance g_m (since, for a given FET technology, g_m/C_f is constant), and this will offset to a great extent any advantage gained from using the lower C_f. So, by far the better solution is to reduce C_y. In the new range of low output-capacitance (LOC) Plumbicon tubes (see Table) this is done by reducing the size of the transparent conductive film in the target.

New range of low output-capacitance diode-gun Plumbicon tubes

Figures in parentheses are typical values of capacitance for conventional counterparts of the LOC tubes

type	XQ3410	XQ3070/02*	XQ3427	
size	30	25	17	mm
loading	rear	rear	front	
C_{as}, intrinsic tube capacitance	2.0 (4.5)	2.0 (4.5)	2.0 (2.5)	pF pF
C_y, capacitance of tube in yoke	3.5 (8.5)	3.0 (7.5)	2.5** (6.5)	pF pF

* Samples already available.

** Measured with centring ring grounded.

TARGET CONSTRUCTION

Figure 1 shows a section through the target of a LOC tube, and for comparison, a section through the target of a conventional Plumbicon tube. The smaller conductive film reduces C_y in two ways: firstly, it reduces the contribution made by the *intrinsic* tube capacitance C_{as};

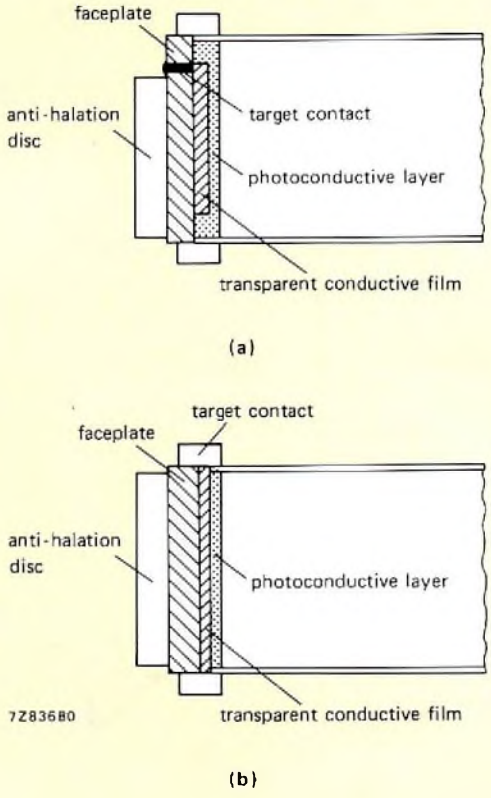

Fig.1 (a) Section through the target of a LOC tube (XQ3427 series); (b) Section through the target of a conventional Plumbicon tube (XQ2427 series)

and secondly, because its perimeter is farther from the yoke, it reduces stray target/yoke capacitances that contribute to C_y. The film is in fact only slightly larger than the scanning area, in contrast to the conventional tube in which the film covers the whole faceplate.

Figure 2 shows the different methods used to make the target contact (i.e. the conductive film to FET connection) in the three series of tubes. To minimise the wiring capacitance C_w the FET should be inside the yoke, allowing the target contact to be as short as possible.

XQ3427 series – development type 74XQ LOC (17 mm diameter, 11 mm diagonal scan). Like conventional 17 mm Plumbicon tubes (XQ2427 series), these have a metal ring surrounding the target; however, it is for centring only: an electrode passing through the faceplate forms the target contact (Fig.2(a)). The anti-halation disc is cut away as shown, allowing the contact to be as short as possible. To avoid charging effects the ring should be grounded, either directly or via a 10 MΩ resistor. The new tubes can be used with existing yokes, provided these are adapted to accommodate the new target contact.

XQ3070 series – development type 73XQ LOC (25 mm diameter, 16 mm diagonal scan). Like their conventional counterparts (XQ1070/02, XQ2070/02, XQ1080 and XQ1500 series), these have a ceramic ring immediately in front of the target with two interconnected gold electrodes (Fig.2(b)). The ring was initially introduced to reduce C_y in the conventional tubes, and has been kept

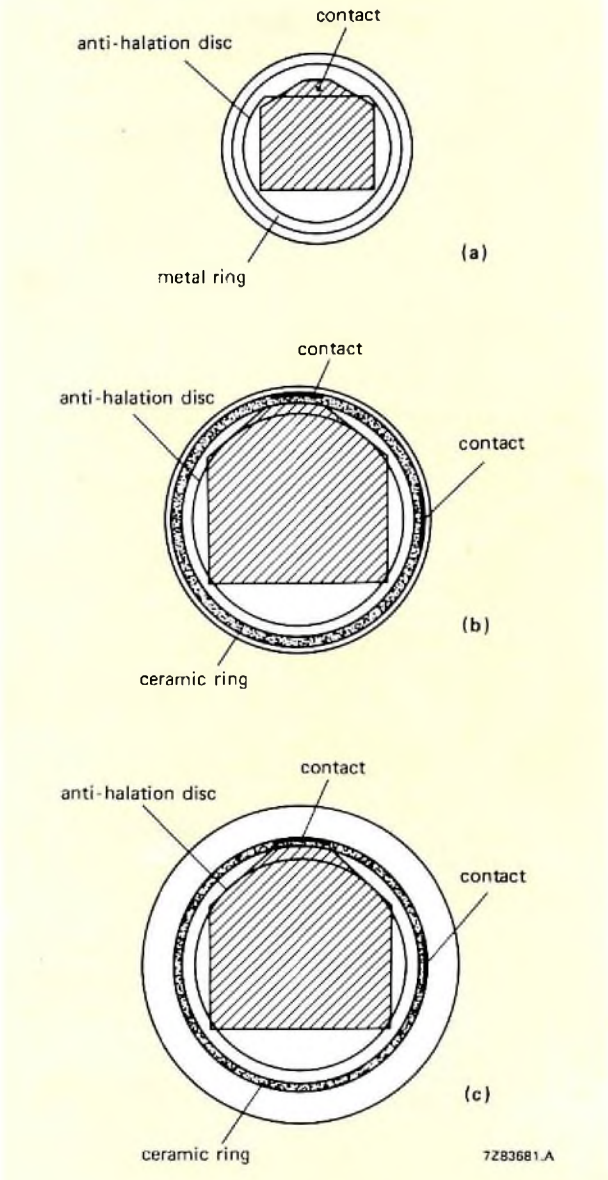

Fig.2 Because of the smaller conductive film in the LOC Plumbicon tubes, the target contact differs from that of the conventional tubes. (a) 17 mm XQ3427 series: an electrode passing through the faceplate forms the target contact; the anti-halation disc is cut away, allowing the electrode to be as short as possible; (b) 25 mm XQ3070 series and (c) 30 mm XQ3410 series: a direct connection between the conductive film and a gold electrode on the ceramic ring forms the target contact

to make the new tubes compatible with existing yokes. A direct connection between the conductive film and the gold electrodes (as shown in the figure) forms the target contact, so the new tubes are both mechanically and electrically interchangeable with conventional tubes.

XQ3410 series – development type 78XQ LOC (30 mm diameter, 16 mm diagonal scan). This series (Fig.2(c)) uses a narrow scan (16 mm) to improve registration. To take full advantage of the reduced capacitance, the metal ring of the conventional 30 mm tubes has (provisionally) been replaced by a ceramic ring in front of the target. As in the XQ3070 Series, the ceramic ring has two interconnected gold electrodes that connect directly with the conductive film to form the target contact. Existing yokes must therefore be adapted slightly to take the new tubes.

PERFORMANCE

The new range of LOC Plumbicon tubes can provide increases of about 3 dB in S/N ratio compared with conventional tubes. Figure 3 compares the performance of the 17 mm LOC tube XQ3427 (C_y = 2.5 pF) and its conventional counterpart the XQ2427 (C_y = 6.5 pF).

To gain maximum advantage from the reduced output capacitance, the FET capacitance must be matched to that of the tube, or more accurately, to the sum of the tube capacitance C_y and the wiring capacitance C_w. This is illustrated by Fig.3 in which the curves for the LOC tube peak at C_f = 3 pF (= C_y + C_w), and those for the conventional tube at C_f = 7 pF.

Figure 3 also shows that the S/N ratio can be increased by using FETs with higher values of g_m/C_f. With present-day FETs g_m/C_f is between 2 mA/V.pF and 4 mA/V.pF. However, improvements in FET technology will probably lead to higher values.

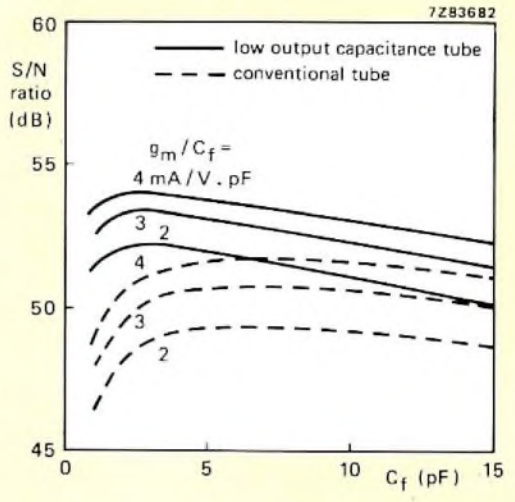

Fig.3 Signal-to-noise ratio of the 17 mm LOC Plumbicon tube XQ3427 (C_y = 2.5 pF) and of its conventional counterpart the XQ2427 (C_y = 6.5 pF) as a function of FET input capacitance C_f, with the ratio g_m/C_f as parameter. For both sets of curves B = 5 MHz, R_t = 1 MΩ, I_s = 200 nA, T = 300 K, and C_w = 0.5 pF

REFERENCES

1. FRANKEN, A. 1978. Electronic Components and Applications 1, 57-59.
2. FRANKEN, A. 1979. Electronic Components and Applications 1, 71-77.
3. FRANKEN, A. and LOHUIS, W. 1980. Electronic Components and Applications 3, 17-21.
4. BENDELL, S. L. and JOHNSON, C. A. 1980. SMPTE Journal 89, 838-841.

Gate turn-off switches combine the high blocking voltage and high switching current of thyristors with the ease of gate drive and speed of transistors. This article explains how to use published GTO data to get the best possible circuit performance.

Understanding GTO data as an aid to circuit design

A. WOODWORTH

The gate turn-off switch (GTO), shown in Fig.1, is a three-junction bistable semiconductor switch for controlling the flow of unidirectional current. Like a thyristor, it can block a high-level forward voltage whilst turned off, and can pass a peak forward current far in excess of its average current rating whilst turned on. Like a transistor however, it can be switched on and off at high speed by controlling a low-level current flowing into or out of its gate. The GTO therefore combines the most desirable characteristics of the thyristor with those of the transistor. Since some of the terms and characteristics in the published data for the GTO are unfamiliar, the design of GTO circuits may appear to be a more formidable task than the design of thyristor circuits. This article will show that, if a few fundamental precautions are observed, just the opposite will more often be the case.

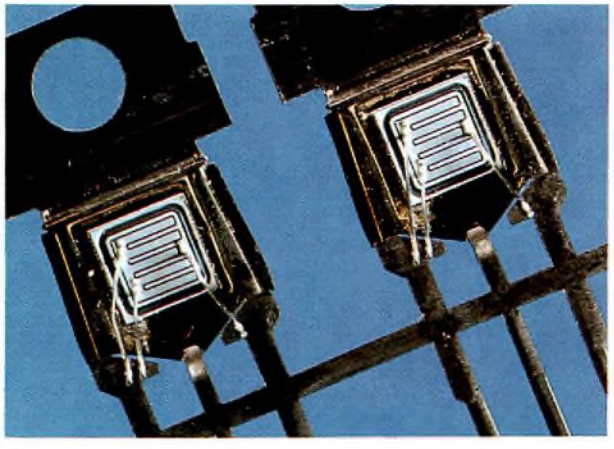

Fig.1 The GTO construction

FORWARD CHARACTERISTIC

Figure 2 continues the thyristor/transistor analogy for the GTO by showing that, when the anode current is less than the latching current I_L, the GTO behaves like a high-voltage transistor with a gate-to-anode current amplification factor I_A/I_G which increases with increasing anode current as shown in Fig.3. If the gate current is less than that required for triggering (I_{GT}), the GTO is in the off-state with a low leakage current flowing between the anode and cathode. If the gate current is greater than or equal to I_{GT}, the GTO is in the on-state with a small potential difference between anode and cathode. As long as the anode current remains below the latching level, however, the GTO may return to the off-state if the gate current falls below I_{GT}. If the anode

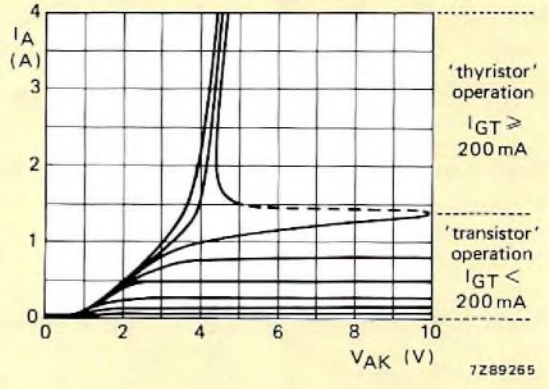

Fig.2 On-state current as a function of on-state voltage with gate current as a parameter, for the BTW58

current is greater than the latching level, the GTO, like a thyristor, will remain latched in the on-state, even if the flow of gate current ceases. Unlike the thyristor however, the GTO can be turned off again by reversing the polarity of the gate drive voltage.

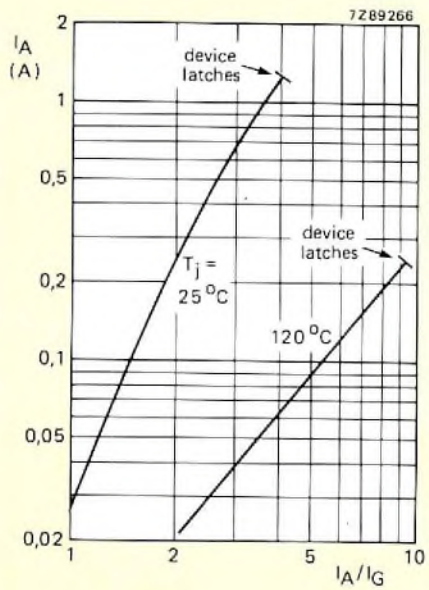

Fig.3 Forward current gain as a function of anode current for the BTW58

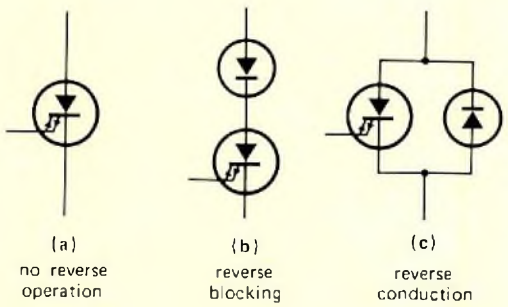

Fig.4 Changing the reverse characteristics of a GTO circuit with additional diodes

REVERSE CHARACTERISTIC

The reverse characteristic of the GTO is equivalent to that of a resistance which is incapable of blocking voltage or conducting significant current. For d.c. switching, this does not present any problem. If reverse voltage blocking is required for a.c. switching, a diode must be connected in series with the GTO as shown in Fig.4. If reverse current must be allowed to flow, a diode must be connected in anti-parallel with the GTO. Suitable diodes are available from our standard range of rectifier diodes. For example, diode BYW19 is suitable for use with the BTW58 GTO.

TURN-ON BEHAVIOUR

Precautions during pulse or capacitor discharge drive

During turn-on, care should be taken to ensure that adequate gate current is available whenever the anode current is likely to be less than the latching level. For example, Fig.5 shows that, if turn-on is achieved by discharging a capacitor into the gate of a GTO with an inductive load, too brief a time-constant may cause the gate-current to fall below I_{GT} before sufficient time has elapsed for the anode current to rise above the latching level. This could cause uncertain triggering. Uncertain triggering could also be caused by some types of anode load which vary considerably both during switch-on and during idling. It has also been observed that, if the anode current is only slightly higher than the latching level, a steep trailing edge of a positive gate pulse may cause the GTO to unlatch as shown in Fig.6. The fall time of the gate drive pulses should therefore be prolonged.

The disadvantage of having to take the foregoing precautions during turn-on is far outweighed by the triggering sensitivity of the GTO (I_{GT} min. = 200 mA for the BTW58).

Minimising switching losses

To minimise losses during fast switching, it essential to minimise the turn-on time of the GTO. As shown in Fig.7, both components of the turn-on time (delay time t_d and rise time t_r) reduce with increasing forward gate current. The ideal waveform for the gate drive current as shown in Fig.8 therefore rapidly rises to a level much higher than the minimum value required to ensure triggering (I_{GT}), and does not reduce to I_{GT} until the anode current has stabilised at a value much higher than the latching level (I_L). In conventional thyristors, a rapidly rising anode current would cause a high level of localised dissipation in the crystal during turn-on. The interdigitated construction of the GTO gate (Fig.1) increases its ability to withstand the stresses caused by fast turn-on.

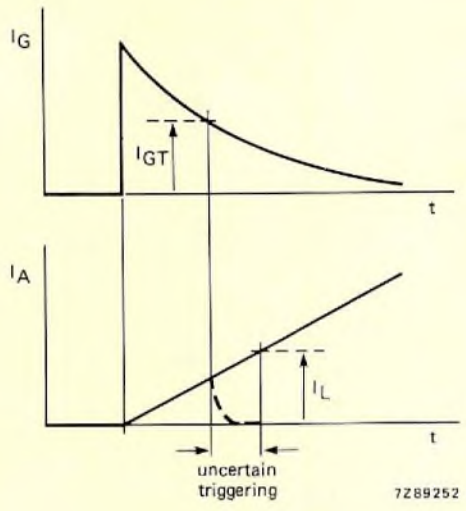

Fig.5 To ensure good triggering the anode current must rise above the latching level before the gate current falls below the minimum level required to ensure triggering

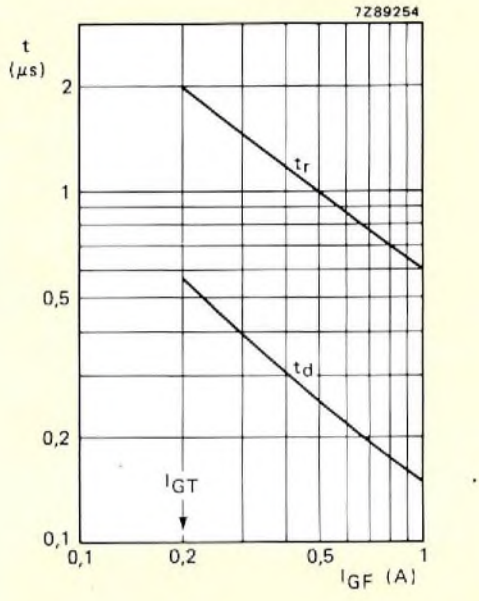

Fig.7 Components of the turn-on time as functions of forward gate current

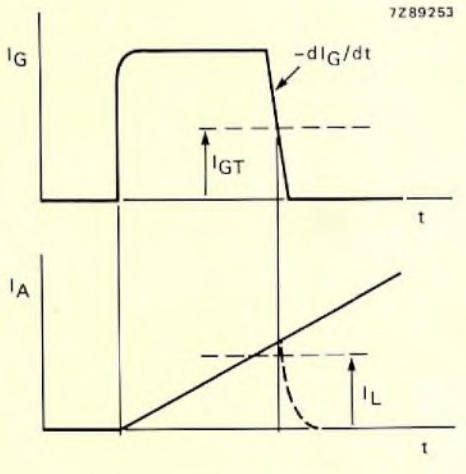

Fig.6 Unlatching can occur if the anode current is only slightly higher than the latching level during a rapid positive to negative transition of the gate current

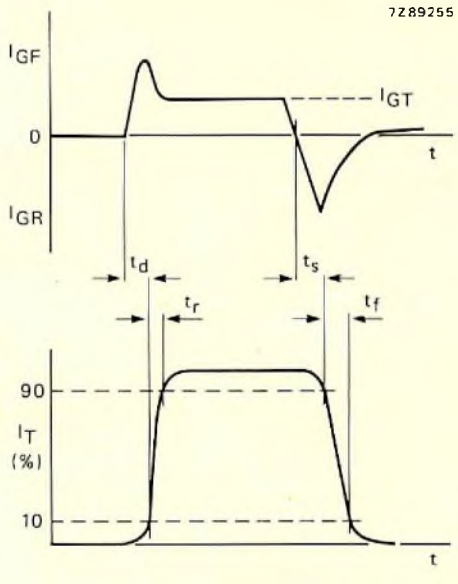

Fig.8 Ideal turn-on and turn-off waveforms for a GTO

Advantages of d.c. gate drive

Like a transistor, the GTO can also be turned on by applying a direct gate current greater than I_{GT}. As shown in Fig.9, this mode of operation has the additional advantage of reducing the voltage drop across the GTO whilst it is conducting, even if the anode current is very much higher than the latching level.

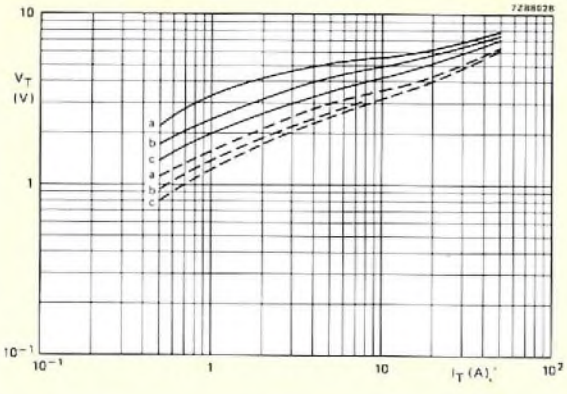

Fig.9 Voltage drop across the GTO as a function of anode current with d.c. gate drive level as a parameter
a: 200 mA;
b: 500 mA;
c: 1 A.
Full line for T_j = 25 °C, dashed line for T_j = 120 °C

TURN-OFF BEHAVIOUR

To understand the turn-off process, it is helpful to have some understanding of the solid-state conduction through the GTO crystal. Figure 10 shows a cross-section through the crystal whilst conduction is taking place between the anode and the cathode. During this on-state, the central region of the crystal is filled with a hole-electron plasma which enables the GTO to conduct a high current with very little potential difference between anode and cathode. To turn-off the GTO this plasma must be interrupted by applying a negative voltage bias to the gate. This causes the plasma to be squeezed to a narrow filament as shown in Fig.11. The period up to the breaking of the plasma filament is the storage phase of the turn-off time. For it to be short, a reasonably strong field (−5 V to −10 V) should be applied between the gate and the cathode. The gate region is so designed that it can withstand short periods (≈20 μs) of operation whilst in reverse avalanche breakdown. The application of a reverse bias voltage which exceeds the reverse breakdown level does not, however, further assist the turn-off process. The relationship between applied reverse gate voltage and the two components of the turn-off delay of a GTO is shown in Fig.12.

When the plasma filament shown in Fig.11 is broken, the anode current falls and the anode voltage rises at a

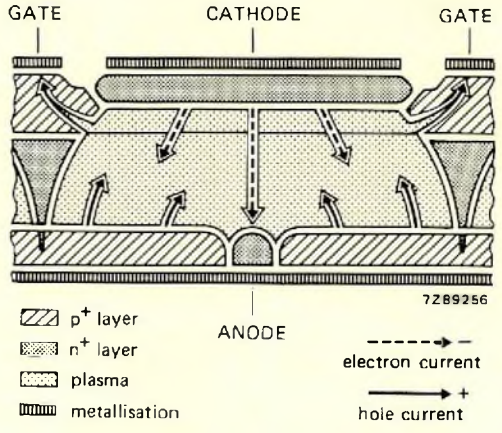

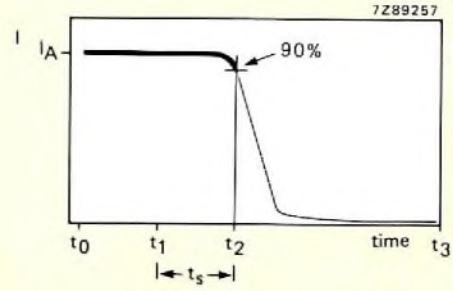

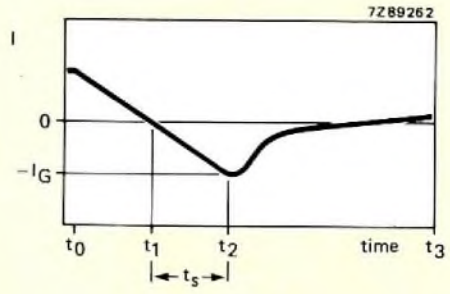

Fig.10 Cross-section of the GTO crystal during the start of turn-off (storage time t_s) when gate current extraction commences

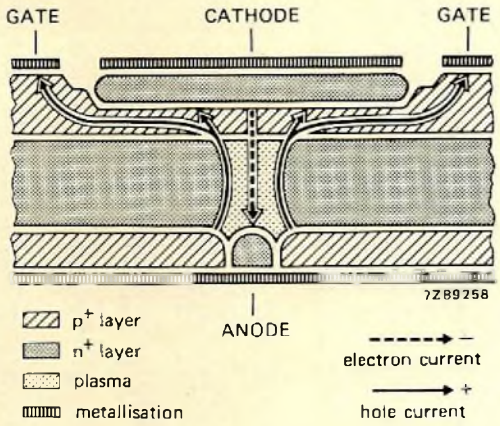

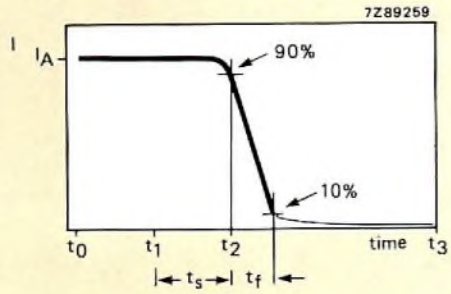

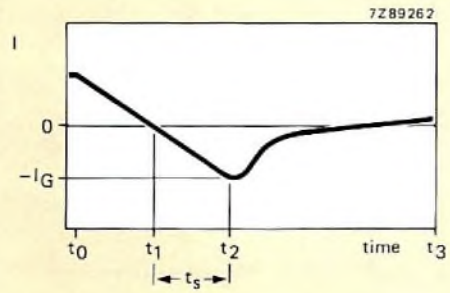

Fig.11 Cross-section of the GTO crystal during the next phase of turn-off, the fall time t_f, during which the conduction is squeezed into a narrow filament that finally breaks

rate dependent on the load. The anode current fall-time depends on the current extracted from the gate as shown in Fig.13. For example, if an anode current of 5 A is switched off by extracting 1 A of gate current, the storage and fall times may be as long as 2.5 μs and 2 μs respectively. Alternatively, if 5 A is extracted from the gate to switch off the same 5 A load, the storage and fall times are reduced to 0.5 μs and 0.25 μs respectively. The ability to withstand the high peak level of reverse gate current which is necessary to ensure fast turn-off is ensured by using a shorted anode structure and a low-impedance base region beneath the cathode. These features are made possible by careful control of the diffusion. Localised hot-spots during turn-off are prevented by using long, narrow cathode fingers (interdigitated construction).

As shown by Fig.14, the final stage of turn-off consists of a small tail of anode current due to charge trapped in the remoter regions of the crystal. Gold doping has been used to ensure that this charge rapidly recombines so that it does not normally have any appreciable influence on the turn-off dissipation.

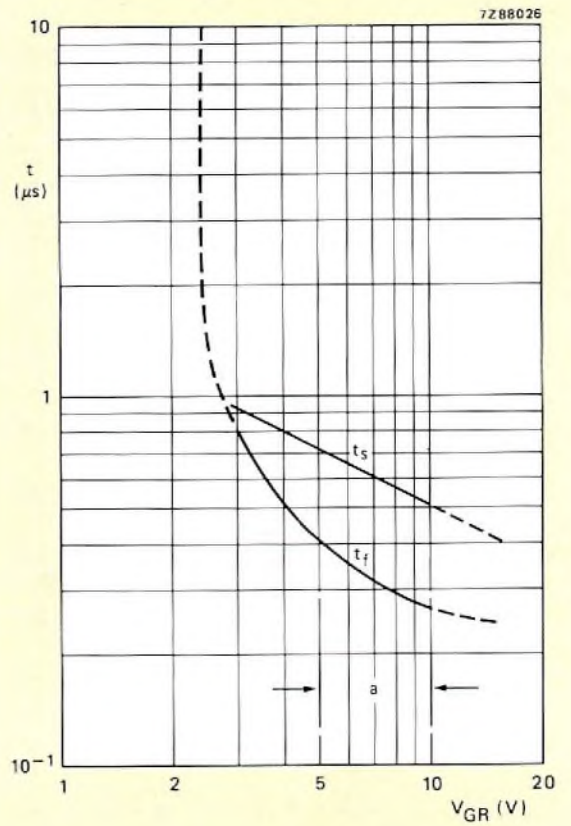

Fig.12 The influence of negative gate voltage on the two components of the turn-off time
a = recommended range of V_{GR}

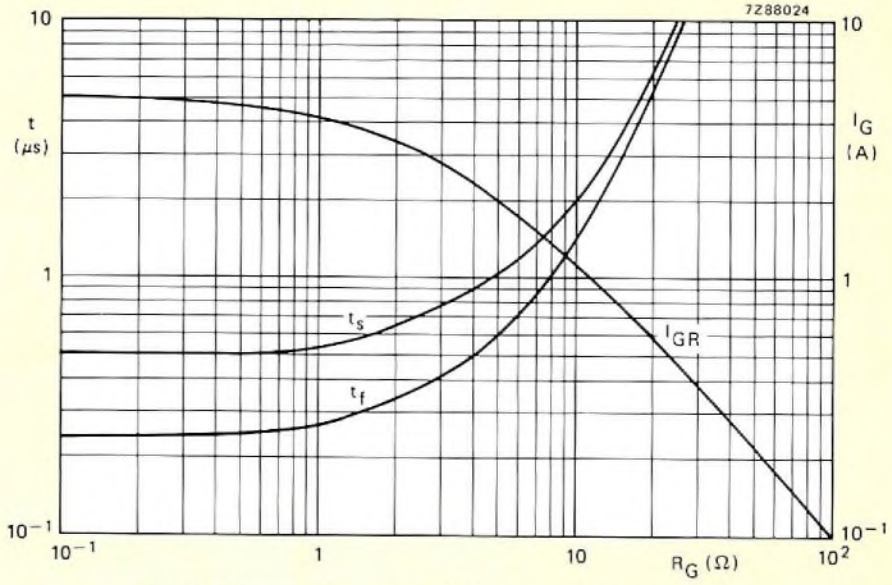

Fig.13 Reverse gate current and the two components of turn-off time as functions of gate series resistance

MAXIMUM CONTROLLABLE ANODE CURRENT

Although the GTO crystal is quite small, it is capable of conducting and switching off currents well in excess of its average anode current rating. For example, the 6.5 A BTW58 can switch off 25 A pulses of anode current. The only condition is that the rate of rise of the voltage between anode and cathode must be limited as shown in Fig.15 for inductive loads. The higher the current that must be switched off, the lower the allowable dV/dt. Figure 15 shows that, as might be expected, for a given dV/dt, the level of current that can be switched off increases with increasing negative bias applied to the gate. In applications where Fig.15 indicates that a slow rise circuit is required, one of the two circuits shown in Fig.16 can be used. Figure16(a) is suitable for use in circuits with a single GTO controlling load currents up to 25 A. Figure 16(b) is for GTO bridge circuits for controlling load currents up to 6 A.

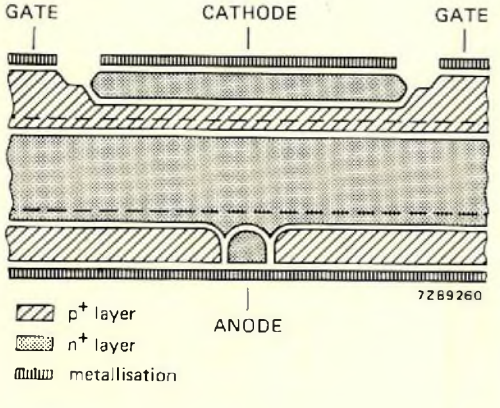

Fig.14 Cross-section of the GTO crystal during the final phase of turn-off (tail time) during which a depletion layer is formed and the charge recombines in the remote n-base

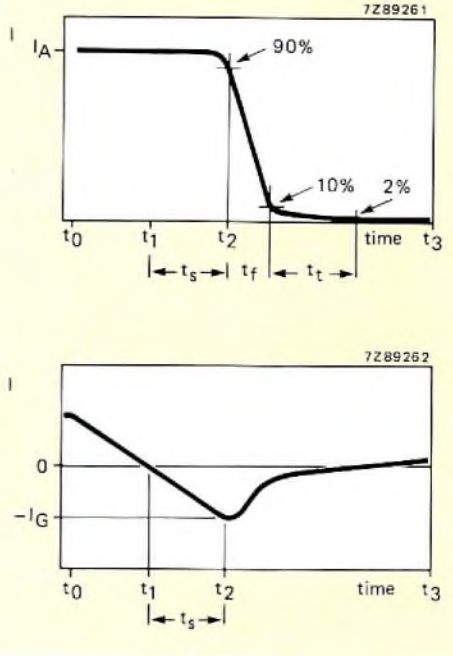

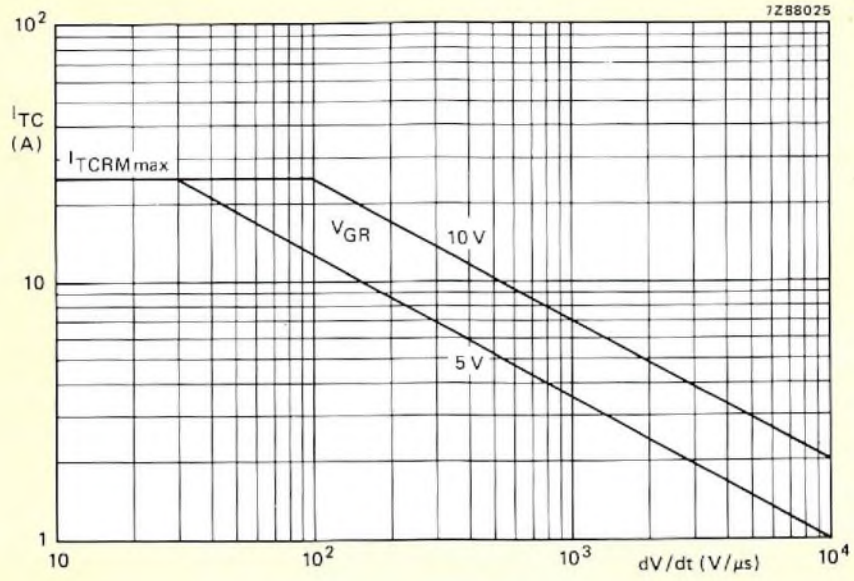

Fig.15 Permitted anode voltage rise time as a function of controllable anode current with reverse bias voltage on the gate as a parameter

SAFE OPERATING AREA (SOAR)

Since the GTO is a switch with two stable states, it cannot remain in a quasi-saturated condition during turn-on or turn-off. There is not therefore a SOAR limitation whilst the GTO is forward biased. The SOAR for a reverse biased GTO is a simple rectangle as shown in Fig.17.

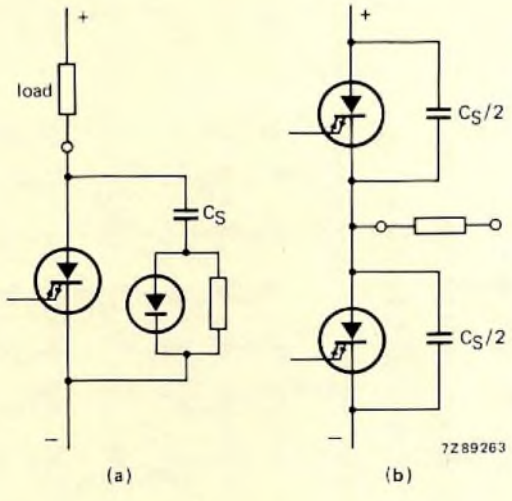

Fig.16 Slow rise circuits

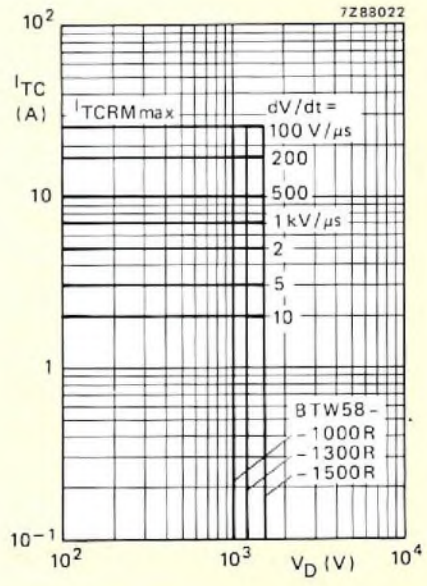

Fig.17 Reverse biased SOAR for the BTW58

GTO DRIVE CIRCUITS

In some applications, the GTO can be switched by a simple direct-drive circuit. In others, the control circuit must be isolated from the GTO switch. There may also be requirements regarding parameters such as switching duty-factor range and switching frequency which demand a more complex drive circuit. Isolation of the control voltage is not usually required in self-contained domestic appliances where low cost is of paramount importance. On the other hand, it is often essential to isolate the control voltage in applications such as industrial SMPS and motor control. In an SMPS, the switching duty factor is usually between 5% and 50% at a switching frequency of the order of tens of kHz. For a.c. motor control, the duty factor of the switching must range from less than 1% to more than 99% at frequencies which are often as low as tens of hertz.

Examples of two simple non-isolated drive circuits will be described. Fully toleranced designs and detailed design methods for both isolated and non-isolated drive circuits will be described in forthcoming publications.

Simple direct gate drive circuit

The simplest, least expensive non-isolated gate drive circuit is shown in Fig.18. This circuit has a limited minimum value for the switching duty factor and can only switch up to 6 A of GTO anode current. The main applications for this circuit are horizontal deflection circuits for tv, and simple series-resonant power supplies (SRPS) such as that used to control a d.c. motor in a washing machine.

The GTO is turned on when TR_1 is conducting. Initially, the GTO gate current flows via C_1 and L_1 ensuring a good switching characteristic. The build-up of charge on C_1 is limited by the supply voltage and by TR_1 as it comes out of saturation. When C_1 is charged, a low-level gate current flows via R_2 to maintain the GTO conduction. When darlington transistor TR_2 is turned on, the GTO conduction ceases because the charge on C_1 is applied negatively to the gate of the GTO via L_1. Charge is therefore extracted from the gate of the GTO and the GTO turns off when the correct relationship exists between negative gate voltage, peak anode current and rate of rise of anode voltage. The minimum duty factor for the switching is limited because the interval between switching the GTO on and off again must be long enough to allow C_1 to charge via TR_1. This is particularly important during the first few switching cycles during which C_1 receives its initial charge.

Direct cathode drive circuit

The non-isolated drive circuit shown in Fig.19 controls the GTO by switching its cathode current with a low-voltage high-current MOSFET. This circuit has the advantages of a MOS-compatible control input, good switching characteristics and a controllable GTO anode current of more than 10 A. The circuit can be used for pulsed switching with an unlimited duty factor range. Since there is no lower limit to the switching frequency, it can also be used to switch d.c. We are currently investigating the use of this type of circuit to control a d.c. motor via an SRPS.

When TR_1 conducts, the GTO is turned on by gate current which initially flows via C_2. When C_2 has charged, the gate current is maintained via R_1. Electrolytic capacitor C_1, which must have a low ESR, ensures that the GTO is rapidly forced into full conduction to achieve fast switching, even if the anode current has a very brief rise time. For turn off, TR_1 must be so driven that the GTO anode current falls at a rate of between 10 and 20 A/μs. The cathode current of the GTO then rapidly diverts to the gate from where it initially flows via C_2 into C_1. When C_2 is fully discharged, the flow of gate current is maintained via D_1.

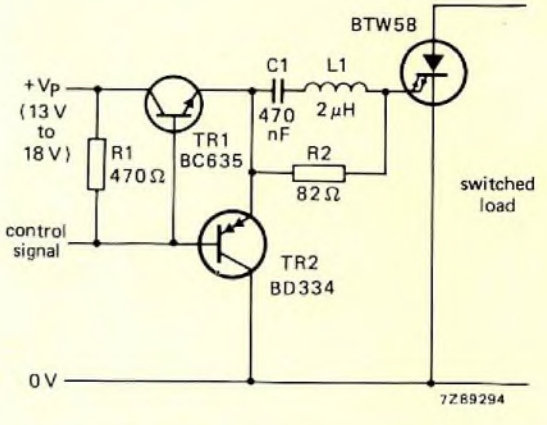

Fig.18 Simple direct gate drive for the GTO

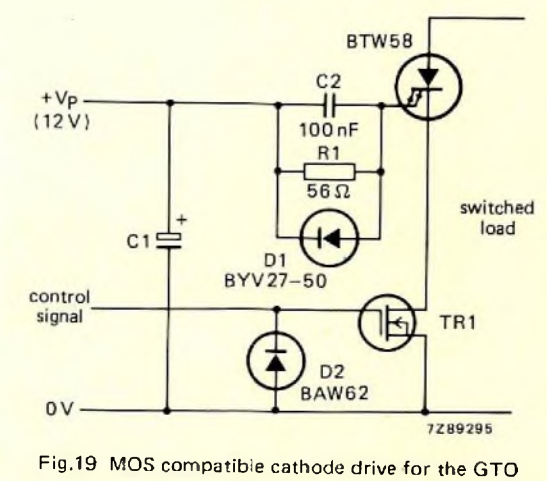

Fig.19 MOS compatible cathode drive for the GTO

Switched-mode power supplies and PWM motor-speed control systems impose severe demands on smoothing capacitors, particularly as regards their ripple-current ratings. This article describes new capacitors designed to meet those demands and tells how to select the best one for each application.

Electrolytic capacitors for industrial applications

J.A. HOULDSWORTH and H. SCHMICKL

A new range of electrolytic capacitors, the 114/115 series, has been purpose-designed for rectified mains smoothing and energy storage in industrial applications. The 114 series are low-voltage types (10 to 100 V) with capacitance values of 1000 to 220 000 μF, while high-voltage requirements are met by the 115 series (250 to 385 V), capacitance values 150 to 4700 μF. A selection of capacitors from the range is shown in Fig.1. The capacitors can be used at temperatures of between –40 to +85°C, and have a typical lifetime of more than 10 000 h when operated at the maximum rated temperature and ripple current. The internal construction of these capacitors ensures that they have ripple current ratings which are superior to existing types. For example, a 2200 μF 385 V type has a ripple current rating of 9 A at 100 Hz and 85°C ambient, with a corresponding figure of 21 A at an ambient temperature of 40°C.

Fig.1 A selection of 114/115 series capacitors

The capacitors will be used principally in switched-mode power supplies (SMPS) and motor control systems, and they are particularly suitable for the mains smoothing function in the Pulse-Width Modulation (PWM) a.c. motor speed control system previously described in Refs.1 to 5. In both SMPS and motor control systems, the values of capacitance required are usually ripple-current determined, and the superior ripple current ratings of the 114/115 types provide a significant advance in economical filter design.

This article describes the features and construction of the 114/115 series capacitors, with particular emphasis on those aspects which contribute to the high ripple current rating. The influence of temperature and frequency on capacitor selection is described, including a method of determining operating conditions for extended life expectancy. Brief descriptions are given of the two major application areas: PWM motor speed control and SMPS, and to facilitate the selection of the correct capacitor, the associated ripple current design equations are presented. These equations are verified by comparing predicted and measured ripple currents in three representative power systems.

PHYSICAL BACKGROUND TO ELECTROLYTIC CAPACITORS

The capacitance C of a parallel plate capacitor is given by:

$$C = \epsilon_0 \epsilon_r \frac{A}{t}, \qquad (1)$$

where ϵ_0 is the permittivity of free space, ϵ_r is the relative permittivity of the dielectric, A is the surface area of

the electrodes, and t is the thickness of the dielectric film. A full list of the symbols used in this article is given in Table 1.

Electrolytic capacitors are characterised by a high capacitance-to-volume ratio. This feature makes their use in many cases highly desirable, and in certain circumstances essential.

The anode of an electrolytic capacitor is made from aluminium foil. This foil is electrochemically etched, which increases its effective surface area by a factor of typically a 100. A large effective surface area is an important factor in achieving a large capacitance-to-volume ratio. The dielectric film is formed by converting the surface of the aluminium foil into aluminium oxide, using anodic oxidation (also referred to as forming). This is a simple process and gives a very homogeneous dielectric film. Anodic films have a relative permittivity of about 8, and a very high dielectric strength which approaches that predicted by the ionic theory of crystals. The thickness of the dielectric layer is determined by the forming voltage used, each volt of forming voltage producing about 1.4 nm of layer thickness. An etched and formed foil is shown in detail in Fig.2.

The second electrode of the capacitor (the cathode) is formed by a low resistance liquid (the electrolyte). This is necessary to ensure effective and uniform contact with the spongelike surface of the dielectric. To achieve electrical contact between the liquid cathode and the cathode terminal of the capacitor, another etched foil is required. This second foil, the cathode contact, has a very thin dielectric layer. The thickness of this layer is about 2 nm, and the voltage drop across the layer will be approximately 1.5 V. This thin dielectric layer is required to give the cathode contact a stored charge (the product of C and V) equal to the CV product at the anode, thereby improving the charge/discharge properties of the capacitor.

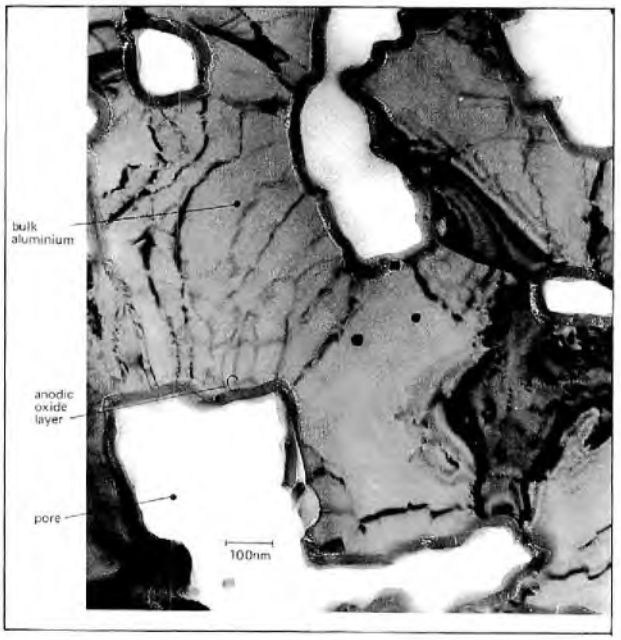

Fig.2 Section parallel to surface of etched and formed anode foil. Magnification: X 63 000
Forming voltage: 12 V

The electrolyte is impregnated into paper tissue spacers to ensure that the liquid cathode remains between the cathode and anode foils.

The anode and cathode foils are extremely thin; 100 μm is a typical thickness for the anode foil while the cathode contact foil is approximately 30 μm thick. The anode/paper/cathode combination is coaxially wound on a winding machine, giving the characteristic cylindrical shape of the electrolytic capacitor (see Fig.1). This compact wound structure is a further factor contributing to a high capacitance-to-volume ratio.

THE ELECTROLYTE

The characteristics of the electrolyte are a major factor in determining the performance and reliability of an electrolytic capacitor. Of the many properties required by the electrolyte, the following are especially important.

- Low resistance, as the electrolyte forms part of the series resistance of the winding
- Stability of electrical and chemical properties over a wide temperature range, –40 to +85°C
- Non-corrosive behaviour towards the materials of the capacitor

CONSTRUCTION OF 114/115 SERIES CAPACITORS

A simplified cross-section of an electrolytic capacitor is shown in Fig.3a. The equivalent circuit of this cross-section is shown in Fig.3b. From this equivalent circuit, it can be seen that an electrolytic capacitor is effectively made-up of a very large number of capacitors arranged in parallel. Figure 3b also indicates the series resistance of the electrolyte and paper spacer.

There will be other parasitic resistances contributing to the total resistance of the capacitor. Potentially, the most significant sources of additional parasitic resistance are the anode and cathode contact foils. In a large electrolytic capacitor these can be many metres long, and if the capacitor is constructed in the conventional way with a single contact to each foil, then the resulting lateral resistance can be large. In the 114/115 series capacitors, the resistance of the foil is minimised by multiple connections to the anode and cathode contact

TABLE 1 List of symbols

Symbol	Definition
A	surface area of a plate in parallel plate capacitor
C	capacitance
D	maximum diode conduction period
f_{IN}	ripple frequency of capacitor input current
f_{OUT}	ripple frequency of capacitor output current
I_{cap}	r.m.s. value of capacitor ripple current
I_{dc}	average d.c. link current
I_{in}	r.m.s. value of a.c. component of capacitor input current
$I_{INP(k)}$	peak value of the k^{th} pulse of the capacitor input current waveform
I_n	capacitor ripple current at a given frequency
I_{out}	r.m.s. value of a.c. component of capacitor output current
I_R	rated ripple current (85°C, 100 Hz)
I_r	capacitor ripple current
$I_{r(T,95)}$	maximum ripple current at ambient temperature T and core temperature 95°C
$I_{r(T,\theta)}$	maximum ripple current at ambient temperature T and core temperature θ°C
i_{CAP}	instantaneous value of capacitor current
i_{cap}	a.c. component of capacitor current
$\overline{i^2}_{cap}$	mean-square value of a.c. component of capacitor current
i_{IN}	instantaneous value of capacitor input current
i_{in}	a.c. component of capacitor input current
$\overline{i^2}_{in}$	mean-square value of a.c. component of capacitor input current
i_{OUT}	instantaneous value of capacitor output current
i_{out}	a.c. component of capacitor output current
$\overline{i^2}_{out}$	mean-square value of a.c. component of capacitor output current
L_{crit}	minimum inductance for continous diode conduction
M_T	temperature multiplier for rated ripple current
m	number of differing pulse amplitudes in capacitor input current waveform
R	effective series resistance
$\sqrt{r_n}$	frequency multiplier for rated ripple current
T	ambient temperature
t	thickness of dielectric in parallel plate capacitor
V_{dc}	average d.c. supply voltage
α_{IN}	diode conduction period
$\alpha_{IN(k)}$	diode conduction period for k^{th} pulse of the capacitor input current waveform
δ_{IN}	capacitor input waveform duty cycle
δ_{OUT}	capacitor output waveform duty cycle
δ_T	duty cycle of either of the transistor drive waveforms in push-pull converter
ϵ_0	permittivity of free space
e_r	relative permittivity of dielectric
θ	core temperature

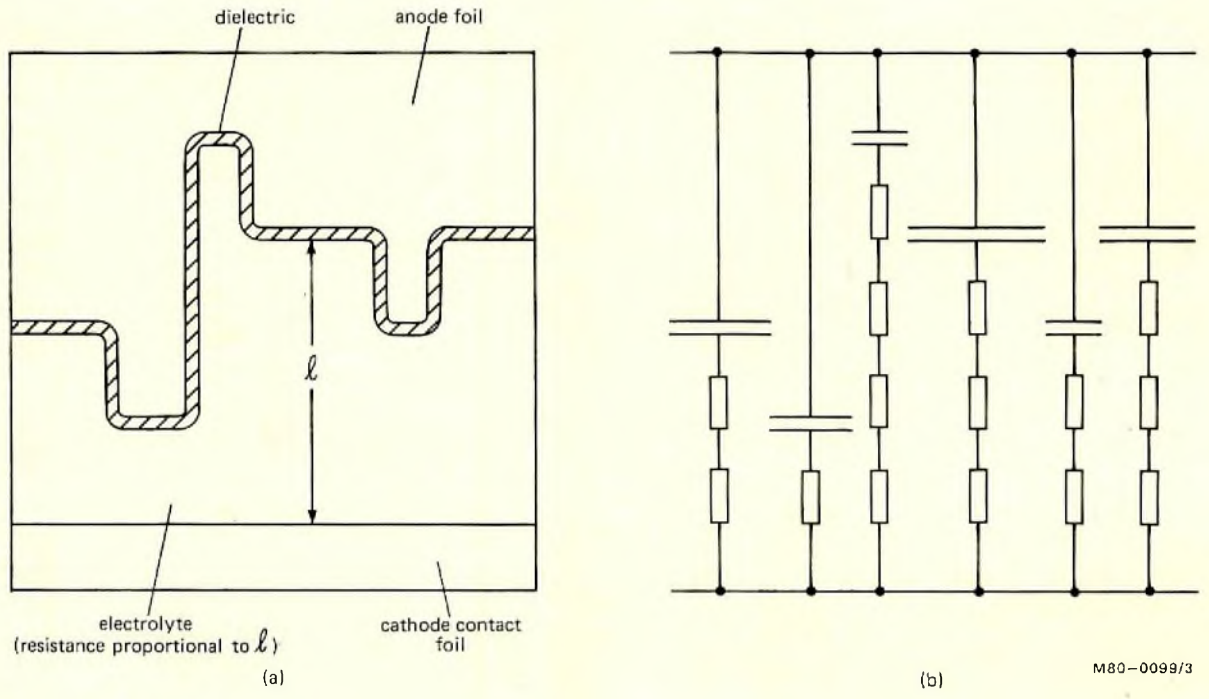

Fig.3 (a) Simplified cross-section of an electrolytic capacitor (not to scale)
(b) Corresponding equivalent circuit

foils. This is illustrated in Fig.4a. From the equivalent circuits of Figs.4b and 4c, it can be seen that as a result of the multiple connections, the effective series resistances of the winding elements are parallel-connected and hence reduced in value.

The method of construction ensures that the effective series inductance of the windings is inherently very low. However, some inductance is inescapable as corresponding anode and cathode connecting tabs must be physically separated to avoid the accidental short-circuiting of the capacitor. In practice the inductance of the winding is reduced to a negligible level by placing corresponding tabs no more than half a turn apart.

The distribution of tab connections in a wound capacitor is shown clearly in Fig.5a. The multiple tab connections are brought out at the top of the winding thereby reducing the equivalent series resistance and inductance due to the leads by minimising their lengths. The method of connecting the tabs to the screw terminals of the capacitor is evident from Fig.5b. Also shown in Fig.5b is the valve which releases excess gases produced by operating the capacitor beyond its specified limits; for example, at too high a temperature or operating voltage, or with incorrect polarity.

MANUFACTURE

Electrolytic capacitors are manufactured in several stages. Aluminium of 99.99% purity is rolled to a thickness of about 100 μm, a width of 50 cm, and a length of approximately 2000 m. The foil is etched electrochemically, and then thoroughly cleaned with deionised water, all in a continuous process. The cleaning process is required to remove all chemical residues prior to the forming of the oxide layer. This ensures the long-term stability of the oxide layer, which contributes to the long-life characteristics of the capacitors.

The next stage is the anodic oxidation of the etched foil, also a continuous process. The foil is passed through the forming liquid, and a constant voltage (known as the forming voltage) is applied to the foil. The application of the forming voltage for a specified time results in the formation of the dielectric layer. The forming voltage is always about 20% higher than the specified working voltage of the capacitor. After forming, the foil is cut to the width required for use in the capacitor.

Anode foil, tissue paper spacers, and cathode contact foil are coaxially wound on a winding machine. The winding machine (see Fig.6) is computer-controlled and determines the appropriate positions for the multiple

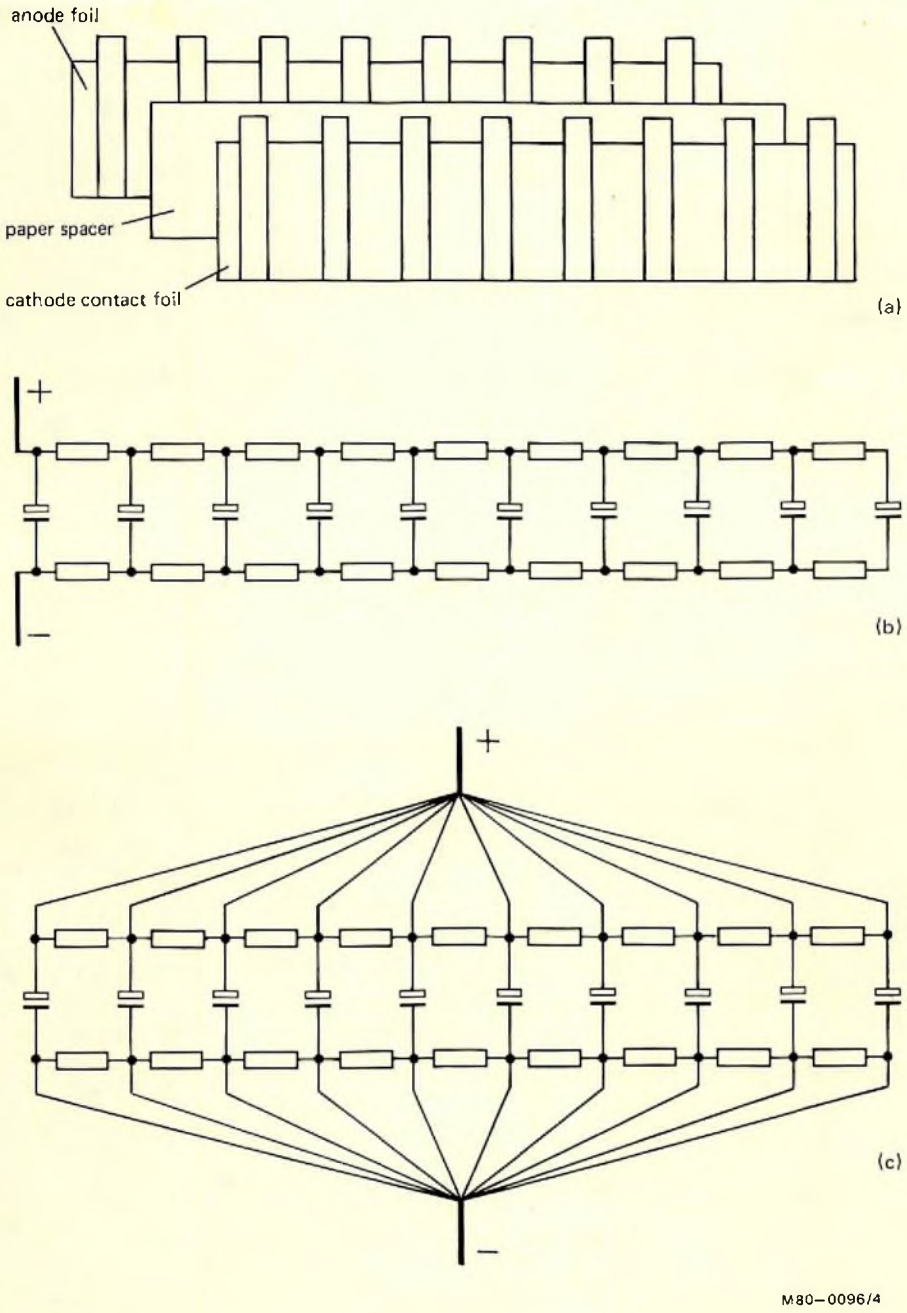

Fig.4 (a) Multi-tab connections – capacitor in unwound state. (b) Simplified equivalent circuit of capacitor with conventional construction. Capacitor on extreme right joined to terminals via full lateral resistance of the foil. (c) Simplified equivalent circuit of capacitor with multi-tap construction

anode and cathode connections. These are cold-welded into place as the capacitor is being wound. All connections in the capacitor are cold-welded, giving a molecular bond with high reliability and excellent life stability. After winding, the top cap of the capacitor (see Fig.5b) is cold-welded to the anode and cathode connection tabs.

The cell is impregnated with electrolyte using vacuum impregnation, and then assembled and sealed into the can. A ring of ethylene-propylene rubber forms the sealing element between the top cap and the can. The winding is clamped in the can by a technique which produces longitudinal rills in the can body. This ensures a good thermal contact between the winding and the can, and gives a very robust assembly.

After assembly, the capacitor is subjected to a prolonged reforming process at a temperature of 85°C,

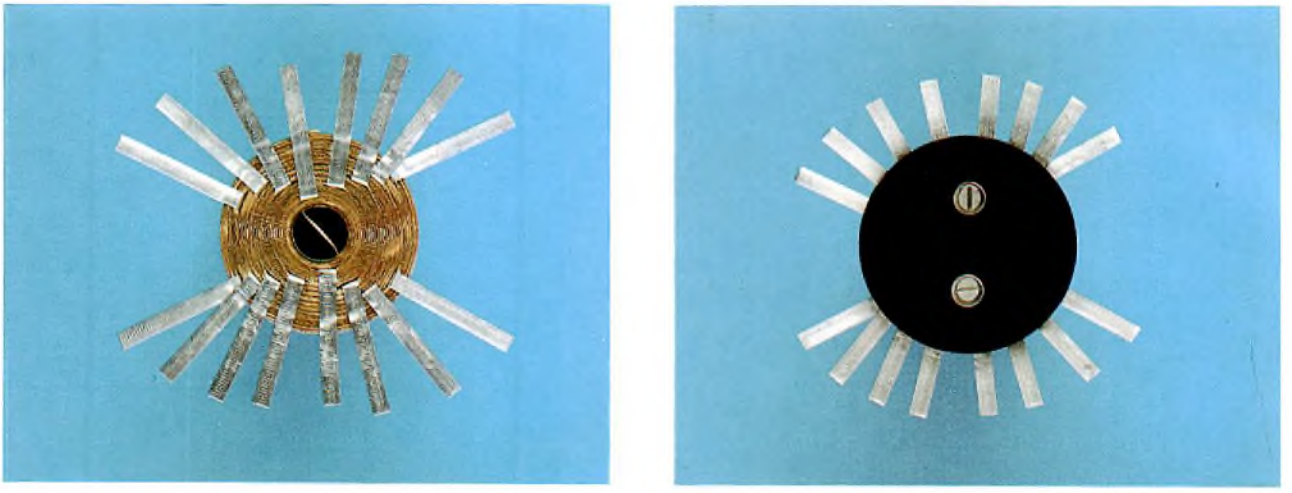

Fig.5 (a) Multiple anode and cathode connections on a wound capacitor. Corresponding anode and cathode connections are brought out so that they are diametrically opposite, half a turn apart. (b) Top cap of capacitor showing connection points for multiple anode and cathode connections

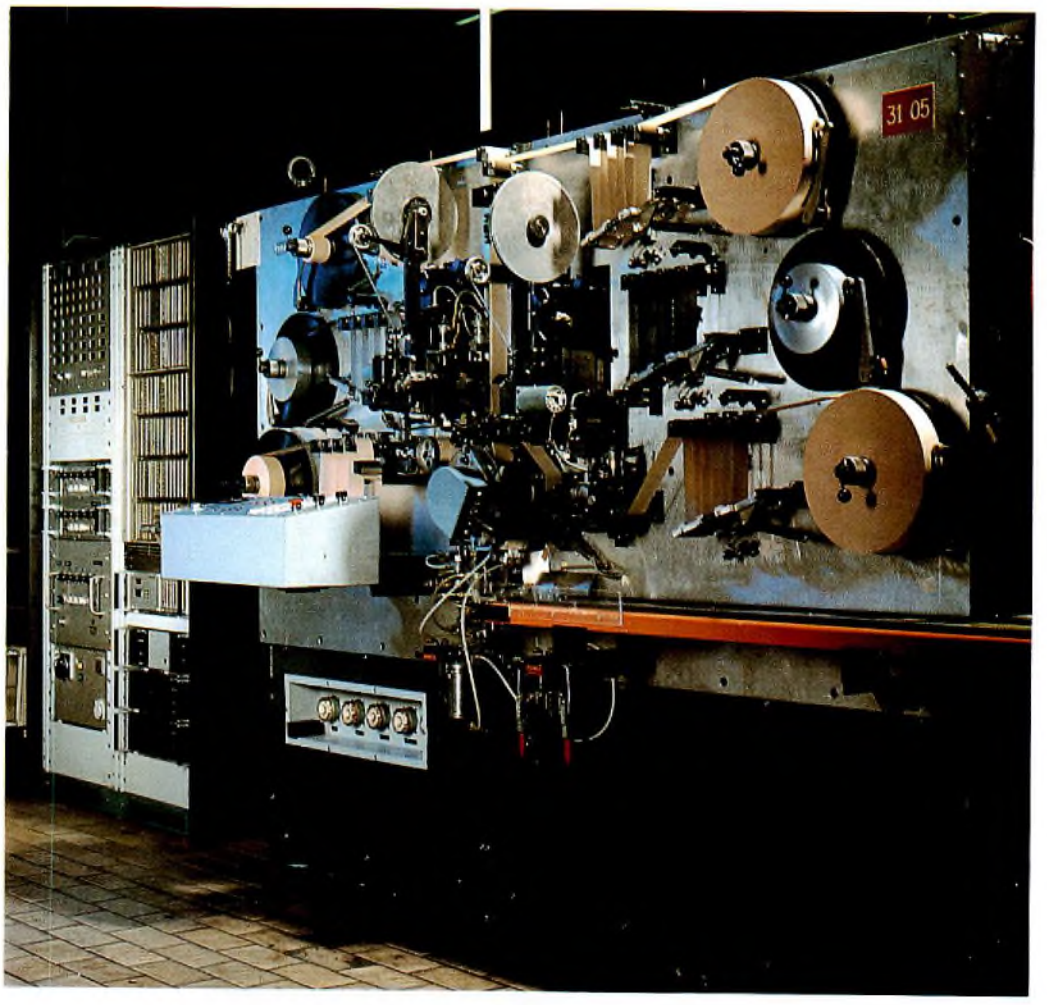

Fig.6 Computer-controlled winding machine

again using a constant forming voltage. This ensures that any spots where the dielectric layer is missing, such as the edge of the cut foil, are anodically oxidised. The reforming process results in a capacitor with an extremely low leakage current.

The capacitor is then insulated in a plastic sleeve before being finally inspected and tested.

CAPACITOR DESIGN AND RIPPLE CURRENT RATING

A ripple current I_r will result in a rate of heat generation substantially equal to $I^2_r R$, where R is the effective series resistance. To produce a capacitor with a high ripple current rating therefore requires a low effective series resistance and efficient heat dissipation. From the above description, the features of the 114/115 series capacitors which contribute to their high ripple current rating can be summarised as follows.

- Multi-tab construction
- Low-resistance electrolyte
- Good thermal contact between winding and can (rilled can construction)

Details of the rated ripple currents for the 385 V 115 series electrolytic capacitors are given in Table 2. (For full details of the complete 114/115 series, see published data). The maximum ripple current is dependent on ambient temperature and frequency, and the influence of these two factors is now considered.

Ambient temperature

The life expectancy of an electrolytic capacitor is determined principally by its core temperature, and the 114/115 series capacitors are designed to operate at a maximum core temperature of 95°C. The core temperature will be determined by the ambient temperature and the heating effect of the ripple current. The 114/115 series capacitors are rated at an ambient temperature of 85°C, and at this temperature the rated ripple current therefore contributes a temperature rise at the capacitor core of 10°C. At lower ambient temperatures, the maximum allowable ripple current (giving a core temperature of 95°C) will contribute a greater temperature rise at the core, and will therefore be greater than the rated ripple current. The maximum ripple at an ambient temperature T is related to the rated ripple current (at 85°C) by:

$$I_{r(T,95)} = I_R \sqrt{\left(\frac{95-T}{10}\right)}, \qquad (2)$$

$$= I_R \times M_T,$$

where $I_{r(T,95)}$ is the maximum ripple current at an ambient temperature T and a core temperature 95°C, I_R is the rated ripple current at 85°C ambient, and M_T is the temperature multiplying factor for ripple current (see Table 3). It should be noted that both ripple currents in Eq.2, $I_{r(T,95)}$ and I_R, are specified at 100 Hz.

TABLE 2

Rated ripple currents for 385 V 115 series electrolytic capacitors

Capacitance μF	Rated ripple current (I_R) 85°C, 100 Hz
150	1.2
220	1.6
330	2.2
470	2.7
680	4.8
1000	7
1500	7
2200	9

TABLE 3

Multiplier for rated ripple current as a function of ambient temperature

Ambient temperature °C	Multiplier (M_T)
85	1.0
80	1.22
75	1.41
70	1.58
65	1.73
60	1.87
55	2.00
50	2.12
45	2.24
≤40	2.35

Frequency

The power dissipated by the dielectric and cathode oxide layers falls with frequency, so that the maximum ripple current can be increased as the frequency is increased. Ripple current ratings are usually standardised at 100 Hz; for non-sinusoidal ripple currents (and hence for multi-frequency ripple currents) the equivalent ripple current at 100 Hz is given by:

$$I_r = \sqrt{\left(\sum \frac{I_n^2}{r_n}\right)}, \qquad (3)$$

where I_n is the ripple current at a given frequency, and $\sqrt{r_n}$ is the multiplying factor at the same frequency (see Table 4).

TABLE 4

Multiplier for rated ripple current as a function of frequency

Frequency Hz	Multiplier ($\sqrt{r_n}$)
50	0.83
100	1.00
200	1.10
300	1.125
400	1.15
1000	1.19
≥2000	1.20

RELIABILITY

The 114/115 series capacitors are the result of an extensive programme of development and testing. As such, they are highly reliable and if properly selected will give long and predictable service. As with all components, however, some failures will occur during the designed service life. For 114/115 series capacitors, this rate of failure is extremely low and relatively constant, and is an indication of reliability.

After a certain time, gradual changes in the properties of the capacitors reach a point signified by a sudden and marked increase in the failure rate. The time taken for this to occur is a measure of the life expectancy of the capacitors.

Fig.7 shows a curve of failure rate as a function of time. The curve can be divided into three distinct zones:

A) failures during manufacture and burn-in procedure (infant mortality);
B) failures during service life;
C) failures at the end of useful life (wear-out period).

For 114/115 series electrolytic capacitors, the failure rate during service life (60% confidence level) at 40°C and rated voltage is 1×10^{-7}/h (catastrophic failures). Temperature and voltage derating have a relatively small influence on this figure. A voltage derating of 50% reduces the failure rate by a factor of approximately 4.5, while a reduction in ambient temperature of approximately 15°C reduces it by a factor of 2.

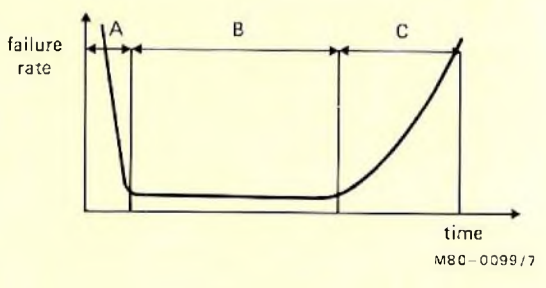

Fig.7 Failure rate as a function of time

SERVICE LIFE

As indicated above, the life expectancy/service life (region B of Fig.7) is largely determined by the core temperature, and for capacitors operated at the maximum core temperature of 95°C, the life expectancy is typically 10 000 h. By lowering the core temperature the life expectancy can be extended, each 10°C reduction in the core temperature resulting in a doubling of the life expectancy. Thus a core temperature of 85°C gives a life expectancy of about 20 000 h, while a core temperature of 50°C gives a life expectancy of some 200 000 h, equivalent to approximately 25 years of continuous operation. The guaranteed lifetime (standard endurance test) is 5000 h at an ambient temperature of 85°C.

A specified extended life expectancy can be obtained by selecting a capacitor to operate at the appropriate core temperature. The method of capacitor selection is best illustrated by an example.

Example – Selection of capacitor for extended life expectancy

Required voltage rating	385 V
Operating frequency	300 Hz
Ambient temperature	60°C
Required ripple current	3 A
Required extended life expectancy	40 000 h

The first step is to determine the ripple current at 100 Hz equivalent to the required ripple current at the operating frequency of 300 Hz. From Eq.3 and Table 4:

$$I_1 = \frac{3}{1.125},$$

$$I_r = 2.7 \text{ A}.$$

To obtain an extended life expectancy of 40 000 h, a capacitor must be selected that will have a maximum core temperature of 75°C, when operated with a ripple current of 2.7 A (referred to 100 Hz), at an ambient temperature of 60°C. The maximum allowable ripple current for an ambient temperature T and a core temperature θ, $I_{r(T,\theta)}$, can be obtained by generalising Eq.2 to

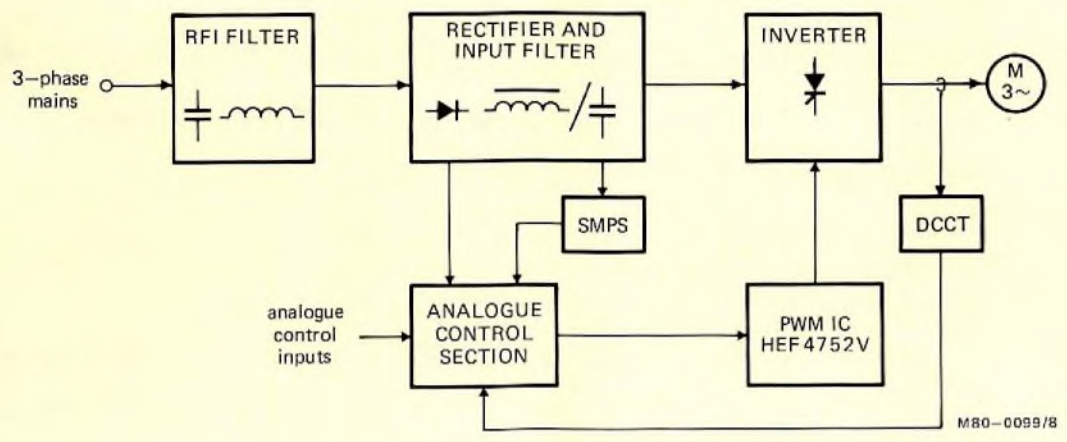

Fig.8 PWM motor drive system

give:

$$I_{r(T,\theta)} = I_R \sqrt{\left(\frac{\theta - T}{10}\right)} . \qquad (4)$$

Substituting for $I_{r(T,\theta)}$, T, and θ, and rearranging to obtain I_R (the rating of the required capacitor) gives:

$$I_R = 2.7 \sqrt{\left(\frac{10}{75 - 60}\right)} ,$$

$$I_R = 2.2 \text{ A.}$$

From Table 2, the required capacitor can be identified as the 330 μF type.

PRINCIPAL APPLICATION AREAS

The 114/115 series capacitors will be used principally in a.c. motor speed control systems and switched-mode power supplies (SMPS). Before introducing the associated ripple current design equations, representative examples of these systems are briefly described.

PWM control of a.c. motors

A block diagram of the PWM a.c. motor speed control system (Refs.1 to 5) is shown in Fig.8. The three-phase mains input is connected to the bridge rectifier via an interference filter. The rectified mains is smoothed by an input filter, and provides a fixed d.c. supply for the inverter. For powers of less than about 4 kW, a capacitor input filter would normally be used, with a choke input filter being employed at higher powers. The output from the inverter consists of three-phase sinewave-weighted pulse-width-modulated waveforms at the selected carrier frequency; this produces sinusoidal motor currents with low harmonic content. The waveforms are synthesised by a purpose-designed LSI circuit, type HEF4752V.

Switched-mode power supplies

Switched-mode power supplies operate at a high switching rate (typically 30 kHz). The transformer required is therefore small compared with 50 Hz types so that the introduction of SMPS has resulted in a considerable reduction in the size and weight of stabilised power supplies operated from single- and three-phase mains. The basic circuit of a forward converter switched-mode power supply is shown in Fig.9.

The mains supply is rectified and smoothed by the capacitor to provide the d.c. link for the high-frequency power switch. The mark/space ratio of this switch is under the control of a feedback loop, providing a constant voltage output within a designed range of load current.

RIPPLE CURRENT DESIGN EQUATIONS

The required ripple current rating of the input smoothing capacitors in both PWM speed control and SMPS, can be analysed by means of the equivalent circuit shown in Fig.10. Referring to Fig.10, by Kirchoff's current law:

$$i_{CAP} = i_{IN} - i_{OUT}, \qquad (5)$$

where i_{CAP} is the instantaneous capacitor current, i_{IN} is the instantaneous current in the capacitor input circuit, and i_{OUT} is the instantaneous current in the capacitor output circuit. If the a.c. components of these currents

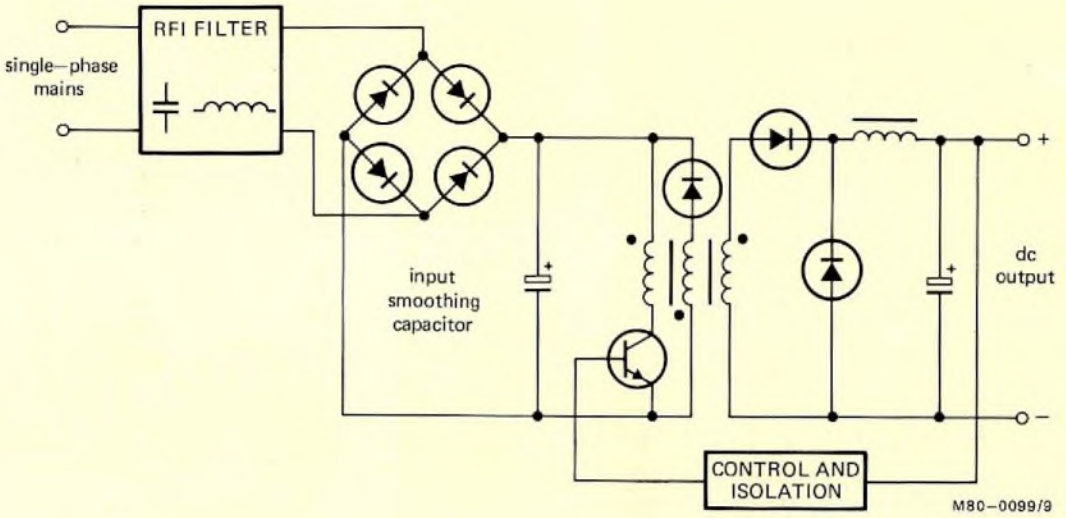

Fig.9 Basic forward converter switched-mode power supply

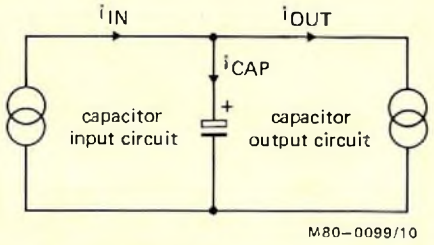

Fig.10 Equivalent circuit for analysis of capacitor ripple currents

are denoted by i_{cap}, i_{in}, and i_{out} respectively, then it can be shown that:

$$\overline{i^2}_{cap} = \overline{i^2}_{in} + \overline{i^2}_{out}, \qquad (6)$$

where $\overline{i^2}_{cap}$ is the mean-square value of i_{cap}, and $\overline{i^2}_{in}$ and $\overline{i^2}_{out}$ are similarly defined. The square-root of $\overline{i^2}_{cap}$ is the r.m.s. value of the capacitor ripple current, so that if $\overline{i^2}_{in}$ and $\overline{i^2}_{out}$ are known for a given circuit configuration, then from Eq.6 the capacitor ripple current can be determined.

Calculation of $\overline{i^2}_{in}$

Expressions for $\overline{i^2}_{in}$ are given for choke input filters with three-phase full-wave rectified supplies (PWM speed control applications), and capacitor input filters with single- and three-phase rectified supplies (PWM speed control and switched-mode power supply applications).

Choke input filters

A choke input filter is used for powers greater than about 4 kW. With a choke input filter, a smaller capacitor may be used giving a lower filter cost at these power levels. The choke input filter has the added advantage of giving continuous diode conduction, which reduces the peak forward current rating required by the rectifier diodes. Continuous diode conduction in a three-phase full-wave rectifier requires an inductance with a value greater than that defined by:

$$L_{crit} = \frac{V_{dc}}{110.6 \times I_{dc} \times f_{IN}}, \qquad (7)$$

where V_{dc} is the average d.c. supply voltage, I_{dc} is the average d.c. link current, and f_{IN} is the ripple frequency of the rectified supply voltage. For a choke inductance L, where L is greater than or equal to L_{crit}, the value of $\overline{i^2}_{in}$ is given by:

$$\overline{i^2}_{in} = \frac{V^2_{dc} \times 42 \times 10^{-6}}{f^2_{IN} \times L^2}. \qquad (8)$$

Capacitor input filters

At power levels of less than about 4 kW, the capacitor input filter is a more attractive option than the corresponding choke input filter design. The cost is lower, and the impedance (viewed from the converter side) is lower, giving improved stability for inverter/motor loads in PWM motor control systems.

For both single- and three-phase full-wave rectified supplies with uniform input current pulses to the capacitor:

$$\overline{i^2}_{in} = \left(\frac{\pi^2}{8\delta_{IN}} - 1 \right) I^2_{dc}, \qquad (9)$$

where δ_{IN} is the capacitor input waveform duty cycle. The value of δ_{IN} can be calculated from:

$$\delta_{IN} = \frac{a_{IN}}{D}, \quad (10)$$

where a_{IN} is the diode conduction period, and D is the maximum diode conduction period. For single-phase full-wave rectified supplies D = 10 ms, and for three-phase full-wave rectified supplies D = 3.3 ms.

If the current pulses of the input current waveform are not identical, then:

$$\overline{i^2}_{in} = \frac{1}{2mD}\left(\sum_{k=1}^{m} I^2_{INP(k)} \times a_{IN(k)}\right) - I^2_{dc}, \quad (11)$$

where m is the number of differing current pulse amplitudes (m = 2 for a single-phase full-wave rectified supply and m = 3 for a three-phase full-wave rectified supply), $I_{INP(k)}$ is the peak value of the k^{th} input current pulse, and $a_{IN(k)}$ is the diode conduction period for the k^{th} input current pulse.

Calculation of $\overline{i^2}_{out}$

Expressions for $\overline{i^2}_{out}$ are given for the HEF4752V PWM speed control system, and flyback converter, forward converter, and push-pull converter switched-mode power supplies.

PWM a.c. motor speed control applications

The value of $\overline{i^2}_{out}$ for a.c. motor speed control applications depends on the inverter switching frequency selected, the 'filter' time-constant of the particular motor used, and the load condition of the motor, the maximum value of $\overline{i^2}_{out}$ occurring at full load. For systems using the HEF4752V PWM method of speed control, standard 380 V mains supplies, and the corresponding motors, then at full load the following empirical formula gives a good approximation for $\overline{i^2}_{out}$:

$$\overline{i^2}_{out} = 0.25 \times I^2_{dc}. \quad (12)$$

SMPS applications

In a conventional flyback converter with bifilar windings to protect the power transistors against overvoltage, the value of $\overline{i^2}_{out}$ is given by:

$$\overline{i^2}_{out} = \left(\frac{4}{3\delta_{OUT}} - 1\right) I^2_{dc}, \quad (13)$$

where δ_{OUT} is the capacitor output waveform duty cycle; $0 < \delta_{OUT} \leq 0.5$.

The conventional forward converter with bifilar windings for magnetisation energy recovery and transistor voltage protection, has a value $\overline{i^2}_{out}$ which is given by:

$$\overline{i^2}_{out} = \left(\frac{1}{\delta_{OUT}} - 1\right) I^2_{dc}. \quad (14)$$

For the conventional push-pull converter, the value of $\overline{i^2}_{out}$ is given by:

$$\overline{i^2}_{out} = \left(\frac{1}{2\delta_T} - 1\right) I^2_{dc}, \quad (15)$$

where δ_T is the duty cycle of either of the transistor drive waveforms; $0 < \delta_T \leq 0.5$.

RIPPLE CURRENT MEASUREMENT

To verify the above design equations, measurements of ripple current were made on three representative power systems and the results compared with the theoretically predicted values. The three systems were:

1) a 4 kW PWM speed control system with a choke input filter;
2) a 4 kW PWM speed control system with a capacitor input filter;
3) a 300 W forward converter switched-mode power supply with a capacitor input filter.

In each case, a suitable starting value for the smoothing capacitor was selected by a preliminary measurement of the capacitor ripple current. The calculation and measurement of the three ripple currents are described in detail for the 4 kW PWM system with a choke input filter. The corresponding results for the remaining two systems are summarised in tabular form.

4 kW PWM speed control system with choke input filter.

The test circuit is shown in Fig.11. The r.m.s. values of the three ripple currents were measured using an a.c. current probe, the calibration of the probe being checked against a thermal ammeter connected in series with the capacitor. The voltage-sharing resistors R_1 and R_2 ensure equal voltage division between the two capacitors. Measurements were made at the full-load condition of 4 kW, which corresponds to the maximum capacitor ripple current. With a three-phase full-wave supply, f_{IN} is 300 Hz, the measured value of V_{dc} was 538 V, and the corresponding value of I_{dc} was 10 A. A value of inductance slightly greater than the critical value was used, ensuring continuous current flow in the rectifier. In the following calculations the r.m.s. values of the a.c. components of the ripple currents are denoted by I_{in}, I_{out}, and I_{cap}.

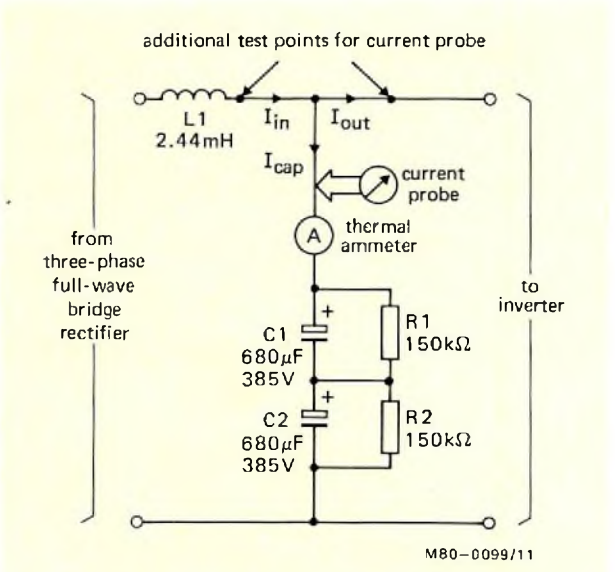

Fig.11 Test circuit for 4 kW PWM speed control system with choke input filter

I_{in}

From Eq.8:

$$\overline{i^2}_{in} = \frac{538^2 \times 42 \times 10^{-6}}{300^2 \times (2.44 \times 10^{-3})^2},$$

$$= 22.69 \text{ A}^2,$$

or: $$I_{in} = 4.76 \text{ A}.$$

This compares with the measured value of 4.8 A.

I_{out}

From Eq.12:

$$\overline{i^2}_{out} = 0.25 \times 10^2,$$

$$= 25 \text{ A}^2,$$

or:

$$I_{out} = 5.00 \text{ A}.$$

This compares with the measured value of 4.9 A.

I_{cap}

From Eq.6:

$$\overline{i^2}_{cap} = 22.69 + 25,$$

$$= 47.69 \text{ A}^2,$$

or:

$$I_{cap} = 6.91 \text{ A}.$$

This compares with the measured value of 6.8 A.

Capacitor selection using calculated ripple currents

It is clear from the above calculations that the ripple current design equations for a PWM speed control system with a choke input filter give calculated ripple currents which are in very close agreement with the corresponding measured values. A confident selection of the appropriate capacitor for the 4 kW PWM speed control system can therefore be made solely on the basis of calculated ripple currents. The selection process is now illustrated.

For three-phase full-wave rectified mains, the frequency of the input ripple current is 300 Hz, and for the PWM speed control system this is also a typical value for the frequency of the output ripple current, since the maximum power usually occurs at an inverter output frequency of 50 Hz. From Table 4 the multiplying factor for 300 Hz is 1.125, so that, applying Eq.3, the calculated input and output ripple circuits are equivalent to a 100 Hz ripple current given by:

$$I_r = \sqrt{\left(\frac{22.69}{1.125^2} + \frac{25}{1.125^2}\right)},$$

$$= 6.1 \text{ A}.$$

Assuming a maximum ambient temperature of 60°C and a required life expectancy of 40 000 h, then from Eq.4:

$$I_R = 6.1 \sqrt{\left(\frac{10}{75-60}\right)} = 5 \text{ A}.$$

From Table 2, the 1000 μF type (I_R = 7 A) is therefore required.

Because the ripple current rating of the selected capacitor exceeds the rating required by the assumed operating conditions, some relaxation of these conditions is clearly possible. If the required life expectancy is fixed at 40 000 h, then the maximum ambient temperature can be obtained by treating T as the unknown in Eq.4:

$$T = 75 - 10\left(\frac{5}{7}\right)^2,$$

$$T = 69.9°\text{C}.$$

Alternatively, if the maximum ambient temperature is limited to 60°C, then the minimum core temperature (and hence maximum life expectancy) can be obtained by treating θ as the unkown in Eq.4:

$$\theta = 60 + 10\left(\frac{5}{7}\right)^2.$$

$$\theta = 65.1.$$

A life expectancy of very nearly 80 000 h will thus be obtained.

4 kW PWM speed control system with capacitor input filter

The test circuit is shown in Fig.12, and the relevant circuit measurements and calculations are summarised in Table 5. The calculated value of I_{in} was obtained from Eq.11, and the calculated value of I_{out} was obtained from Eq.12. The peak values of the input current pulses and the diode conduction periods were obtained from Fig.14.

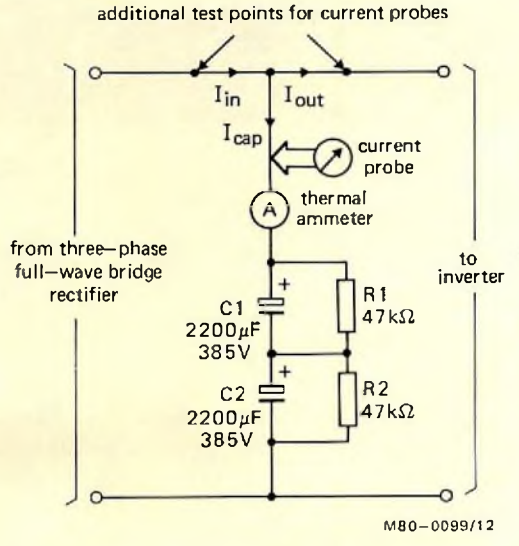

Fig.12 Test circuit for 4 kW PWM speed control system with capacitor input filter

300 W forward converter switched-mode power supply with capacitor input filter

The test circuit is shown in Fig.13, and the relevant circuit measurements and calculations are again summarised in Table 5. The value of I_{in} was calculated from Eq.9, with the value of δ_{IN} being obtained from Fig.15. Equation 14 was used to calculate I_{out}, and the capacitor output waveform duty cycle δ_{OUT} was obtained from Fig.16.

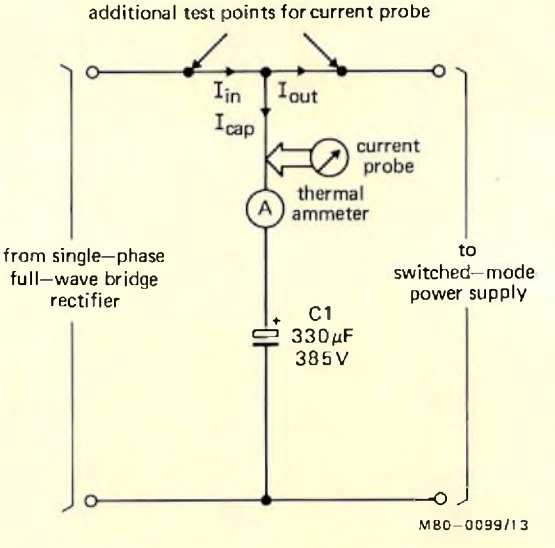

Fig.13 Test circuit for 300 W switched-mode power supply with capacitor input filter

TABLE 5

Data for circuits of Figs.12 and 13

	Fig.12		Fig.13	
Average d.c. supply voltage	540	V	275	V
Average d.c. link current	10	A	1.34	A
Measured r.m.s. value of a.c. component of capacitor input current	12.3	A	2.4	A
Calculated r.m.s. value of a.c. component of capacitor input current	12.14	A	2.66	A
Measured r.m.s. value of a.c. component of capacitor output current	4.9	A	2.1	A
Calculated r.m.s. value of a.c. component of capacitor output current	5.0	A	2.05	A
Measured r.m.s. capacitor ripple current	13.2	A	3.2	A
Calculated r.m.s. capacitor ripple current	13.13	A	3.36	A
Frequency of capacitor input ripple current	300	Hz	100	Hz
Frequency of capacitor output ripple current	300	Hz	30	kHz

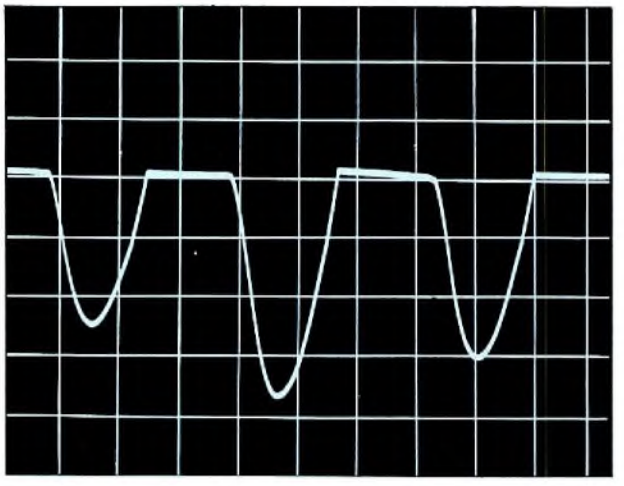

Fig.14 Capacitor input current waveform (asymmetrical) for PWM speed control system with capacitor input filter
Horizontal scale: 1 ms/division
Vertical scale: 10 A/division

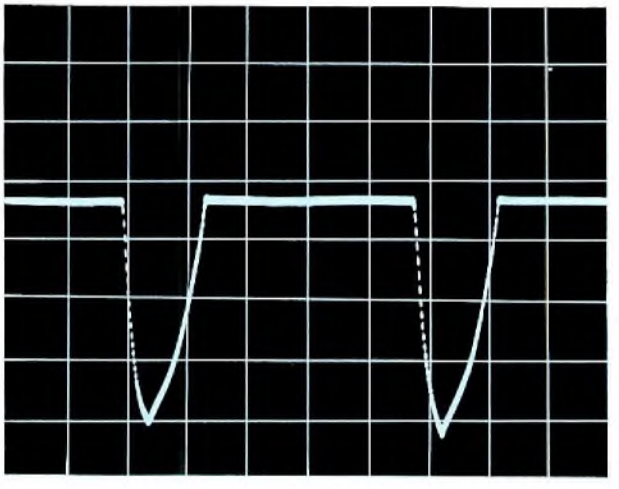

Fig.15 Capacitor input current waveform (symmetrical) for 300 W forward converter switched-mode power supply with capacitor input filter
Horizontal scale: 2 ms/division
Vertical scale: 2 A/division

This article is the sixth in a series covering various aspects of our PWM variable speed drive. The seventh, and final, article in the series will be devoted to the switched-mode power supply.

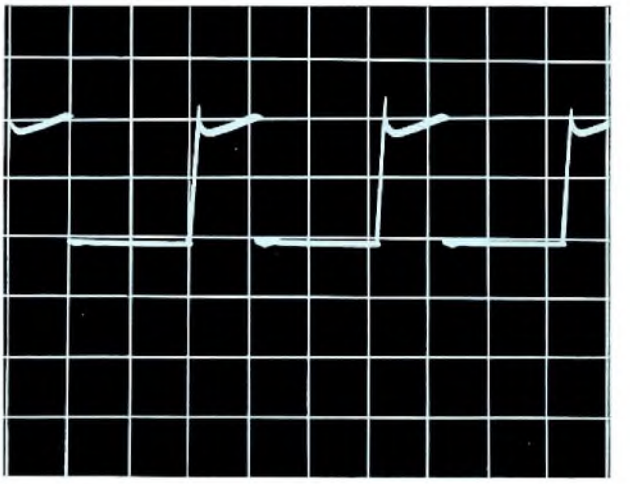

Fig.16 Switching stage collector current for 300 W forward converter switched-mode power supply
Horizontal scale: 10 μs/division
Vertical scale: 2 A/division

ACKNOWLEDGEMENT

The authors wish to thank D. Fidder and H. Voeten of Philips Zwolle, and L. Hampson of the Mullard Application Laboratory Mitcham, for technical assistance with this article.

REFERENCES

1. HOULDSWORTH, J.A. and ROSINK, W.B., Introduction to PWM speed control system for 3-phase AC motors', Electronic Components and Applications, Vol.2, No.2, February 1980, pp.66 to 79.
2. BURGUM, F. and NIJHOF, E.B.G., Inverter circuit for PWM motor speed control system', Electronic Components and Applications, Vol.2, No.3, May 1980, pp.130 to 142.
3. STARR, B.G. and van LOON, J.C.F., 'LSI circuit for AC motor speed control', Electronic Components and Applications, Vol.2, No.4, August 1980, pp.219 to 229.
4. ROSINK, W.B., 'Analogue control system for an AC motor with PWM variable speed drive', Electronic Components and Applications, Vol.3, No.1, November 1980, pp.6 to 15.
5. HOULDSWORTH, J.A., 'Purpose-designed ferrite toroids for isolated current measurement in power electronic equipment', Electronic Components and Applications, Vol.3, No.2, February 1981, pp.101 to 109.

Bandswitching diode for a.m. radios

The mechanical waveband switch in a.m. radios has been giving faithful service for many years. It is bidirectional and has low series resistance and capacitance. It is, however, space consuming, costly to manufacture, and subject to wear and contamination; and, since it must be located close to the tuned circuit it controls, it must be either positioned where it is inconvenient to operate or connected to its manual control via a mechanical linkage. We have now overcome this last barrier to the construction of entirely solid-state radios by developing a.m. band-switching diode BA423 to replace the mechanical switches that are customarily used to select the long, medium, and short wavebands. The following features of the BA423 enable it to overcome all the drawbacks of the mechanical switch and to offer several additional advantages.

- High reliability and long life.
- Its steep V/I characteristic and long minority charge carrier lifetime result in a low forward a.c. resistance at a.m. radio frequencies. The low forward resistance is achieved with a low-level forward bias voltage applied to the diode. The low-level voltage for the required forward bias is available in mains-powered a.m. radios and even in car radios where the d.c. supply is only 12 V.
- Its low forward resistance causes minimum losses when connected in series with the coil of a parallel tuned circuit.
- The low capacitance in parallel with its high-resistance reverse-biased junction prevents spurious resonances within the selected waveband.
- It can be switched by a direct voltage from a simple, conveniently positioned switch, or by remote switching or microcomputer.

A circuit arrangement for the BA423 in a m.w./l.w. radio is given in Fig.4. If the Q of the m.w. tuned-circuit with C_1 set to 200 pF is assumed to be 80 with the diode short-circuited, the inherent series resistance of the tuned circuit is

$$R_S = \frac{Z}{Q} = \frac{\sqrt{(L_1/C_1)}}{80} = 12.5\Omega$$

When the diode is connected into the circuit, its forward current is

$$I_F = \frac{V_B - V_F}{R_1} = \frac{7 - 0.9}{620} = 10\,\text{mA}$$

At this current, Fig.2 shows that the forward resistance (r_D) of the diode is 0.9Ω. The Q of the m.w. tuned

Brief specification for the BA423

Forward current (d.c.):	I_F max	50 mA
Forward voltage at I_F max:	V_F max	0.9V
Series resistance (f = 1 MHz)	r_D typ	
at I_F = 2 mA:		2.2Ω
at I_F = 5 mA:		1.3Ω
at I_F = 10 mA:		0.9Ω (1.2Ω max.)
Continuous reverse voltage:	V_R max	20 V
Reverse current at V_R max:	I_R max	100 nA
Diode capacitance	C_d max	
at V_R = 3 V, f = 1 MHz:		2.5 pF (1.6 pF typ.)
C_d/V_R curve:		Fig.1
Junction temperature:	T_j max	150 °C
Thermal resistance:	$R_{th\ j\text{-}a}$	400 K/W
Envelope:		submin. glass SOD 68

circuit with C_1 set to 200 pF is therefore reduced from 80 to

$$Q = \frac{Z}{R} = \frac{\sqrt{(L_1/C_1)}}{R_s + r_D} = 74.6$$

This is only about 7% less than the Q without the diode, which means that the introduction of the diode has little effect on the selectivity of the tuned circuit.

When the diode is reverse-biased with 3 V (l.w. operation), Fig.1 shows that its capacitance will be about 1.6 pF. This low capacitance, together with other parasitic capacitances and the m.w. coil, cause a spurious resonance at about 2.8 MHz which is well above the upper frequency limit of the long-wave band.

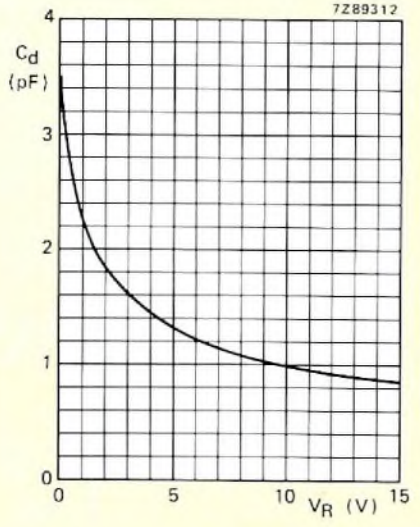

Fig.1 Typical diode capacitance as a function of reverse voltage; f = 1 MHz, T_j = 25 °C.

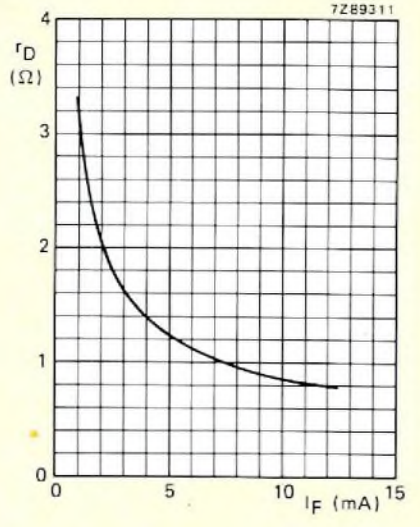

Fig.2 Typical forward a.c. resistance as a function of forward current; f = 1 MHz, T_j = 25 °C.

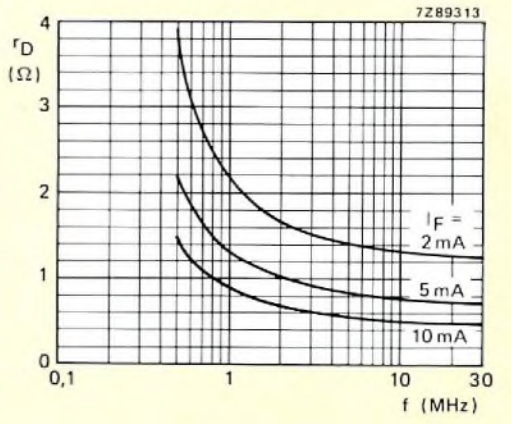

Fig.3 Typical forward a.c. resistance as a function of frequency, with forward current as parameter.

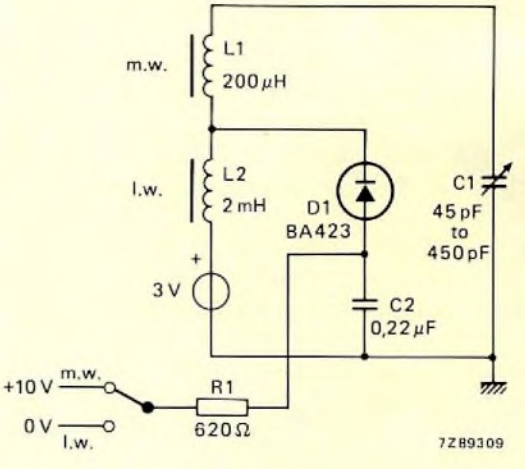

(a) Circuit arrangement

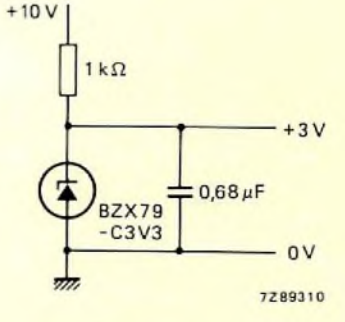

(b) Typical voltage source

Fig.4 Operating principles of diode band switching.

To radiate a useful signal from the antenna the output stages of a broadcasting transmitter must be capable of generating powers up to several hundred kilowatts. Only thermionic tubes can handle such powers, and today, as in the past, all broadcast transmitters use thermionic output stages. Our transmitting tubes are designed to meet the severe demands of modern transmitters: grid construction and metallurgy ensure stable operation by providing low primary and secondary emission and high thermal emissivity; and advanced cathode and envelope design enhances reliability and prolongs life.

Transmitting tubes for radio and TV broadcasting

D. VAN HOUWELINGEN and J. C. VAN WARMERDAM

Modern transmitters demand a lot from their hardware, particularly from the output stages, which may have to generate powers approaching megawatt levels. The transmitting tubes used in these stages, commonly tetrodes, must be able to generate these powers, and must continue to do so, without trouble, for more than 10 000 operating hours – a period that may span several years of operation.

The wide range of transmitting tubes available today (from those producing a few kilowatts to the 500 kW models used in large transmitters and high energy physics) is a result of continuous innovation over the last half century. With few exceptions, there have been no major breakthroughs in transmitting tube design, just steady improvement. The table lists our current range of transmitting tubes for radio and tv broadcasting. The power ratings given in the table represent the anode output power; the power delivered to the load will depend upon circuit efficiency. In the design of these tubes, particular attention has been paid to cathode, grid and envelope construction, since these contribute greatly to the performance.

Tubes for radio and TV transmitters and transposers

	VHF transmitters		VHF transposers		UHF transmitters		UHF transposers		AM	
	output power (kW)	gain (dB)	output power (kW)	gain (dB)	output power (kW)	gain (dB)	output power (kW)	gain (dB)	output power (kW)	gain (dB)
YL1540	1.1	20								
YL1440	1.5	14.1	0.55	14.8						
YL1420	8.6	13.8	2.5	14.8						
YL1430	18.4	14	7	15						
YL1520	27.5	14.5	10.5	16.2						
YL1610	12	17								
YL1630	38	17	20	17						
YL1590					0.6	15.4	0.22	15.6		
YL1560					5.5	16.5	2.2	16.5		
YL1580					12	17	4.4	17		
YL1640									125	21
YL1660									520	21

VHF/UHF figures apply to sync level, AM figures to carrier level.

CATHODE DESIGN – RIGID OR FLEXIBLE?

The tubes use a directly-heated cylindrical mesh cathode (Fig.1) of carburised thoriated-tungsten. The cathode must maintain its size and shape over the life of the tube, at operating temperatures up to 1800 °C. It must therefore be rigid enough not to sag at high temperatures, and flexible enough to withstand the compressive and tensile stresses introduced by the thermal inertia of its supports during the rapid heating and cooling that occurs when the tube is switched on and off.

The rigidity (C) of a cylindrical mesh structure depends on its diameter, on the number, thickness, and length of the wires forming it, and on the ratio of welded to total wire crossings. When the structure is fixed at both ends it experiences a maximum gravitational stress (due to its weight), σ_1, inversely proportional to C, and a maximum deformation stress (due to its expansion relative to the supports), σ_2, directly proportional to C and to its length.

Fig.1 Cylindrical mesh cathode

Figure 2 shows how σ_1 and σ_2 vary with C. Their upper limits $\hat{\sigma}_1$ and $\hat{\sigma}_2$ depend, among other things, on the physical properties of the mesh material, and must be determined experimentally. A gravitational stress greater than $\hat{\sigma}_1$, which occurs when C is less than C_1, means that the structure is too flexible and will sag at high temperature. Increasing the structure's rigidity by increasing C will cure this. But if C exceeds C_2, the deformation stress will exceed $\hat{\sigma}_2$; the structure is then too rigid and will very likely fracture when the tube is switched on or off. So the cathode must be designed with C between C_1 and C_2. For the smaller tubes this presents no problem, since a wide margin exists between C_1 and C_2. This margin gets less, however, as cathode length increases,

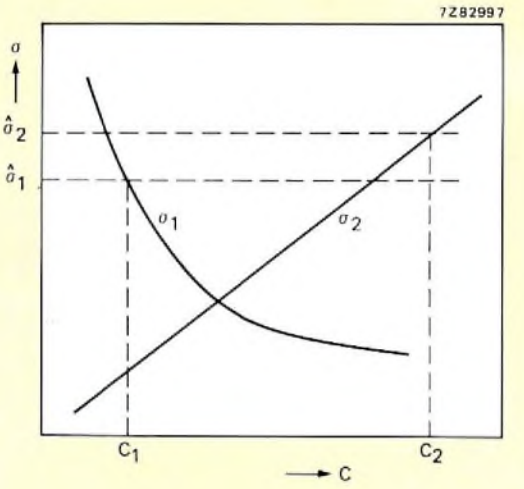

Fig.2 Gravitation stress σ_1 and deformation stress σ_2 experienced by the cathode mesh, both as a function of its rigidity C. When C is less than C_1, the mesh is too flexible and will sag at high temperature; when C is greater than C_2, the mesh is too rigid and will very likely fracture when the tube is switched on or off

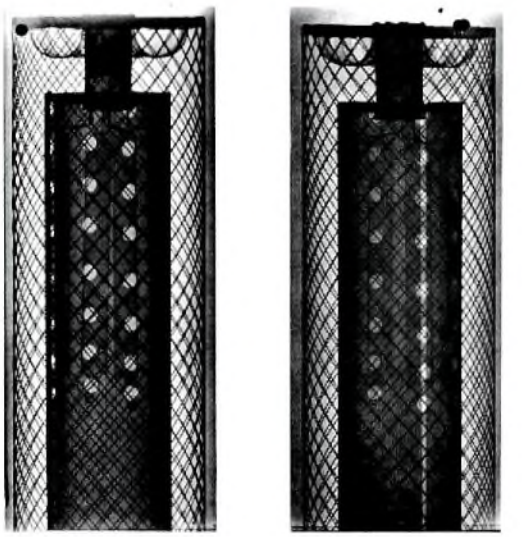

Fig.3 X-ray photograph of a rigid cathode fixed at one end and flexibly mounted at the other end, (a) zero hour and (b) after 8145 hours and 24 435 switching cycles

and above a certain length (about 200 mm), it effectively disappears. For such cathodes, a compromise between the required rigidity and flexibility is impossible to achieve. So these cathodes are either too flexible to maintain their shape at high temperature, or too rigid to withstand the stresses introduced during fast on or off switching.

To overcome this problem, our high power tubes with cathodes longer than 200 mm use a rigid cathode fixed at one end and flexibly mounted at the other. The unrestricted axial expansion this construction allows, entirely eliminates the deformation stresses in the mesh. This construction has so far proved highly successful, as indicated by the X-ray photographs shown in Fig.3.

There is no doubt that careful attention to cathode design pays handsome dividends. Not only does it improve the reliability and stability of the tubes in operation, it also minimises the risk of failure when switching them on and off. With most of our transmitting tubes, the full filament voltage can be applied immediately upon switching on, no warm-up time or switch-on procedure being needed.

THE K-GRID

The grids, usually in the form of a squirrel cage, surround the cathode and are radially aligned with each other to limit obstruction of the electron beam. Their operating conditions, and their proximity to the hot cathode (essential for efficient high-frequency operation) impose severe demands upon them. Not only do they absorb a high proportion of the heat radiated by the cathode, they also intercept the electron beam, converting a significant part of its kinetic energy into heat. Moreover, high-frequency capacitive currents flowing in the grids result in further generation of heat.

The net result is that the grids are forced to work at temperatures in the region of 1200 °C. Their primary and secondary emission must, however, be low, and must remain low even after contamination by material evaporated from the cathode (which inevitably occurs as the tube ages). In addition, their evaporation and mechanical stability must remain within acceptable limits throughout the life of the tube.

To meet these requirements, we introduced the K-grid about 25 years ago (Refs 1 and 2). The K-grid is a spot welded structure of molybdenum wire, doped to prevent brittleness and re-crystallization. To relieve stress, the grid is fired at 1500 °C. After this it is baked at over 2000 °C to de-gas the molybdenum wire and increase its ductility. The grid is then coated with zirconium carbide (sintered at about 2000 °C), and finally with platinum.

The grid is mechanically very stable, and exhibits no signs of brittleness or re-crystallization, even after extensive use. The high work function provided by the platinum reduces primary emission to a minimum. Moreover, the surface structure of the grid material helps to keep secondary emission low, and its high thermal emissivity (about 90%) means that even at grid loadings as high as 25 W/cm^2, grid temperatures rarely exceed 1300 °C.

In the 25 years the K-grid has been in use it has amply proved itself; even today its performance is comparable with that of more recently developed grids (for example the pyrolytic graphite grid).

THE ENVELOPE

To describe the external structure of a transmitting tube as an envelope is to some extent misleading, since it not only encloses the working components of the tube but is itself a functional part of it. It comprises the copper anode, the coaxial connections for the grids and cathode, and the ceramic insulators.

The anode

The compact design of a modern transmitting tube means that the anode often has to contend with extremely high heat densities, so it is usually the largest and most massive structure in the tube. Its inside is blackened to increase its absorptivity and assure stable tube operation.

Anode cooling

The anode may be cooled by water or by air. Water cooling (either in liquid or vapour phase) is generally preferred for high power tubes (above say 50 kW). In the design shown in Fig.4, water is constrained by a surrounding jacket to flow through spiral grooves machined in the anode's outer surface. Anodes of this design can dissipate more than 1kW/cm^2 from their inner surfaces. They are quiet and reliable (especially if operated with a closed cooling system containing water of high purity). Vapour-cooled anodes offer no particular advantage over this design, and they do have the added complication of needing a boiler.

Fig.4 A water-cooled anode is quiet and efficient, and can dissipate more than 1 kW/cm^2 from its inner surface

Fig.5 Forced-air-cooled anodes have copper fins brazed to their outsides. They can dissipate powers up to about 500 W/cm^2

Lower power tubes usually use forced-air-cooled anodes (Fig.5). These have copper cooling fins brazed to their outsides. Forced-air-cooled tubes have a maximum dissipation of about 500 W/cm^2 (on the inner surface of the anode). They are highly reliable and are therefore popular in systems where maintenance may be infrequent (in unmanned transposer stations for instance), and in systems remote from water supplies or working in sub-zero conditions.

Coaxial connections and ceramic insulators

The cathode and grids are mounted on ring-shaped Kovar terminals, coaxially arranged on high-purity alumina insulators. The insulators are metallised to allow them to be brazed to the Kovar terminals (which are silver coated to increase their conductivity).

This construction is sturdy, and ensures that the inductance is low (especially important at high frequencies). The use of low-loss ceramic results in minimum capacitive current heating of the insulators. Moreover, the high melting point of alumina means that the tubes can be efficiently de-gassed at high temperature, allowing a good and enduring vacuum to be obtained (better than 10^{-4} Pa, maintained by getters located inside the tube).

The brittleness of alumina is, however, a potential cause of failure. Slight structural flaws, not in themselves fatal, can act as stress raisers, and can in time lead to fracture. The risk of such fracture can be significantly reduced, however, by minimising the stresses within the insulators.

Designing for minimum stress

The stresses set up as a result of a flaw can be described in terms of the stress intensity factor K_I, which is proportional to the applied stress and the square root of the flaw size (Refs 3 and 4). A crack produced by this flaw will grow with a speed proportional to K_I^n, where for alumina n lies between 30 and 60 (see Fig.6).

If K_I exceeds a critical value K_{IC}, the crack propagates so quickly that fracture occurs almost immediately. So it is obvious that the ceramic insulators must be designed to ensure that K_I never exceeds K_{IC}. But this in itself is not enough; the long life of modern transmitting tubes means that even in the subcritical condition ($K_I < K_{IC}$), crack growth may ultimately lead to fracture. To prevent this, the applied stresses must be reduced as much as possible. Thanks to computer-aided design of the ceramic/metal construction, the ceramic insulators of our transmitting tubes are virtually stress-free.

Figure 7 illustrates the power of the computer-aided design technique. Figure 7(a) is a computer-generated analysis of the stresses occurring in a ceramic insulator at its maximum operating temperature (240 °C) induced mainly by the expansion of the copper anode. The figure clearly shows the highly stresses regions – the regions where fracture is more likely to occur. Redesigning the ceramic/metal construction as shown in Fig.7(b), completely eliminates these stresses, and in so doing, removes any chance of structural flaws within the ceramic causing fracture.

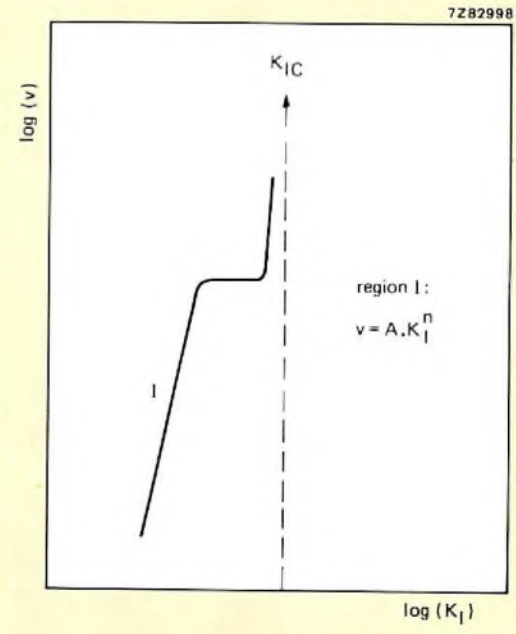

Fig.6 Variation of crack growth velocity (v) with stress intensity factor K_I. For K_I less than the critical value K_{IC} (in region I), v is proportional to K_I^n, where for alumina n lies between 30 and 60

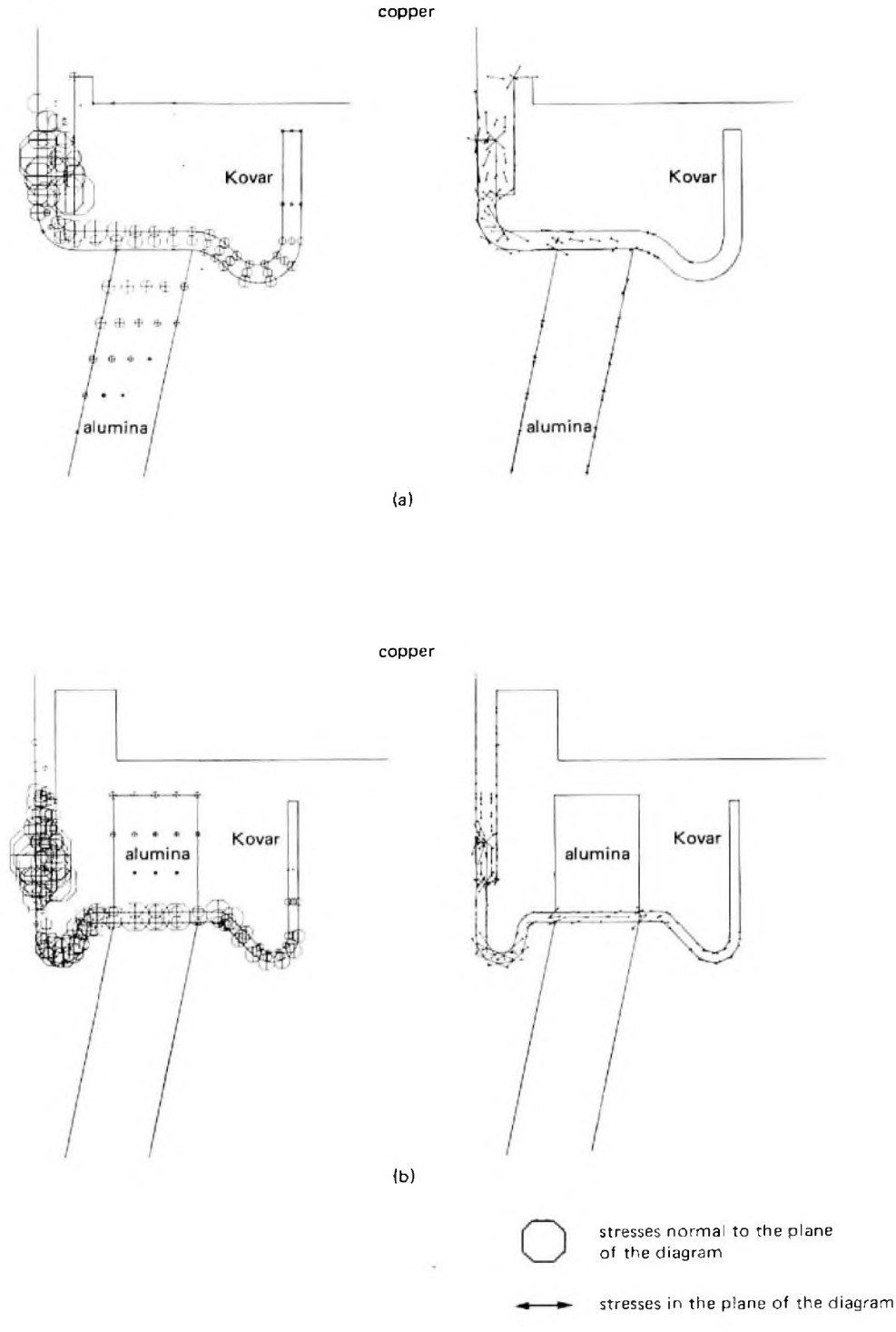

Fig.7 (a) Computer generated analysis of the stresses occurring in a ceramic insulator at its maximum operating temperature (240°C) showing the highly stressed regions; (b) Redesigning the ceramic/metal construction eliminates the dangerous stresses, removing the chance of structural flaws within the ceramic causing fracture

RELIABILITY

Transmitting tubes are expensive items, and customers rightly expect them to be reliable. Failures are inconvenient and often costly; so no effort is spared to make the product as reliable as possible.

This starts with the initial design, which must meet target specifications agreed between Development, Quality Control, Commercial and Production departments. Once development of a new tube is complete, pilot production begins, and continues until a quality consistent with the envisaged application is reached. This signals the release for full production, at which point the Development department hands over responsibility for the product to the Production department. This formal procedure ensures that the product attains its optimum quality before it is ever relased for production.

This, of course, is not the whole story. Line testing helps to maintain the quality by revealing adverse process trends and spotting defective components before they are passed on for further processing; final electrical testing makes sure that the completed tube meets its specification; and finally, life testing and customer feedback provide information on how the tubes perform in the field.

Line testing and final electrical testing

Line testing starts with inspection of incoming materials by the Quality Control department. It includes:

- checking the thoriated tungsten wire for thoria content, structure, thickness, weldability and ductility
- examining the copper and molybdenum wire for impurities that may influence performance
- measuring elastic constants (K_{IC}, strength etc.) of the ceramic insulators, as well as testing the quality of metallization and of brazing
- checking the dimensions of the cathode and grids, and the K-material coating of the grids for blemishes
- checking alignment of the grids after mounting.

The final electrical testing, performed on every tube at the end of the production run, includes the following measurements:

- filament current at nominal voltage
- cathode saturation current
- grid emission at grid loads higher than encountered in practice
- tube characteristics (by means of selected static measuremenets)
- vacuum (via related parameters)
- high-voltage behaviour
- output power and gain.

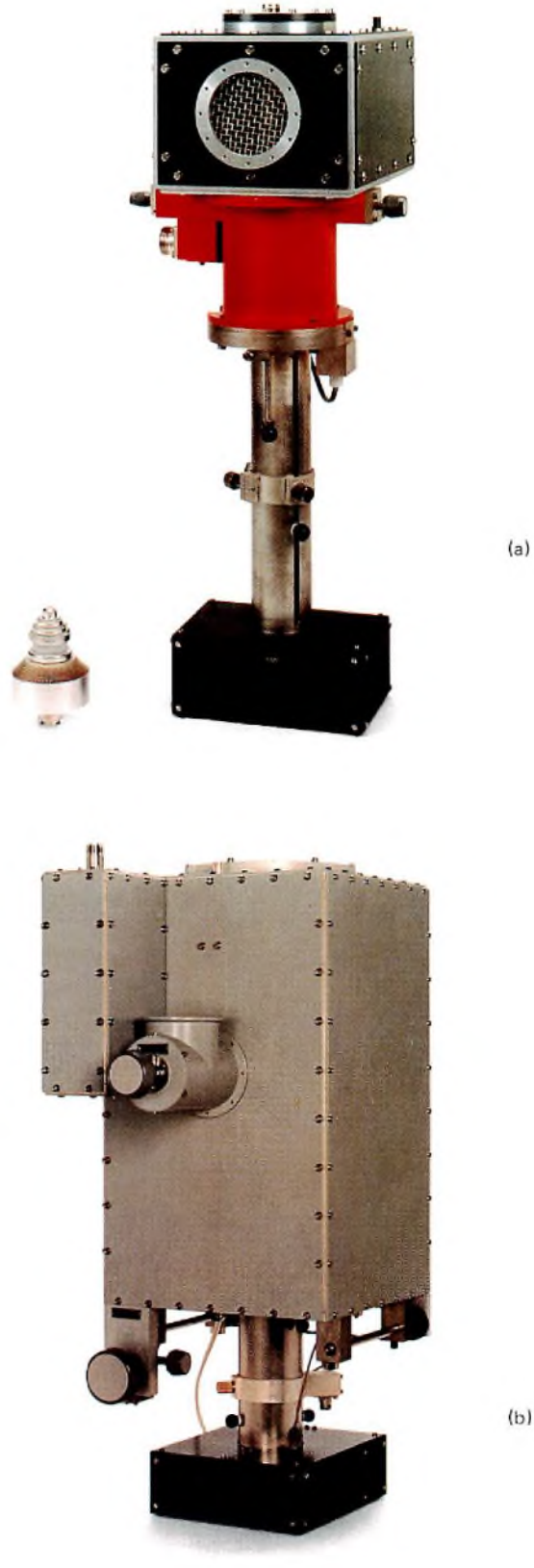

(a)

(b)

Fig.8 UHF cavities developed in our Application Laboratory.
(a) for the YL1590 and (b) for the YL1560

Life tests

Our Quality Control department performs life tests on randomly selected samples to assess the reliability of the tubes in their operating environment. The life tests usually relate to the published operating conditions, and include a regular on/off switching procedure. The long lifetime of the tubes, however, means that for the larger tubes at least (above about 20 kW), the cost of regular life testing is prohibitive. These tubes, therefore, normally undergo short life tests, the results of which are extrapolated to give an indication of actual lifetime.

Field data

There is no better way of assessing a product's reliability than by observing how it performs in the field. Our Development and Production departments, therefore, rely heavily on field data to supplement the data gathered from in-house life testing. The inclusion of customers' and users' experience in the quality-control feedback loop greatly increases the effectiveness of corrective action, and enables us to spot design or processing deficiencies that may not be initially apparent. Moreover, it enables the Quality Control department to monitor the reliability of our tubes.

APPLICATION SUPPORT

No transmitting tube works in isolation. Every tube works in a system the design of which is every bit as important as that of the tube (Fig.8). Our Applications Laboratory helps users to design and set up their systems, and provides support for systems already in use (see Ref.5 which describes a 500 kW r.f. amplifier for plasma research developed in our Application Laboratory).

If failures occur, they may be the fault of the tube, but they may also arise from incorrect operation. Should the latter be the case, the Application Laboratory is available to advise on the best corrective action. In this way, users get a double benefit: not only a very reliable tube, but a sound back-up services as well.

REFERENCES

1. KROL J. W. A., DBR-Auslegeschrift 1.021.502/1957.
2. DORGELO E. G., Le Vide, 67 (1957) 3-8.
3. DAVIDGE R. W., "Mechanical behaviour of ceramics". Cambridge University Press 1979.
4. EVANS A. G. and WIEDERHORN S. M., Int. Journ. of Fracture 10 (1974) 379-392.
5. ADAM J., KUUS H. and WARRINGA J. J. M., "Fusion Technology 1978". 207-262, Pergamon Press.

Abstracts

Miniature Plumbicon tube for portable TV cameras

Deposition of electrodes directly on the glass envelope considerably reduces the size of a new camera tube with 8 mm scan diagonal; together with its deflection coil it occupies a third the space of an 11 mm scan-diagonal tube, weighs a third as much, and consumes a quarter the power. The rigidity of the electrode structure affords a freedom from microphony that suit it especially for use in camera/recorder combinations.

Wideband, variable-persistence storage oscilloscope tube

In a storage oscilloscope tube, ions generated by flood electrons charge unwritten parts of the storage mesh and shorten the storage time. The described transfer-storage tube uses two meshes in cascade: a small-capacitance one for fast writing and a large-capacitance one for long storage. Maximum horizontal writing speed is 9 mm/ns; a quadrupole lens with a scan magnifying factor of 1.8 gives a vertical sensitivity of 5.3 V/cm.

High-fidelity and stereo/dual sound for TV

To achieve high-fidelity sound reception in a TV set it is necessary to reorganise the sound channel into a quasi-split system. Doing this also opens the way for the reception of forthcoming stereo/dual-sound transmissions. This article describes new integrated circuits for quasi-split sound systems and gives details of a decoder for stereo/dual sound which is under development. It also describes a circuit which simulates the new decoder, thereby allowing designers to build stereo/dual-sound channels before the integrated circuit embodying it becomes available.

Low output-capacitance Plumbicon tubes

The signal-to-noise ratio of a television camera increases as the output capacitance of the camera tube is reduced. In the new low output-capacitance Plumbicon tubes a smaller conductive film in the target reduces the intrinsic tube capacitance as well as the stray capacitance between target and yoke, giving about 3 dB improvement in S/N ratio.

Understanding GTO data as an aid to circuit design

The gate turn-off switch (GTO) combines the high blocking voltage and high switching current of the thyristor with the ease of gate drive and speed of the transistor. This article explains how to use the published GTO data to achieve the best possible performance.

Electrolytic capacitors for industrial applications

The 114/115 series electrolytic capacitors have been designed for rectified mains smoothing and energy storage in industrial applications. Detailed guidance on capacitor selection includes the two major applications areas: PWM motor speed control systems and switched-mode power supplies.

Transmitting tubes for radio and TV broadcasting

The design of modern transmitting tubes reflects the heavy demands imposed upon them by present-day transmitters. The tubes use special K-grids for low primary and secondary emission and high thermal emissivity. Moreover, computer-aided design of the ceramic/metal construction virtually eliminates stress in the ceramic insulators, reducing the risk of fracture.

Miniaturisierte Plumbicon-Röhre für tragbare Fernsehkameras

Durch direktes Auftragen der Eletroden auf den Glaskolben ergeben sich erheblich verringerte Abmessungen einer neuen Kameraröhre mit 8 mm Abtastdiagonale. Zusammen mit der Ablenkspule hat diese Einheit einen Raumbedarf von nur einem Drittel von dem einer Röhre mit 11 mm Abtastdiagonale, sie wiegt nur ein Drittel und benötigt nur ein Viertel des Betriebsstromes. Der stabile Elektrodenaufbau gewährleistet eine Mikrophoniefreiheit, durch die diese Röhre vor allem für Kamera/Recorder-Kombinationen geeignet ist.

Breitband-Speicheroszilloskopröhre mit einstellbarer Speicherdauer

Bei einer Speicheroszilloskopröhre laden die von den Flutelektronen erzeugten Ionen die unbeschriebenen Teile des Speichernetzes und begrenzen damit die Speicherzeit. Die Transferspeicher-Röhre enthält zwei hintereinander angeordnete Netze: eines mit kleiner Kapazität für schnelles Schreiben und eines mit grosser Kapazität für lange Speicherung. Die maximale Schreibgeschwindigkeit beträgt 9 mm/ns; eine Vierpollinse mit 1,8facher Abtastvergrösserung ermöglicht eine vertikale Empfindlichkeit von 5,3 V/cm.

HiFi und Stereo-/Zweiton Wiedergabe beim Fernsehempfang

Für eine HiFi-Tonwiedergabe im Fernsehempfänger ist es erforderlich, das Quasi-Paralleltonverfahren für die Tonsignalaufbereitung zu verwenden. Diese Konzept öffnet auch den Weg für den Empfang von in Kürze zu erwartenden Stereo-/Zweiton-Übertragungen. In diesem Artikel werden neue integrierte Schaltungen für einen nach dem Quasi-Parallelton verfahren arbeitenden Tonkanal beschrieben und Einzelheiten über einen Fernseh-Stereo-/Zweiton-Decoder, der sich in der Entwicklung befindet, mitgeteilt.

Plumbicon-Röhren mit niedriger Ausgangskapazität

Das Signal-Rauschverhältnis einer Fernsehkamera steigt an wenn die Ausgangskapazität der Kameraröhre vermindert wird. Bei der neuen Reihe der Plumbicon–Röhren mit niedriger Ausgangskapazität (LOC: Low Output Capacitance) wird mit einem kleineren transparenten leitenden Belag in der Speicherschicht sowohl die innere Röhrenkapazität als auch die Streukapazität zwischen der Speicherschicht und der Spule reduziert, so dass der Signal-Rauschabstand um etwa 3 dB verbessert wird.

Verständnis der GTO-Kennwerte als Hilfe beim Schaltungsentwurf

Der abschaltbare Thyristor (GTO) besitzt einerseits die hohe Blockierspannung und den hohen Schaltstrom eines Thyristors und anderseits die leichte Steuerbarkeit und die niedrigen Schaltzeiten eines Transistors. In diesem Artikel wird beschrieben, wie die GTO-Thyristoren aufgrund der publizierten Kennwerte am besten eingesetzt werden können.

Elektrolytkondensatoren für industrielle Anwendungen

Die Elektrolytkondensatoren der Serien 114/115 sind für die Glättung gleichgerichteter Netzwechselspannungen und zur Energiespeicherung in industriellen Anlagen entwickelt worden. Auf die Auswahlkriterien für diese Kondensatoren, die auch die beiden grossen Anwendungsbereiche "Motor-Drehzahlregelung mit Impulsbreitensteuerung" sowie "Schaltnetzteile" einbeziehen, wird ausführlich eingegangen.

Senderöhren für Rundfunk und Fernsehen

Die hohen Ansprüche, die an moderne Rundfunk- und Fernsehsender gestellt werden, wirken sich auch auf den Entwurf und die Konstruktion von modernen Senderöhren aus. Diese Röhren sind mit speziellen K-Gittern für niedrige Primär- und Sekundäremission und hohes Wärmeemissionsvermögen ausgerüstet. Ferner werden mit Hilfe des computergestützten Entwurfs (CAD) bei diesen Metall-Keramikröhren von vornherein thermische Spannungen in den Keramik-Isolationsbereichen vermieden.

Tube Plumbicon miniature pour camera TV portable

Le dépôt des électrodes directement sur l'enveloppe de verre réduit considérablement les dimensions de ce nouveau tube de prise de vues de 8 mm de diagonale de balayage. Avec sa bobine de déviation, il n'occupe que le tiers du volume nécessaire à un tube de 11 mm de diagonale de balayage, il ne pèse que le tiers de son poids et ne consomme que le quart de l'énergie. La rigidité de la structure donne une bonne protection contre la microphonie, ce qui rend ce tube particulièrement adapté à l'utilisation dans des ensembles caméra-magnétoscope.

Tube d'oscilloscope a mémoire, persistance variable et large bande

Dans un tube d'oscilloscope á mémoire à grille de mémoire unique, les ions générés par le canon auxiliaire chargent les parties non écrites de la grille et diminuent le temps de stockage. Le tube à transfert de mémoire utilise deux grilles en cascade: l'une à faible capacité pour l'écriture rapide et l'autre à grande capacité pour le stockage prolongé. Les électrons du canon auxiliaire transfèrent la trace de l'une à l'autre et permettent sa visualisation. La vitesse d'écriture horizontale maximale est de 9 mm/ns, une lentille quadrupolaire dont le grandissement est de 1,8 permet une sensibilité verticale de 5,3 V/cm.

Haute fidélité et stéreo/son double pour TV

Pour obtenir une réception sonore à haute fidélité sur un récepteur TV, il est nécessaire de réorganiser la voie de reproduction sonore dans un système à F.I. son quasi-séparée. Ceci ouvre la voie à la réception des transmissions stéréo/son double de l'avenir. Cet article décrit les nouveaux circuits intégrés destinés aux systèmes "quasi-séparée" et donne des détails sur un décodeur stéréo/son double actuellement en cours de développement. Il décrit également un circuit qui simule le nouveau décodeur, ce qui permet au concepteur de construire une voie stéréo/son double avant que le circuit intégré spécifique soit disponible.

Tubes Plumbicon à faible capacité de sortie (LOC)

Le rapport signal/bruit d'une caméra de télévision augmente lorsque la capacité de sortie du tube de prise de vue diminue. Dans les tubes Plumbicon LOC une pellicule conductrice transparente dans la cible réduit la capacité intrinsèque du tube, ainsi que les capacités parasites entre cible et bobine de déviation. Les tubes assurent une amélioration d'environ 3 dB du rapport signal/bruit.

La comprehension des caractéristiques du thyristor GTO, une aide à la conception des circuits

Le thyristor GTO rassemble des qualités telles que haute tension de blocage et courant de commutation élevés, inhérentes aux thyristors classiques avec la facilité de commande et la rapidité de commutation des transistors bipolaires. Le présent article explique comment utiliser les caractéristiques publiées du thyristor GTO pour obtenir la meilleure performance possible.

Condensateurs électrolytiques à usage industriel

Les condensateurs électrolytiques de la série 114/115 ont été conçus pour la régulation de la tension secteur redressée et le stockage de l'énergie dans des applications industrielles. Des recommandations détaillées sont données sur le choix du condensateur et sur deux principaux types d'application: régulation de la vitesse des moteurs par modulation de largeur d'impulsion et alimentación conmutadas.

Tubes d'émission pour télévision et radiodiffusion

La conception des tubes d'èmission modernes illustre les exigences sévères que leur imposent les émetteurs modernes. Les tubes emploient des grilles "K" spéciales pour une faible émission primaire et secondaire. En outre, la conception par ordinateur de la construction céramique/métal élimine pratiquement toute contrainte dans les isolants en céramique, réduisant ainsi le risque de rupture.

Tubo Plumbicon miniatura para cámaras TV portátiles

La deposición de electrodos directamente sobre la ampolla de vidrio reduce considerablemente el tamaño de un nuevo tubo de cámara con una diagonal de exploración de 8 mm: junto con su bobina desviadora ocupa un tercio del lugar de un tubo con diagonal de exploración de 11 mm, pesa un tercio de su peso y consume un cuarto de potencia. La rigidez de la estructura del electrodo y la ausencia de hilos de conexión internos aseguran una libertad de microfonía que lo hace especialmente adecuado para el empleo en combinaciones de cámara/grabadora.

Tubo catódico de almacenamiento de persistencia variable, de banda ancha

En un tubo catódico de almacenamiento con una sola malla de almacenamiento, los iones generados por el flujo de electrones cargan las piezas no grabadas de la malla y acortan el tiempo de almacenamiento. El tubo de transferencia-almacenamiento usa dos mallas en cascada: una de pequeña capacidad para grabación rápida y otra de gran capacidad para almacenamiento largo. La velocidad máxima de registro horizontal es de 9 mm/ns: una lente cuádruple con un factor de amplificación de exploración de 1,8 ofrece una sensibilidad vertical de 5,3 V/cm.

Sonido de alta fidelidad y estéreo/doble para TV

Para obtener una recepción de sonido de alta fidelidad en un aparato de TV se requiere reorganizar el canal de sonido en un sistema casi-dividido. Al hacer esto, se abre también el camino para la recepción de futuras transmisiones de sonido estéreo doble. Este artículo describe nuevos circuitos integrados para sistemas de sonido casi-dividido y da detalles de un decodificador para sonido estéreo doble que está en proceso de desarrollo. También describe un circuito que simula el nuevo decodificador, permitiendo con ello a los diseñadores construir canales de sonido estéreo doble antes de que se disponga del CI que lo incorpora.

Tubos Plumbicon de baja capacidad de salida

La relación señal/ruido, de una cámara de televisión aumenta al reducir la capacidad de salida del tubo de cámara. En la nueva gama de tubos Plumbicon de baja capacidad de salida (LOC), una pequeña película conductora transparente en la tarjeta reduce la capacidad intrínsica del tubo, así como las capacidades parásitas entre tarjeta y yugo. Los nuevos tubos dan una mejora en la relación señal/ruido de unos 3 dB.

Comprensión de los datos del GTO como una ayuda para el diseño de circuitos

El interruptor controlado por puerta GTO combina la alta tensión de bloqueado y la alta corriente de conmutación del tiristor con la facilidad de excitación de puerta y la velocidad del transistor. Este artículo explica cómo utilizar los datos del GTO publicados para obtener el mejor funcionamiento posible.

Condensadores electrolíticos para aplicaciones industriales

Las series 114/115 de condensadores electrolíticos han sido diseñadas para rectificación y filtrado de la red y almacenamiento de energía de aplicaciones industriales. Se da una guía detallada sobre la selección de condensadores, incluidas las dos áreas principales de aplicación: sistemas de control de velocidad para motores por modulación de anchura de impulsos y fuertes de alimentatión.

Tubos de transmisión para difusión por radio y TV

El diseño de tubos modernos de transmisión refleja las grandes demandas que les son impuestas por los transmisores de hoy en día. Los tubos utilizan rejillas-K especiales para la emisión primaria y secundaria baja y alta emisividad térmica. Además, el diseño ayudado por computadora de la construcción de cerámica/metal elimina virtualmente la tensión en los aisladores cerámicos, reduciendo el riesgo de fractura.

Authors

A. A. J. Franken was born in Roosendaal, The Netherlands, in 1941 and studied physics and electronics at the University of Amsterdam. Two years after taking his doctorate in 1965 he joined Philips where, in the applications group of the Medical Systems Division, he specialised in X-ray image-intensifier TV systems; since 1976 he has worked in the camera tube applications group of the Electronic Components and Materials Division.

Ulf Buhse was born in 1945 in Kollmar am Elbe and graduated in electrical engineering at the University of Braunschweig in 1973. Since then he has worked in the television group of the Application Laboratory, Valvo Bauelemente G.m.b.H., Hamburg, where his specialities are vision and sound i.f., selectivity, and, lately, stereo-dual sound processing.

D. van Houwelingen was born in Giessendam, The Netherlands, in 1938. He studied applied physics at the Dordrecht Polytechnic and joined Philips' Research Laboratories in 1958, specialising in low-temperature physics. On completing his studies at the Eindhoven University of Technology, graduating in 1969, he moved to the Electronic Components and Materials Division where he worked on the development of neutron generator tubes. Since 1975 he has specialised in the development of transmitting tubes.

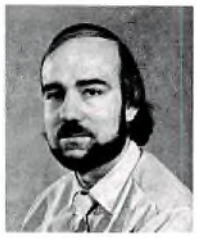

John Houldsworth took his B.Sc. in electronics at the University of Salford and his M.Sc. in control engineering at the University of Manchester Institute of Science and Technology. He joined Mullard in 1969 and is now team leader of the motor control group at the Systems Application Centre for Power at Mitcham. He is a chartered engineer and member of the Power Electronic Equipment Committee of the IEEE.

Helfried Schmickl studied mechanical and electrical engineering and took his doctorate at the University of Technology, Graz, Austria, in 1970. After working on capacitor development for Siemens G.m.b.H., Deutschlandberg, he joined Philips in 1973 and since 1977 has been in charge of electrolytic capacitor development, first at Klagenfurt and, since 1979, as development chief at Zwolle. He is a reader in television engineering at the University of Technology, Graz.

Henning Schwarz was born in Hamburg in 1950. After taking his degree in Electrical Engineering at the University of Technology, Hannover, in 1979 he joined the Application Laboratory of Valvo Bauelemente G.m.b.H., where he specialises in vision and sound i.f. and stereo/dual sound circuitry.

Klaus Zeppenfeld was born in Halle, Germany, in 1940. After taking his doctorate in physics at Hamburg in 1970 he joined Philips' Research Laboratories at Aachen. In 1973 he transferred to the Eindhoven laboratory and in 1975 joined the Energy Systems group. Since 1977 he has been engaged in cathode-ray tube development for the Electronic Components and Materials Division at Heerlen, The Netherlands.

Jan van Warmerdam was born in Haarlemmermeer, The Netherlands, in 1921. He studied electrical engineering at the Amsterdam Polytechnic and joined Philips in 1942. Since that time he has been chiefly concerned with the development of electron tubes, with particular emphasis on transmitting tubes.

Arthur Woodworth was born in Manchester in 1945. He took a B.Sc. in electrical Engineering at Salford University in 1968 and later that year joined Mullard, Stockport, where he is now head of the Electrical Development Department responsible for the specification and evaluation of a wide range of rectifiers, thyristors, triacs, and GTOs.

Electronic components and materials

for professional, industrial and consumer uses

from the world-wide Philips Group of Companies

Argentina: FAPESA, Av. Crovara 2550, Tablada, Prov. de BUENOS AIRES, Tel. 652-7436/7478.
Australia: PHILIPS INDUSTRIES HOLDINGS LTD., Elcoma Division, 67 Mars Road, LANE COVE, 2066, N.S.W., Tel. 427 08 88.
Austria: ÖSTERREICHISCHE PHILIPS BAUELEMENTE Industrie G.m.b.H., Triester Str. 64, A-1101 WIEN, Tel. 62 91 11.
Belgium: M.B.L.E., 7, rue du Pavillon, B-1030 BRUXELLES, Tel. (02) 242 7400.
Brazil: IBRAPE, Caixa Postal 7383, Av. Brigadeiro Faria Lima, 1735 SAO PAULO, SP, Tel. (011) 211-2600.
Canada: PHILIPS ELECTRONICS LTD., Electron Devices Div., 601 Milner Ave., SCARBOROUGH, Ontario, M1B 1M8, Tel. 292-5161.
Chile: PHILIPS CHILENA S.A., Av. Santa Maria 0760, SANTIAGO, Tel. 39-40 01.
Colombia: SADAPE S.A., P.O. Box 9805, Calle 13, No. 51 + 39, BOGOTA D.E. 1., Tel. 600 600.
Denmark: MINIWATT A/S, Emdrupvej 115A, DK-2400 KØBENHAVN NV., Tel. (01) 69 16 22.
Finland: OY PHILIPS AB, Elcoma Division, Kaivokatu 8, SF-00100 HELSINKI 10, Tel. 1 72 71.
France: R.T.C. LA RADIOTECHNIQUE-COMPELEC, 130 Avenue Ledru Rollin, F-75540 PARIS 11, Tel. 355-44-99.
Germany: VALVO, UB Bauelemente der Philips G.m.b.H., Valvo Haus, Burchardstrasse 19, D-2 HAMBURG 1, Tel. (040) 3296-1.
Greece: PHILIPS S.A. HELLENIQUE, Elcoma Division, 52, Av. Syngrou, ATHENS, Tel. 915 311.
Hong Kong: PHILIPS HONG KONG LTD., Elcoma Div., 15/F Philips Ind. Bldg., 24-28 Kung Yip St., KWAI CHUNG, Tel. 12-24 51 21.
India: PEICO ELECTRONICS & ELECTRICALS LTD., Ramon House, 169 Backbay Reclamation, BOMBAY 400020, Tel. 295144.
Indonesia: P.T. PHILIPS-RALIN ELECTRONICS, Elcoma Div., Panim Bank Building, 2nd Fl., Jl. Jend. Sudirman, P.O. Box 223, JAKARTA, Tel. 716 131.
Ireland: PHILIPS ELECTRICAL (IRELAND) LTD., Newstead, Clonskeagh, DUBLIN 14, Tel. 69 33 55.
Italy: PHILIPS S.p.A., Sezione Elcoma, Piazza IV Novembre 3, I-20124 MILANO, Tel. 2-6994.
Japan: NIHON PHILIPS CORP., Shuwa Shinagawa Bldg., 26-33 Takanawa 3-chome, Minato-ku, TOKYO (108), Tel. 448-5611.
(IC Products) SIGNETICS JAPAN, LTD, TOKYO, Tel. (03)230-1521.
Korea: PHILIPS ELECTRONICS (KOREA) LTD., Elcoma Div., Philips House, 260-199 Itaewon-dong, Yongsan-ku, C.P.O. Box 3680, SEOUL, Tel. 794-4202.
Malaysia: PHILIPS MALAYSIA SDN. BERHAD, Lot 2, Jalan 222, Section 14, Petaling Jaya, P.O.B. 2163, KUALA LUMPUR, Selangor, Tel. 77 44 11.
Mexico: ELECTRONICA S.A. de C.V., Varsovia No. 36, MEXICO 6, D.F., Tel. 533-11-80.
Netherlands: PHILIPS NEDERLAND B.V., Afd. Elonco, Boschdijk 525, 5600 PB EINDHOVEN, Tel. (040) 79 33 33.
New Zealand: PHILIPS ELECTRICAL IND. LTD., Elcoma Division, 2 Wagener Place, St. Lukes, AUCKLAND, Tel. 894-160.
Norway: NORSK A/S PHILIPS, Electronica, Sørkedalsveien 6, OSLO 3, Tel. 46 38 90.
Peru: CADESA, Rocca de Vergallo 247, LIMA 17, Tel. 62 85 99.
Philippines: PHILIPS INDUSTRIAL DEV. INC., 2246 Pasong Tamo, P.O. Box 911, Makati Comm. Centre, MAKATI-RIZAL 3116, Tel. 86-89-51 to 59.
Portugal: PHILIPS PORTUGESA S.A.R.L., Av. Eng. Duharte Pacheco 6, LISBOA 1, Tel. 68 31 21.
Singapore: PHILIPS PROJECT DEV. (Singapore) PTE LTD., Elcoma Div., Lorong 1, Toa Payoh, SINGAPORE 1231, Tel. 25 38 811.
South Africa: EDAC (Pty.) Ltd., 3rd Floor Rainer House, Upper Railway Rd. & Ove St., New Doornfontein, JOHANNESBURG 2001, Tel. 614-2362/9.
Spain: COPRESA S.A., Balmes 22, BARCELONA 7, Tel. 301 63 12.
Sweden: A.B. ELCOMA, Lidingövägen 50, S-11584 STOCKHOLM 27, Tel. 08/67 97 80.
Switzerland: PHILIPS A.G., Elcoma Dept., Allmendstrasse 140-142, CH-8027 ZÜRICH, Tel. 01/43 22 11.
Taiwan: PHILIPS TAIWAN LTD., 3rd Fl., San Min Building, 57-1, Chung Shan N. Rd, Section 2, P.O. Box 22978, TAIPEI, Tel. (02)-5631717.
Thailand: PHILIPS ELECTRICAL CO. OF THAILAND LTD., 283 Silom Road, P.O. Box 961, BANGKOK, Tel. 233-6330-9.
Turkey: TÜRK PHILIPS TICARET A.S., EMET Department, Inonu Cad. No. 78-80, ISTANBUL, Tel. 43 59 10.
United Kingdom: MULLARD LTD., Mullard House, Torrington Place, LONDON WC1E 7HD, Tel. 01-580 6633.
United States: (Active devices & Materials) AMPEREX SALES CORP., Providence Pike, SLATERSVILLE, R.I. 02876, Tel. (401) 762-9000.
(Passive devices) MEPCO/ELECTRA INC., Columbia Rd., MORRISTOWN, N.J. 07960, Tel. (201) 539-2000.
(IC Products) SIGNETICS CORPORATION, 811 East Arques Avenue, SUNNYVALE, California 94086, Tel. (408) 739-7700.
Uruguay: LUZILECTRON S.A., Avda Rondeau 1576, piso 5, MONTEVIDEO, Tel. 91 43 21.
Venezuela: IND. VENEZOLANAS PHILIPS S.A., Elcoma Dept., A. Ppal de los Ruices, Edif. Centro Colgate, CARACAS, Tel. 36 05 11.
For all other countries apply to: PHILIPS INDUSTRIES, Electronic Components and Materials Division, Marketing Communications, Building BA, 5600 MD EINDHOVEN, THE NETHERLANDS, Telex 35000, Tel. (040) 72 3142

A20

Printed in The Netherlands